Visualizing neural circuits with concurrent single pulse TMS-fMRI

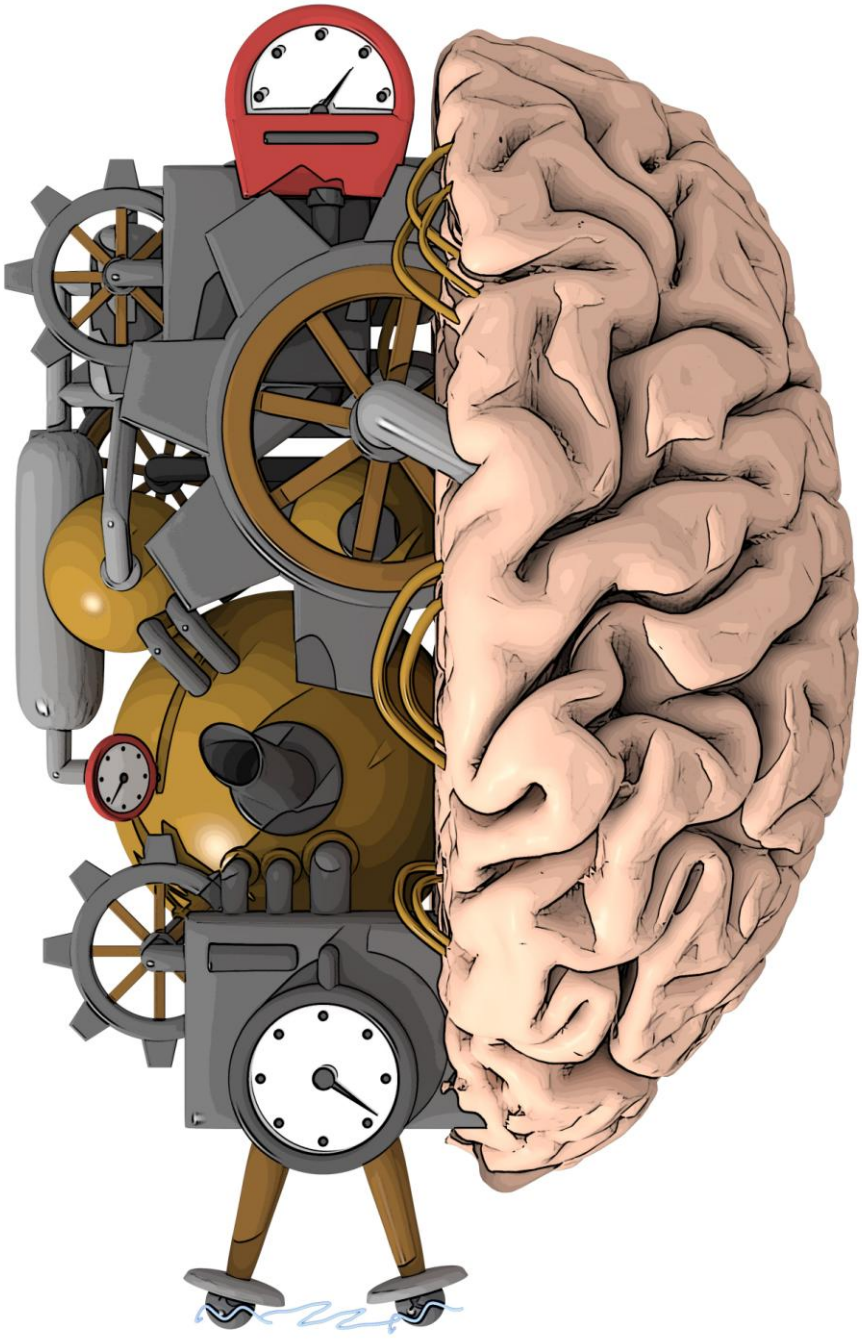

Author details

Author:	J.J.T. Vink, BSc.
Student number:	
E-mail:	
Master degree:	Technical Medicine
Master track:	Medical Sensing & Stimulation

Graduation committee

Chairman:	prof. dr. Ir. M.J.A.M. van Putten
Medical supervisor:	dr. F.S.S. Leijten
Technical supervisor:	dr. S.F.W. Neggers
Process supervisor:	drs. P.A. van Katwijk
External member:	dr. B. ten Haken

Table of contents

Abbreviations

Abbreviations in order of appearance

MDD	Major depressive disorder
TR-MDD	Treatment resistant MDD
TMS	Transcranial magnetic stimulation
rTMS	Repetitive TMS
E-field	Electrical field
M1	Primary motor cortex
MRI	Magnetic resonance imaging
fMRI	Functional MRI
sgACC	Subgenual anterior cingulate cortex
DLPFC	Dorsolateral prefrontal cortex
RMT	Resting motor threshold
HDRS	Hamilton depression rating scale
PET	Positron emission tomography
GMV	Grey matter volume
DBS	Deep brain stimulation
ECT	Electroconvulsive therapy
MEP	Motor-evoked potential
NAc	Nucleus accumbens
BDNF	Brain derived neurotrofic factor
HF	High frequency
LF	Low frequency
FDI	First dorsal interosseous
APB	Abductor pollicis brevis
EEG	Electroencephalography
BA	Brodmann area
ACC	Anterior cingulate cortex
PPC	Posterior parietal cortex
OFC	Orbitofrontal cortex
BOLD	Blood oxygen level dependent
EMG	Electromyography
CSF	Cerebrospinal fluid
GM	Grey matter
RF	Radiofrequency
GLM	Generalized linear model
HRF	Hemodynamic response function
FWE	Family wise error
A1	Primary auditory cortex
SMA	Supplementary motor area
S1	Primary sensory cortex
B0	Static magnetic field
FEF	Frontal eye fields
V5	Middle temporal visual area
SEF	Supplementary eye fields
vPFC	Ventral PFC
V1	Primary visual cortex
V2	secondary visual cortex

Introduction

Major depressive disorder (MDD) is a highly complex disorder that severely affects mood and pleasure in everyday activities. Its complexity appears through its diverse manifestations and its treatment resistant nature. Importantly, MDD is one of the leading causes of disability and the most prevalent mental disorder worldwide. In the first chapter, we show that MDD is associated with a specific dysfunctional brain network and that a response to treatment correlates with normalization of dysfunctional regions within this network. We shed some light on the role of individual regions brain in the pathology of MDD and we relate the complexity of the dysfunctional network to the diverse and treatment resistant nature of MDD.

In chapter 2 we introduce non-invasive brain stimulation methods, that can directly target the dysfunctional network associated with MDD. We specifically focus on repetitive transcranial magnetic stimulation (rTMS). Repetitive TMS is a treatment modality for patients with MDD, which uses electromagnetic induction to modulate DLPFC excitability to realize an antidepressant effect. We lay out the advantages of rTMS and identify ways to improve the limited response rate to rTMS treatment. We stress the importance of the localization of the functional regions rather than relying on brain anatomy for targeting stimulation. Finally, we emphasize the need for more understanding of how the electrical field induced by TMS (TMS E-field) interacts with neuronal populations in the cortical layer.

In chapter 3 we propose concurrent TMS-fMRI as an innovative method to determine the brain's response to single pulses of TMS in order to increase understanding of the effects of TMS. We validate concurrent TMS-fMRI through the delivery of TMS pulses to the functional representation of the hand in the primary motor cortex (M1) and verify TMS-induced network activity through a comparison with voluntarily induced motor network activation and literature findings on motor networks. We debate the complex interaction between the TMS E-field and the neuronal populations in the cortical layer and provide suggestions for future research.

Chapter 4 reviews the networks that are activated in response to TMS pulses delivered to the left DLPFC. We relate these networks to established network connectivity and literature findings. Finally, based on our expertise, we provide suggestions for future research to further increase the understanding of TMS treatment in MDD and to improve the application of concurrent TMS-fMRI.

Chapter 1

Neural circuits involved in major depressive disorder

Major depressive disorder

Major depressive disorder (MDD) is a complex disorder which is characterized by a depressed mood or loss of interest or pleasure in (almost) all activities, for at least a two-week period. MDD is accompanied by at least 4 of the following symptoms: significant loss of weight, feelings of worthlessness or guilt, fatigue, psychomotor agitation or retardation, insomnia or hypersomnia, lack of concentration and recurrent thoughts of death[1]. In light of these symptoms, patients with MDD experience strong impairment in social, occupational and other areas of function, which greatly impairs their daily life. The severity of depressive symptoms is commonly documented with the Hamilton Depression Rating Scale (HDRS), scoring individual depressive symptoms in detail[2].

The global prevalence of MDD is a staggering 4.7%, making it the most prevalent mental illness worldwide[3]. MDD is the leading cause of disability with, in the United States alone, an estimated annual cost of approximately $83 billion due to treatment and decreased overall performance[4]. MDD has an average age of onset of 30 years and risk of development is increased for the middle aged, Caucasian and low income population[5].

The manifestations of MDD are highly diverse, which was elegantly demonstrated by Fried et al. who identified over 1,000 unique symptom profiles[6]. MDD is also exceptionally difficult to treat. Up to two thirds of the patients with MDD do not respond to the first medication prescribed and approximately 15 to 33% of patients has treatment resistant MDD (TR-MDD)[7]. Patients with TR-MDD do not show significant clinical improvement to treatment with antidepressants of at least two different pharmacological classes[4]. Altogether, its diverse manifestations, high prevalence, disabling impact and treatment resistant nature make MDD a heavy burden on societies, which stresses the need for more understanding of its complex pathology.

Neural circuits in MDD

Before we review the neural circuits that are of importance in MDD, we discuss investigational methods that have led to the implication of these neural circuits in the pathology of MDD. In the past decades, the understanding of MDD has greatly increased. The first neuroimaging studies investigated changes in grey matter volume (GMV) in anatomical brain scans that discriminated patients with MDD from healthy individuals. Other researchers would compare metabolic activity between patients with MDD and healthy individuals. This was done through the injection of a radioactive tracer that accumulates in regions with increased metabolic activity. The dose of radioactive tracer was then measured with positron emission tomography (PET). This would provide researchers insight in whether brain activity was different in patients with MDD and whether this related to changes in structural anatomy. After abnormalities in baseline activity were well established, researchers started to investigate metabolic brain activity before and after treatment with antidepressants and identified changes in metabolic activity that were uniquely related to a response to treatment. This would provide them with better understanding of what regions were actively involved in the experience of depressive symptoms and how changes in metabolic activity in these regions related to the relief of depressive symptoms. More recently, neuroscientists started to measure brain activity during a functional magnetic resonance recording (fMRI) while the participant performed specific tasks to identify task-related differences between patients with MDD and healthy individuals. Finally, electroconvulsive therapy (ECT) and deep brain stimulation (DBS) became subjects of interest. With DBS it was possible to modulate the activity of

specific neuroanatomical regions that were found to be dysfunctional in patients with MDD. Researchers started to document metabolic changes in response to DBS treatment, further increasing the knowledge on MDD.

The aforementioned research approaches have identified a number of regions which are relevant in MDD. These regions are part of two major networks: the fronto-limbic network and the reward network. In the following sections we discuss these regions and identify how these regions play a role within the pathology of MDD (Fig. 1.1).

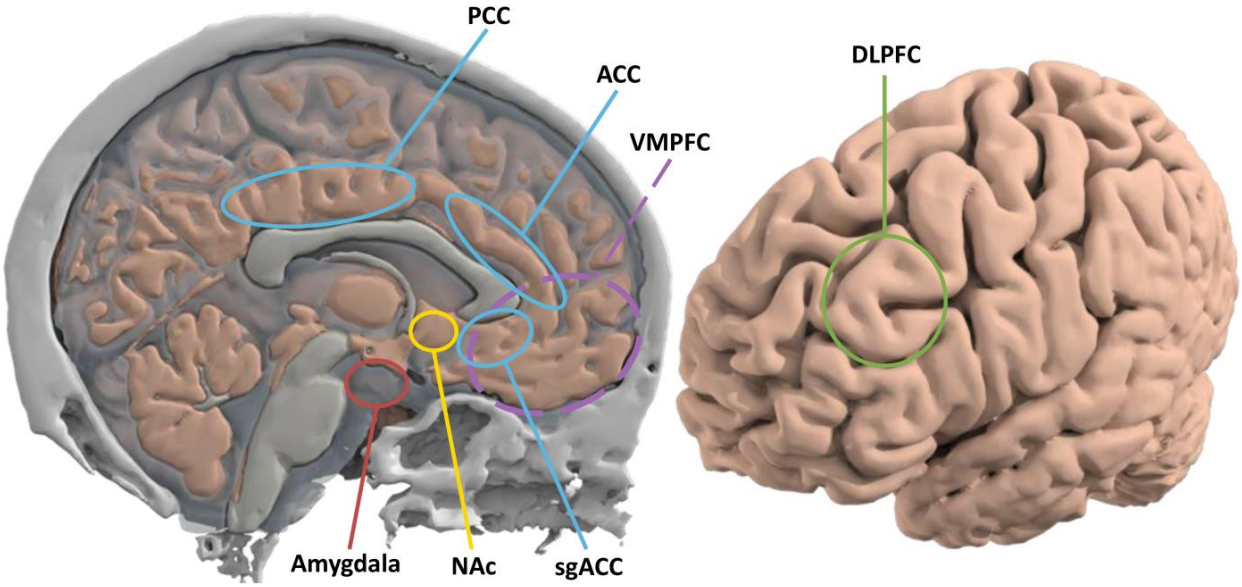

Figure 1.1 *Medial (left) and lateral (right) view on the left hemisphere. A number of neuroanatomical regions relevant to major depressive disorder are encircled. The amygdala is located more deeply than indicated. PCC: posterior cingulate cortex; ACC: anterior cingulate cortex; sgACC: subgenual anterior cingulate cortex; NAc: nucleus accumbens; DLPFC: dorsolateral prefrontal cortex.*

The fronto-limbic network

In 1878, Paul Broca identified the 'great limbic lobe' in addition to previously established cerebral lobes[8]. According to Paul Broca, the 'great limbic lobe' covered the white matter connection between the two hemispheres deep in the brain. He argued that intelligence evolved with the expansion of the frontal lobe because it was only seen in intelligent mammals, such as primates. He observed that frontal lobe expansion occurred simultaneously with the reduction of the olfactory system, an important part of his 'great limbic lobe'. He concluded that through evolution, the frontal lobe had obtained dominance over the ‘great limbic lobe’, because intelligence had obtained dominance over the bestial sense. Thus, the primal instincts were represented in the ‘great limbic lobe’.

Sixty years later, James Papez made a major contribution to the understanding of the limbic system with his theory of emotion[9]. He was able to relate specific cognitive and emotional processes to the limbic network, further specifying the role of the limbic network within the brain. His work included patients with cingulate lesions, who presented with impaired memory and personality changes. Today, the fronto-limbic network has been associated with a large number of complex cognitive and emotional processes, which are linked to a substantial number of neuroanatomical structures. In this chapter we discuss the neuroanatomical structures that are strongly associated with MDD: the cingulate cortex, the prefrontal cortex and the amygdala.

The subgenual cingulate cortex

James Papez was the first to emphasize the role of the cingulate cortex in his theory of emotion[9]. The cingulate cortex is a large grey matter region that embodies the outer surface of the corpus callosum and consists of an anterior and posterior division[10][11]. Although different parts of the cingulate cortex can be affected in MDD, the subgenual anterior cingulate cortex (sgACC) has attracted most attention. The sgACC is the most ventral part of the ACC and is located inferior to the corpus callosum genu. It is one of the most intensively researched brain areas in relation to MDD and other mood disorders.

Drevets et al. investigated neuroanatomical changes in patients with mood disorders and discovered that the GMV of the sgACC was significantly reduced in patients with MDD[12]. The reduction in sgACC volume was also observed in early-onset MDD and young adults with a high familial risk for the development of MDD[13][14], indicating sgACC volume reduction as a precursor of the development of depressive symptoms in patients with a genetic predisposition for MDD. These structural changes are associated with increased metabolic activity that has been observed in the sgACC[12][15]. More specifically, Mayberg et al. found that normalization of the increased metabolic activity in the sgACC was correlated with a response to antidepressant treatment[16]. The fact that treatment outcome correlates with normalization of sgACC activity has become a well-established observation[16][17][18].

Multiple lines of evidence converge upon the idea that increased activity of the sgACC plays a role in the development of depressive symptoms and that successful treatment has a neuromodulatory effect on the increased metabolic activity in the sgACC. Mayberg et al. argued that DBS could be used to modulate the abnormal activity in the sgACC. DBS electrodes were implanted near the sgACC in 6 patients with TR-MDD. Four of these patients showed sustained remission and showed decreased activity in the sgACC and normalized activity in a number of other regions[17]. Holtzheimer et al. followed up on these findings with a single-blind study on 17 patients with MDD, who received DBS of the sgACC[19]. 92% of these patients responded to treatment and 58% went into remission (defined as a 90% decrease on the HDRS). These findings provide further evidence that successful normalization of abnormal sgACC activity through neuromodulation, is associated with an antidepressant effect.

The dorsolateral prefrontal cortex

The prefrontal cortex is the entire cortical region ventral to the motor cortex and is associated with complex cognitive and executive function as well as emotional and behavioral processes. The representation of these complex functions was famously demonstrated in the case report on Phineas Gage, who experienced substantial personality changes after both his prefrontal cortices were severely damaged in a railroad construction accident[20]. The prefrontal cortex can be divided into four quadrants: the dorsolateral, dorsomedial, ventrolateral and ventromedial prefrontal cortex. Two of these quadrants have drawn attention because of their relevance in depression: the ventromedial prefrontal cortex, which inhabits the sgACC, and the DLPFC[21].

One of the major symptoms of MDD is psychomotor impairment, a symptom that is related to abnormal executive function. Patients with MDD show reduced executive function in different neuropsychological and cognitive tests[21]. Interestingly, they also show reduced metabolic activity in the DLPFC[21], an area associated with executive function[22]. Korgaonkar et al. further investigated prefrontal dysfunction in MDD by using standardized tests during an fMRI recording. They found reduced activity in the DLPFC during a working memory task and conscious negative emotion processing in patients with MDD compared to healthy controls[23]. Moreover, Brody et al. investigated the correlation between DLPFC dysfunction and abnormal executive function in relation to treatment. They investigated the response to antidepressant treatment in 30 patients with MDD and correlated the improvement on several aspects of the HDRS to metabolic changes[24]. They found that cognitive improvement on the HDRS was uniquely correlated with increased metabolic activity in the DLPFC.

Finally, patients with bilateral DLPFC lesions show significantly higher levels of depression compared to patients with non-frontal lesions[25], indicating that DLPFC dysfunction can also have a causal role in the development of depressive symptoms.

Amygdala

The amygdala is a subcortical structure located in the temporal lobe, which plays an important role in the regulation of emotional processes and the integration of emotion and memory[26]. Amygdala volume is significantly reduced in unmedicated patients with MDD[27]. Paradoxically, medicated patients with MDD show significantly larger amygdala volumes compared to healthy controls[28]. This is likely due to the increased release of brain-derived neurotrophic factor (BDNF) in response to antidepressants[29].

Drevets et al. observed increased metabolic activity in the amygdala in patients with MDD compared to healthy controls[30], and found that the level of metabolic activity also correlated with symptom severity[31]. They also showed that increased metabolic activity of the amygdala normalized after successful antidepressant treatment[30].

The reward network

An important symptom of MDD is a 'markedly diminished interest or pleasure in (almost) all activities most of the day, nearly every day (as indicated by subjective account or observation).'[1] This core symptom of MDD is called anhedonia, the inability to experience pleasure from activities which were found pleasurable before. Anhedonia has been related to dysfunctional reward processing[32].

The reward network has been investigated intensively, which has led to the identification of a number of structures involved in goal-directed behavior[33]. The dorsal and ventral striatum play an important role in goal-directed behavior and reward processing. The nucleus accumbens (NAc) is part of the ventral striatum and serves as the key region for the integration of information to regulate goal-directed behavior. It receives input from the aforementioned sgACC, integrating emotional processes in the regulation of goal-directed behavior[34]. The caudate nucleus and putamen make up the dorsal striatum and play a role in the motor coordination of goal-directed behavior[35].

Nucleus accumbens

As discussed previously, MDD has been associated with dysfunctional metabolic activity of several neuroanatomical regions. However, these metabolic disturbances have not been observed for striatal regions except for two reports of metabolic dysfunction in the caudata nucleus[36]. Although, evidence for metabolic dysfunction of striatal structures is lacking, abnormal activity can be observed specifically during reward processing in fMRI recordings. Pizzagalli et al. investigated brain responses to the anticipatory and consummatory phases of reward processing in patients with MDD during an fMRI recording[37]. They found that during the consummatory phase, unmedicated patients with MDD showed weaker responses in the left NAc and the bilateral caudate nucleus compared to healthy controls. Reduced activation in the left putamen was seen during the anticipatory phase of reward processing. Smoski et al. also observed reduced activity in striatal regions in response to reward anticipation, selection and feedback. They also measured reduced activity in the bilateral DLPFC during reward selection and found that this correlated with depression severity[38].

DBS treatment of the NAc has also been investigated in patients with MDD. Schlaepfer et al. implanted DBS electrodes in the bilateral NAc of three patients with TR-MDD and found increased metabolic activity in the NAc, amygdala and DLPFC and reduced metabolic activity in the VMPFC and the caudate nucleus in responders[39]. Interestingly, these findings correlate well with observations by Mayberg et al. for DBS treatment of the sgACC[17]. Since the sgACC projects directly onto the NAc, it is possible that stimulation of the sgACC induces neuromodulatory changes of prefrontal

regions through the NAc. However, metabolic changes in the NAc have not been reported in response to DBS of the sgACC. Malone et al. investigated the response to DBS of the NAc in 17 patients with MDD. They found similar response and remission rates compared to DBS treatment of the sgACC with response and remission rates of 40% and 20%, respectively[40].

Table 1.1 *Summary of differences in baseline activity, grey matter volume and task-related activity observed in patients with MDD compared to healthy individuals.*

Brain region	**Baseline activity**	**Grey matter volume**	**Task-related activity**
sgACC	Increased	Reduced	-
DLPFC	Reduced	-	Reduced
Amygdala	Increased	Reduced	-
NAc	-	-	Reduced
Caudate nucleus	Reduced	-	Reduced

Discussion

We discussed how a network consisting of several neuroanatomical regions that exhibit abnormal activity fits in the pathology of MDD (Table 1.1). However, a coherent framework that explains the interactions between these key regions in light of the pathology and pathogenesis of MDD is lacking. The design of such a coherent framework for a complex multidimensional disorder poses significant challenges.

First, the key regions that we discussed in the previous sections are all part of a bigger integrated network. We saw that within an integrated network, one dysfunctional region can affect other regions and that modulating the activity of one region can result in normalization of abnormal activity in other regions. For example, we saw that patients with bilateral DLPFC lesions are at higher risk of depression and that neuromodulation of the sgACC can cause normalization of activity in the DLPFC. Therefore, I would argue that dysfunctional activity in the DLFPC can be both a consequence and a cause of a network dysfunction, since it is part of an integrated network. This dual role complicates inference on causality within integrated networks.

Second, the network of interest is made up of billions of communicating neurons. Neuroimaging techniques enable us to measure the activity in neuroanatomical structures and identify dysfunctional structures in depressed brains. However, these structures consist of large numbers of neuronal populations with complex interactions within and between these neuronal populations. It is important to note that we make inferences based on dysfunctional activity on a macroscopic scale, while network communication takes place on a microscopic scale.

Finally, MDD presents itself in a large number of unique symptom profiles. I argue that the substantial variation in symptom profiles arises from a significant diversity in network dysfunction. This strong variation in network dysfunction requires a coherent framework that can explain the variability in network dysfunction.

Conclusion

Major depressive disorder is a highly complex disorder that severely affects mood and pleasure in everyday activities. We saw that its complexity appears through its diverse manifestations and its treatment resistant nature. We showed that MDD is associated with a specific brain network consisting of dysfunctional neuroanatomical regions. We saw how abnormal activity in an individual regions relates to symptoms observed in patients with MDD and that successful treatment correlates with the normalization of abnormal activity in these regions. Finally, we emphasized the need for a coherent framework that explains the role of different neuroanatomical regions in the pathology of MDD.

Chapter 2

Non-invasive brain stimulation in major depressive disorder

Introduction

In chapter one, we discussed the enormous impact of MDD on individuals and their communities. We saw that approximately 20% of the patients with MDD does not respond to conventional treatment with antidepressants. We showed that MDD is associated with a network consisting of several dysfunctional regions and that a response to treatment correlates with normalization of dysfunctional regions within this network. Over the last decades new treatment modalities have emerged that specifically target these dysfunctional regions. We already discussed DBS, a highly invasive treatment alternative, which is considered if all other treatment options are exhausted. However, we did not discuss non-invasive brain stimulation methods that are available for the treatment of patients with MDD, like electroconvulsive therapy (ECT) and repetitive transcranial magnetic stimulation (rTMS). ECT induces an electrical current into the brain to induce an epileptic seizure. ECT is shown to be effective in patients with TR-MDD, but requires anesthesia for its application and is accompanied by severe side effects[41]. rTMS is a more patient-friendly alternative to ECT, with only mild side effects. rTMS utilizes electromagnetic induction to induce a focal electrical field in the brain[42]. For treatment of patients with MDD, the local electrical field is induced in the left DLPFC (Fig. 2.1), one of the regions that we discussed in chapter one. In the following sections we discuss rTMS as a treatment modality for MDD in more detail.

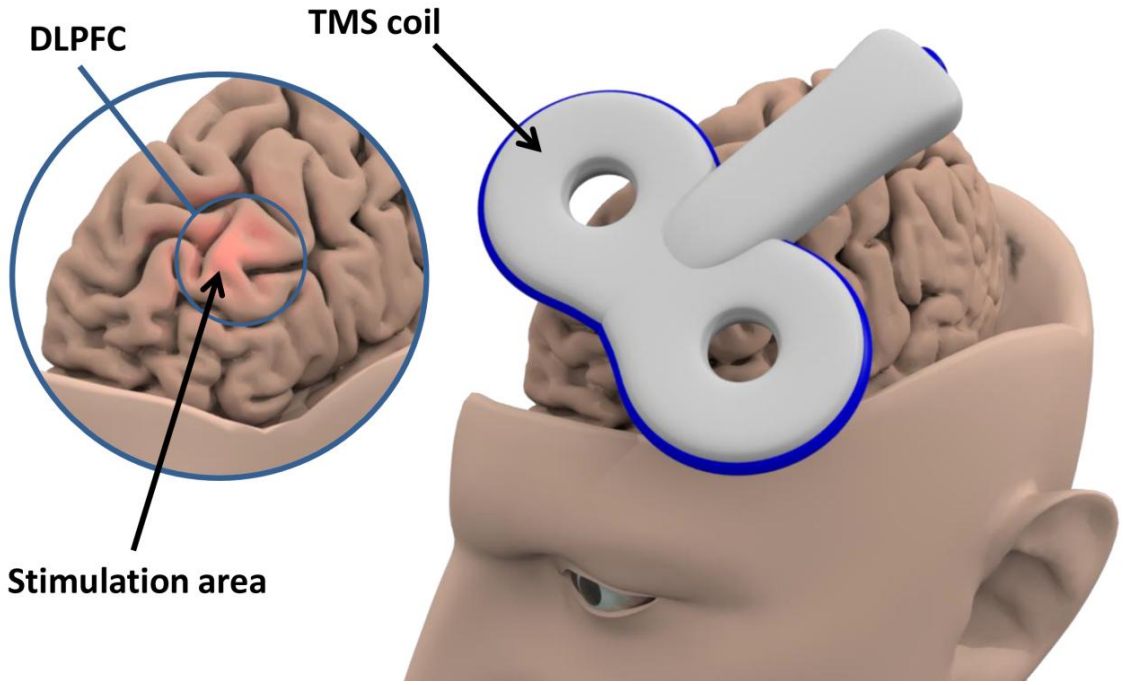

Figure 2.1 *A TMS coil positioned over the left DLPFC. The left panel shows a projection of the electrical field on the cortical surface. DLPFC: dorsolateral prefrontal cortex.*

Transcranial magnetic stimulation

TMS is a non-invasive brain stimulation technique, which induces a focal electrical field through Faraday's laws of electromagnetic induction[42]. An electrical current flows through

windings of copper wire to induce a time-varying magnetic field, which again induces an incident electrical field in the brain (Fig 2.2). This electrical field interacts with the neuronal populations in the cortex, which produce an evoked potential in response to stimulation. For example, a TMS pulse delivered to the functional representation of the hand within M1, evokes a potential that travels to connected brain regions and to the muscles in the contralateral hand resulting in a muscle contraction. Therefore, single pulse TMS can be used to measure cortical excitability or to determine network connectivity.

The repetitive delivery of pulses of TMS (rTMS) causes different effects compared to delivery of single pulses. During rTMS, an incident electrical field is induced in the cortex with a specific frequency which causes changes in cortical excitability that outlast the duration of treatment[43]. The frequency of stimulation determines whether the long-term excitability of neuronal populations is inhibited or excited. The principle that the behavior of neuronal populations changes in response to changes in input is called neuroplasticity. High frequency (HF) rTMS delivers pulses at a frequency of 5 Hz or higher, which causes a long-term increase in excitability of the stimulated neuronal populations[44]. Low frequency (LF) rTMS (< 1 Hz) causes a long-term decrease in excitability. When we use rTMS to change plasticity of neuronal populations, we talk about neuromodulation. Finally, during rTMS, pulses are delivered with an intensity relative to the patient's resting motor threshold (RMT), to individualize TMS pulse intensity[45]. The RMT is determined based on the amplitude of the motor-evoked potential (MEP) in the first dorsal interosseous (FDI) or abductor pollicis brevis (APB) muscle in response to single TMS pulses delivered to the thumb representation in the contralateral motor cortex.

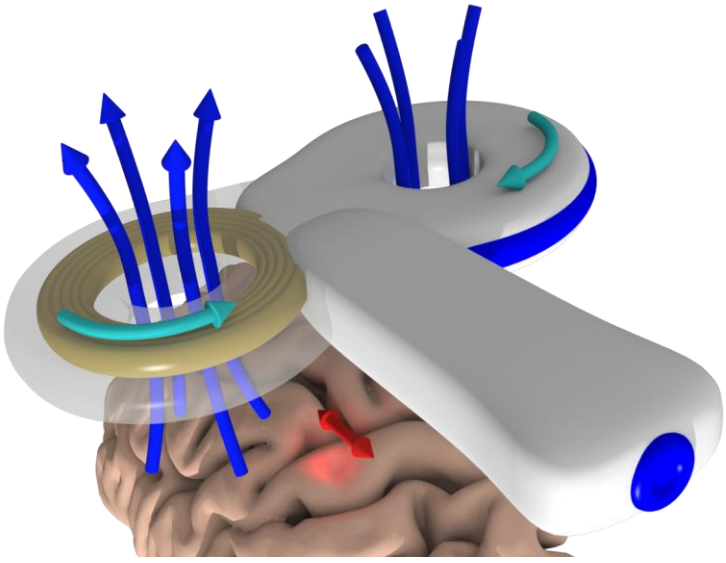

Figure 2.2 *TMS coil located above the cortical surface. The light blue arrows indicate the direction of the current flowing through the copper windings. The dark blue arrows illustrate the direction of the time-varying magnetic field. The red arrow shows the orientation of the incident TMS electrical field.*

The interaction between the electrical field induced by TMS (TMS E-field) and the neuronal populations in the cortical layer is of great importance in understanding the effects of TMS on neuronal populations. Rahman et al. investigated the effects of two different E-field orientations on neuronal cells in cortical slices of rats[46]. They found that tangential E-fields, which are oriented parallel to the cortical surface, produce different effects compared to radial E-fields, which are oriented perpendicular to the cortical surface (Fig. 2.3). They concluded that tangential E-fields modulate synaptic efficacy during stimulation, through hyper- or depolarization of afferent axons and their synaptic terminals. Differently, radial E-fields modulate the cell bodies of cortical neurons, affecting output that travels to other brain regions. According to this simplified theoretical framework, the induction of a radial E-field is crucial in the production of network activity in

response to single pulse TMS. Importantly, the induction of radial or tangential E-fields in response to TMS is highly variable due the complex morphology of the gyri of the brain. Thus, a single TMS E-field has completely different effects in different regions of the stimulation area, depending on the morphology of the gyri.

Kammer et al. demonstrated the relevance of the direction of the TMS E-field with respect to the orientation of the gyrus. They showed that TMS E-fields oriented perpendicular to the orientation of the gyrus induced stronger effects (based on phosphene thresholds in response to stimulation of the visual cortex) compared to E-fields oriented parallel to the orientation of the gyrus (Fig 2.4). Additionally, Fox et al. observed that TMS-induced activity is predominantly present in the sulcal regions, rather than on the superficial gyral surfaces in TMS-PET measurements[47]. Based on their observations, they proposed Rushton's cosine principle, which isolates the radial component of the TMS E-field, to determine the effective TMS E-field. Rushton's cosine principle can be incorporated in a finite element model to estimate the effects of the TMS coil location and orientation on the TMS E-field (Fig. 2.5). Janssen et al. were able replicate the observations by Kammer and Fox et al. on the effect of the TMS coil orientation with respect to the underlying gyrus using FEM[48]. It is important to note that Rushton's cosine principle is a crude approach to predict the effects of the TMS E-field, but more sophisticated approaches are lacking.

Furthermore, the effects of TMS are prone to the complex biochemical and neurophysiological state of the brain. For example, changes in the biochemistry of the brain in response to alcohol can influence the excitability of the cortex[49] and slight contraction of the muscle or observation of movement, i.e. facilitation, increase cortical excitability of M1[50]. Furthermore, the effects of TMS are significantly affected by pre-existing oscillatory activity of the cortical neuronal populations[51][52]. These biochemical and neurophysiological processes diversify the effects of TMS between people.

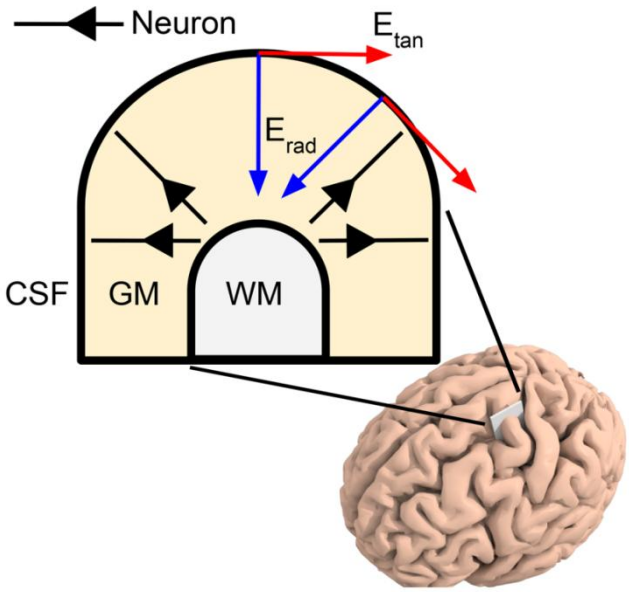

Figure 2.3 *Simplified schematic of the orientation of cortical neurons in the cortical layer of the gyrus. The direction of the radial electrical field (E_{rad}) and the direction of the tangential electrical field (E_{tan}) are shown in blue and red, respectively. WM: white matter; GM: grey matter; CSF: cerebrospinal fluid.*

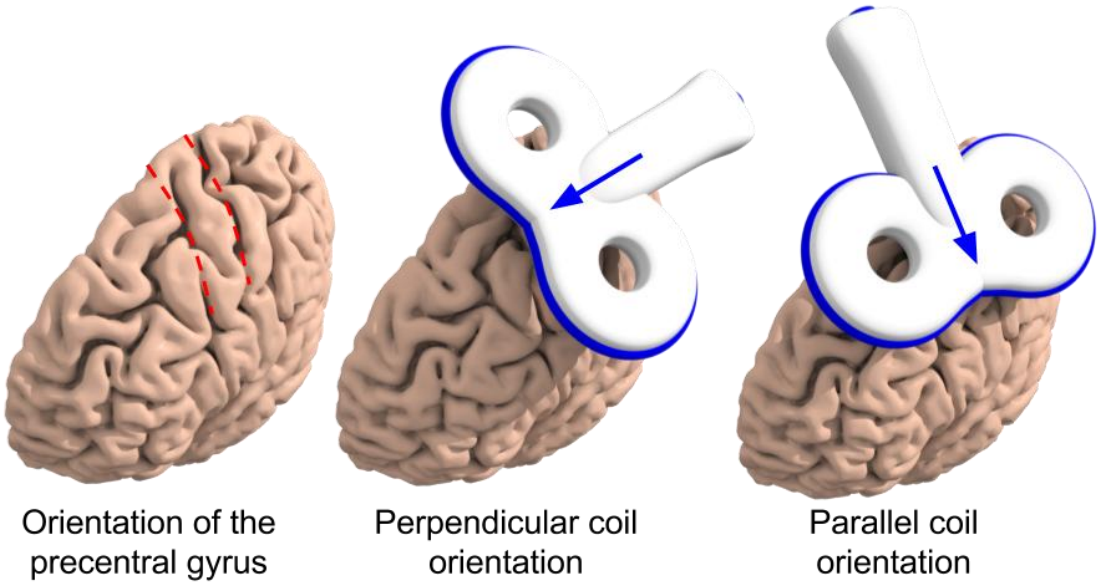

Figure 2.4 *Orientation of the precentral gyrus in red and coil orientations perpendicular and parallel to the orientation of the precentral gyrus. The direction of the TMS E-field is indicated with a blue arrow.*

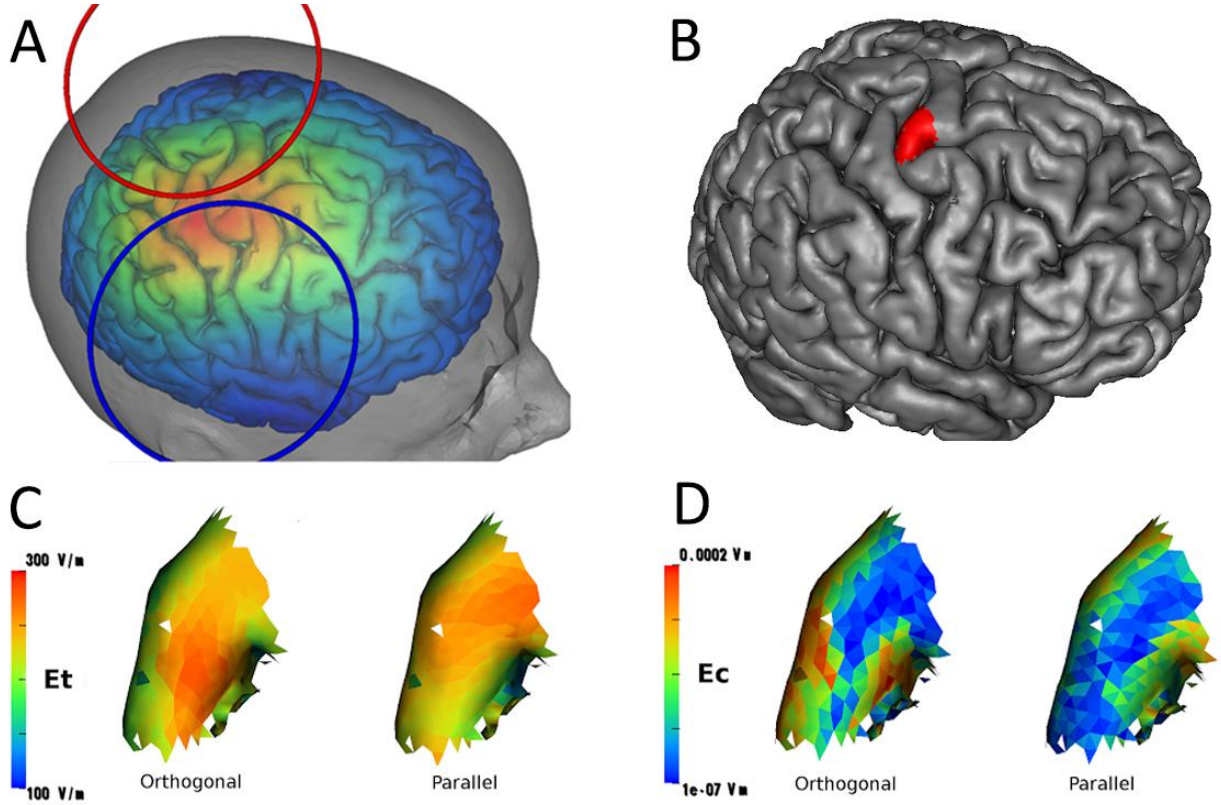

Figure 2.5A *Projection of the TMS E-field on the cortical surface.* ***Figure 2.4B*** *The location of the cortical area shown in panels C and D.* ***Figure 2.4C*** *Projection of the E-field strength on the cortical surface for orthogonal and parallel orientations of the TMS coil.* ***Figure 2.4D*** *Application of Rushton's cosine principle to determine the strength of the E-field perpendicular to the surface (radial component of the E-field) for orthogonal and parallel orientation of the TMS coil. Courtesy of Petar Petrov (manuscript currently under review).*

Repetitive TMS in MDD

As we discussed in chapter 1, the metabolic activity of the left DLPFC is reduced in patients with MDD and normalization of this activity through antidepressant treatment correlates with treatment outcome. HF rTMS attempts to increase the excitability of the left DLPFC directly in order to normalize the abnormal activity in this region. The effects of rTMS are not limited to the area of stimulation, but propagate to different brain regions, as we demonstrate later in this chapter. However, little is known about the pattern of propagation and the distant neuromodulatory effects.

In 2008, the United States Food and Drug Administration (FDA) approved 10Hz rTMS of the left DLPFC as a treatment option for patients with MDD. O'Reardon et al. investigated the clinical effects of rTMS treatment in 155 unmedicated patients with MDD[53]. They observed a significant clinical benefit of rTMS compared to sham TMS with a response rate up to 25% and a remission rate of approximately 15% (subtle variations between depression rating scales) for active rTMS. A disadvantage of rTMS is treatment duration and the necessity for maintenance treatments. Patients with MDD are treated daily with rTMS protocols consisting of 37.5 minutes of treatment during a period of 4 to 6 weeks[42]. Moreover, the antidepressant effects of rTMS wear off in about half of the patients treated[54]. In these cases, rTMS treatments are repeated in order to maintain the antidepressant effect[54]. Consequently, rTMS is a demanding and time-consuming treatment for both patients and personnel. Although rTMS is clearly beneficial in the treatment of MDD, the response rate is limited. Limited treatment effects can be attributed to inaccurate coil positioning because conventional coil placement methods have no regard for individual brain morphology. Ideally, the TMS target is based on the representation of functional regions in the brain, as we will see later in the next section. Finally, the complex interaction between the TMS E-field and the neuronal populations in the cortex affect the efficacy of stimulation. This interaction is modulated by a number of parameters including coil orientation and angulation, cortical morphology and TMS pulse intensity.

Improving rTMS treatment

The widespread application of rTMS in the treatment of MDD faces two significant challenges. rTMS is a time-consuming procedure and its response rate is limited[53]. In order to overcome the time-consuming nature of rTMS, research has focused on the design of accelerated rTMS protocols[55]. These accelerated protocols are beyond the scope of this thesis and are therefore not discussed.

However, the limited response rate remains a significant challenge. One factor that restricts the response rate is the accuracy of coil placement[56]. Conventional coil placement methods navigate to the DLPFC based on the location of the thumb area in the left M1 (as determined through contralateral thumb movement in response to single pulse TMS), the 5cm rule, or based on the 10-20 system used in electro-encephalography (EEG). However, the first method does not take into account individual brain size and morphology while the latter only disregards patient-specific brain morphology. An alternative to these conventional methods is MRI-guided neuronavigation, which uses a patient-specific MRI scan to navigate coil placement to the left DLPFC. Fitzgerald et al. showed that MRI-guided neuronavigation is superior to conventional coil placement methods in the treatment of MDD[56].

Taking into account individual brain morphology increases the response to rTMS treatment. However, the representation of functional regions within the anatomically defined regions shows substantial variability between individuals[57][58]. In order to further increase the response to TMS, the functional parcellation of the human brain should be taken into account. This was elegantly demonstrated by Sack et al. who showed that fMRI-guided neuronavigation (based on functional regions) increased TMS effect size[59].

The relevance of functional regions was also demonstrated by Fox et al.[60]. They hypothesized that the antidepressant effect of HF rTMS could be explained by an indirect neuromodulatory effect on the sgACC. They identified the region inside the left DLPFC which showed

the strongest correlation with the sgACC based on resting state fMRI data and subsequently targeted this region with HF rTMS. They observed that stimulation of cortical regions with a stronger negative correlation with the sgACC showed better treatment outcome. Best treatment outcome was observed for rTMS of Brodmann area 46 (BA46), which makes up the DLPFC together with a part of BA9. Fox et al. were the first to establish the relevance of functional regions in rTMS treatment of MDD. Baeken et al. further investigated the relevance of functional connectivity between the sgACC and the DLPFC[61]. They confirmed the findings by Fox et al. by observing that responders to HF rTMS of the DLPFC had stronger connectivity at baseline compared to non-responders. In addition, they found a positive correlation between the sgACC and the DLPFC in responders after treatment. There was no treatment-induced change in correlation for non-responders. Hopman et al. also confirmed these findings in their work[62].

We discussed that stimulation of functional regions increases the effects of TMS compared to conventional methods. We also saw that stimulation of functional regions that are connected to the sgACC, increased the response to rTMS treatment for MDD, specifically. Consequently, an anatomical and functional MRI scan are required to guide TMS coil placement, in order to increase the efficacy of rTMS in the treatment of MDD. As stated previously, coil placement is even further complicated by the complex interaction between the TMS E-field and the neuronal populations in the cortical layer. The integration of all these different elements is required to guarantee best possible treatment for an individual patient. This is achieved through the design of a personalized brain model that simulates the effect of the TMS E-field on the neuronal populations and shows the functional parcellation of the brain in order to guide coil placement. Subsequently, this coil position can be replicated during TMS sessions with MRI-guided neuronavigation.

Effects of high frequency rTMS of the DLPFC

In a previous section, we discussed that TMS-induced activity propagates to other brain regions causing distant modulatory effects. This was first visualized by Teneback et al. when they applied rTMS to the left DLPFC in 22 unmedicated patients with MDD[63]. Prior to treatment, they found that metabolic activity in the left DLPFC, the left caudate nucleus and the bilateral medial temporal lobes negatively correlated with depression severity. They identified that an increase, and thus normalization, in metabolic activity in the left DLPFC and left caudate nucleus was uniquely associated with a response to treatment. In chapter one, we discussed the relationship between normalization of DLPFC activity and treatment outcome. However, the increased activity in the caudate nucleus observed by Teneback et al. contradicts findings by Schlaepfer et al., who observed reduced caudate nucleus activity in responders to DBS.

Zheng et al. also investigated metabolic activity in patients with MDD and observed a significant increase in metabolic activity of the left ACC[64]. However, reliability is limited because they had little control over the TMS target (they used the 5cm rule), a small sample of 5 patients, and no associations with treatment outcome. Lan et al. investigated the effects of rTMS treatment of the left DLPFC on grey matter volume (GMV) in 27 patients with MDD[65]. They observed increased grey matter volume in the left ACC, left insula, left superior temporal gyrus and right angular gyrus. The increase in GMV of the left ACC specifically was correlated with a reduction in HDRS symptom severity.

Investigation of the neuromodulatory effects of rTMS of the left DLPFC has not been limited to patients with MDD. De Raedt et al. measured whole brain effects of HF rTMS of the left DLPFC in healthy individuals using fMRI[66]. They recorded BOLD during an attentional processing task of emotional information before and after HF rTMS of the left DLPFC. They observed reduced engagement of angry faces after treatment, which was associated with increased activity in the right DLPFC, the dorsal anterior cingulate cortex (ACC), the right posterior parietal cortex (PPC) and the left orbitofrontal cortex (OFC).

Conclusion

We discussed HF rTMS of the left DLPFC as a non-invasive treatment option for patients with MDD, which is currently applied clinically. However, the response rate to rTMS is limited and the treatment protocol is time-consuming. Accelerated treatment protocols and patient-specific coil placement provide a solution to these problems. In this chapter we specifically discussed the necessity of increased understanding of TMS E-field interactions and the use of functional topography in order to guide coil placement. These elements can be combined in a personalized brain model that contains both structural and functional information of an individual patient to guarantee most efficacious treatment.

Research goals

We propose concurrent TMS-fMRI as an innovative method to measure the direct effects of TMS in order to guide the design of a personalized brain model that incorporates the individual structural and functional anatomy of the brain to simulate the TMS effect. During concurrent TMS-fMRI, pulses of TMS are delivered during the acquisition of the blood oxygen level dependent contrast (BOLD) in functional MRI scans in order to visualize TMS-induced activity. In order to use concurrent TMS-fMRI for clinical purposes, we set out to achieve the following goals:

1. Identify the reliability of concurrent TMS-fMRI in the identification of neural networks by stimulation of the motor network and comparing this with voluntary motor activity.
2. Identify the neural circuits activated by stimulation of the left DLPFC and to put these circuits in the perspective of TMS treatment of patients with MDD.
3. Guide the design of patient-specific head models with concurrent TMS-fMRI data.

Chapter 3

Validation of concurrent single pulse TMS-fMRI in the identification of the motor network

Introduction

In chapter 2, we saw that rTMS is an increasingly popular treatment modality for patients with MDD and that more precise targeting of functional regions has a positive effect on treatment outcome[60][59]. We also discussed the complexity of the interaction between the TMS E-field and the neuronal populations in the cortical layer[46][67]. We proposed a personalized brain model that integrates information on the functional topography and brain morphology of the patient to provide a way to guide coil placement. In order to guide the design of such a model, a method to identify network activation in response to single pulses of TMS is required. This can be achieved by concurrent single pulse TMS-fMRI.

During concurrent TMS-fMRI, TMS pulses are delivered to the brain during the acquisition of the blood oxygen level dependent contrast (BOLD) in a functional MRI scan. In this way, the hemodynamic changes in response to TMS pulses can be visualized with a high spatial resolution. This enables us to accurately determine network activity in response to TMS and to relate this to neural circuits described in the literature. Furthermore, this allows us to investigate the effect of different parameters such as the stimulation intensity and coil orientation on TMS-induced network activity. Concurrent TMS-fMRI can increase insight on the interaction of the TMS E-field and the neuronal populations to guide the design of personalized brain models. Finally, it can validate patient-specific brain models that integrate functional and anatomical information.

Concurrent TMS-fMRI is an innovative method applied by only a few research groups, worldwide. Concurrent TMS-fMRI is in the early phase of development and a number of significant technical challenges remain, restricting its widespread use. Because concurrent TMS-fMRI is still in its early phase of development, we aim to identify the reliability of concurrent TMS-fMRI in the identification of neural networks by stimulation of the motor network and comparing this with voluntary motor activity.

Methods

We validated our concurrent TMS-fMRI setup through stimulation of the motor network by stimulating the hand area within the left M1, which allowed us to compare network activation in response to voluntary thumb movements to TMS-induced network activity. The motor network is optimal for validation because it is an extensively investigated network with well-known involvement of several neuroanatomical structures. Furthermore, stimulation of the hand area in the left M1 allows validation of correct coil placement through observation of contralateral thumb movements.

The experimental procedure was approved by the medical ethical committee of the University Medical Center Utrecht (UMCU), Utrecht, The Netherlands. MRI data were acquired in 6 right-handed participants (mean age: 20.8 (19-23 years); 1 male; 5 female; mean RMT: 75.9 (66-83%)). All participants provided written informed consent and were screened for MRI and TMS exclusion criteria. During the experimental procedure, we strictly adhered to the guidelines and recommendations for TMS endorsed by the International Federation for Clinical Neurophysiology[42].

All MR sequences were performed in a 3T MR scanner (Philips Achieva, The Netherlands) and TMS was applied with a Magstim Rapid^2 (Magstim Inc., UK) with an MR-compatible TMS coil

(Magstim Inc., UK) and custom designed TMS filter box (Magstim Inc., UK). The experiment was divided into two parts: an intake session and a TMS session. During the intake, a T1 weighted anatomical scan and a functional scan were obtained. The first was used for neuronavigation during the TMS session, while the latter was used to identify network activation during voluntary thumb movements and the localization of the right thumb area in the anatomical scan. In the TMS session, neuronavigation was used to determine the location and orientation of the TMS coil for stimulation of the right thumb area in the left M1. Thereafter, the participant underwent a combined TMS-fMRI sequence in which single TMS pulses were delivered to the hand area of the left M1. A T2 weighted scan was made to verify coil placement.

Intake session

Thumb movements were recorded during the functional scan with an electromyogram (EMG) of the right anterior pollicis brevis (APB) muscle. The ground electrode was attached to the wrist, the reference electrode was located on the lower arm while the recording electrode was placed over APB muscle. The wireless MR-compatible electrocardiography device (Invivo, The Netherlands) was used to record the EMG. The EMG was sampled at a frequency of 496Hz, insufficient for quantification of MEPs but sufficient to detect muscle contractions.

First, a T1 weighted anatomical scan was acquired with a TR/TE of 10.015/4.61ms, a flip angle of 8°, voxel size of 0.75x0.75x0.8mm, scan duration of 677s, 225 slices with a slice gap of 0mm. The T1 weighted image was then segmented with SPM to obtain a grey matter, white matter and CSF mask.

Thereafter, a single-shot EPI sequence was acquired with 250 dynamics, a TR/TE of 2,000/23ms, flip angle of 70, voxel size of 4x4x4mm, scan duration of 510s, 30 slices with a slice thickness of 3.6mm and a slice gap of 0.4mm. During the EPI sequence, the participant was asked to move the right thumb at random moments during the scan, which were captured in the EMG recording. Custom Matlab code was used to detect the thumb movements in the EMG recordings. The thumb movements were modeled with the canonical hemodynamic response function (HRF) and its first-order derivative in a standard event-related GLM analysis with 2 nuisance regressors: the average BOLD signal in the white matter and the CSF. Statistical images were constructed based on an F-statistic with the F-threshold at $P < 0.05$, family wise error (FWE) corrected[68]. The statistical maps were used to determine the location of the hand area in the left M1.

TMS session

For each participant, the T1 weighted image acquired during the intake session was segmented with SPM12 to obtain skin, skull, cerebrospinal fluid (CSF), white matter and grey matter (GM) masks[68]. The 3D surface renderings of the skin and grey matter masks were visualized in the Neural Navigator (Brain Science Tools, The Netherlands). Subsequently, the location of the hand area in the left M1 was derived from the statistical map acquired during the intake session and marked in the Neural Navigator. Each patient was provided with bathing cap on which the location of the thumb area in the left M1 after was marked after successful neuronavigation. Neuronavigation was performed in the preparation room of the MRI scanner with chin support to minimize head movements during the navigation procedure. Eight facial markers were used to align world space with the MRI coordinates: the upper and lower left and right ear, the left and right inner eye lid, the tip of the nose and the nasion (Fig 3.1).

After successful alignment of the 3D model and the position of the participant's head, the location of the hand area in the left M1 was marked on the bathing cap along with the orientation of the precentral gyrus. This was done so that the coil could be positioned with the direction of the electrical field orientated perpendicular to the precentral gyrus (Fig. 2.3). In this way, the coil orientation was personalized based on brain morphology. Neuronavigation was then used to guide the TMS coil to the motor area of the thumb. The RMT was determined by decreasing the TMS stimulator output until a response in the APB muscle was visible in 5 out of 10 TMS pulses[45].

The participant was then accompanied to the scanner room. The head was positioned in a custom designed setup between 2 circular radio frequency (RF) receive loop coils (Fig 3.2). The receive coils were fixed to 2 plastic side plates with Velcro. The TMS coil was attached to a custom made mount which was positioned over the participant's head. The custom made mount was approved by the UMCU medical technical department and allowed flexible coil position. The TMS coil plane was always positioned perpendicular to the B0 field to minimize Lorentz forces during TMS pulse delivery. The head was tilted backwards and rotated slightly to match the coil position with the markings on the swimming cap. The TMS coil was positioned so that the direction of the electrical field was oriented perpendicular to the orientation of the precentral gyrus. The head and neck of the participant were supported with cushions to increase comfort and to minimize head movement during the scan. The MR bed was then moved into the MR bore. In case of M1 stimulation, once inside the bore, one or two TMS pulses of 115% RMT were delivered to determine correct positioning of the coil.

After successful TMS coil positioning, two sequences were acquired. First, a T2-weighted scan with a TR/TE of 13,609/80ms, flip angle of 90°, voxel size of 2x2x2mm, scan duration of 218s and a slice gap of 0 mm was made. The purpose of this scan was to visualize the coil location and orientation with respect to the head. This was done by attaching 6 fluid markers to the back of the TMS coil which appear hyper intense on a T2 weighted scan. To avoid spatial shift of the markers by the magnetic field distortions around the coil, the water fat shift was minimized. Second, a single-shot EPI sequence was acquired with 500 dynamics, a TR/TE of 2,000/23ms, flip angle of 70°, FOV of 256x119.6x208mm, matrix of 64x63, voxel size of 4x4x4mm, scan duration of 1020s, 30 slices with a slice thickness of 3.6mm and a slice gap of 0.4mm. During the EPI sequence, single pulses of TMS with an intensity of 115% RMT were interleaved with pulses with an intensity of 60% RMT. TMS pulses were delivered with a random interval of 5 to 8 dynamics (10 to 16s) to avoid habituation. Further details are discussed in appendix A.

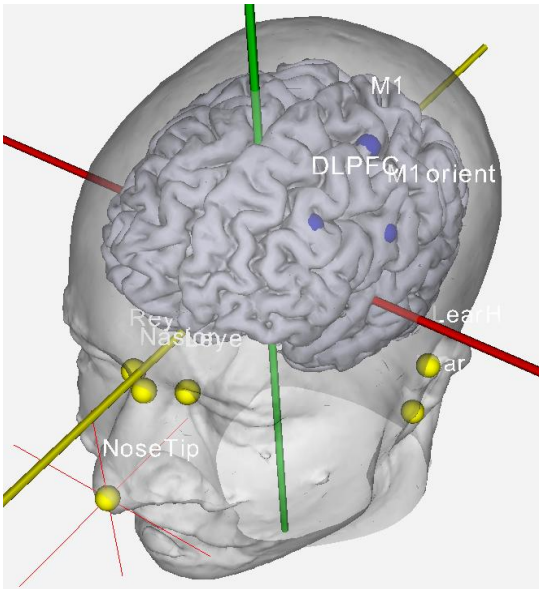

Figure 3.1 *Location of facial markers and TMS targets in the Neural Navigator. Facial markers: tip of the nose; nasion, left and right inner eyelid; left and right upper and lower ear. TMS targets: primary motor cortex (M1); dorsolateral prefrontal cortex (DLPFC).*

Data analysis

Analysis of the structural and fMRI data was performed with custom scripts and SPM12[68] in the Matlab R2014a environment (Mathworks Inc., USA).

The location of the isocenter of the TMS coil was reconstructed with respect to the brain based on the location of the fluid markers on the TMS coil. The TMS coil isocenter is of interest

because it represents the location of the maximum TMS E-field, theoretically. Prior to the experiment, we captured the location of the TMS coil isocenter with respect to the location of the fluid markers on the coil. In order to reconstruct the TMS coil isocenter with respect to the brain, the T2-weighted scan was co-registered to the T1-weighted scan using SPM12, so that the locations of the fluid markers in the T2-weighted scan were the same with respect to the brain as in T1-weighted scan. We then determined the location of the fluid markers in the T2-weighted scan and used the relative location of the TMS coil isocenter to reconstruct the location of isocenter with respect to the brain. Thereafter, the EPI volumes were realigned using SPM12. Next, the mean EPI scan was co-registered to the T1-weighted scan. The inverse of the EPI to T1 affine transformation and the inverse of the EPI realignment affine transformations were used to create a head movement-corrected reconstruction of the location of the TMS coil isocenter. We assumed that the TMS coil was stationary throughout the TMS session, since it was mounted to the setup. Finally, the EPI volumes were normalized and subsequently smoothed with a FWEH of 8mm.

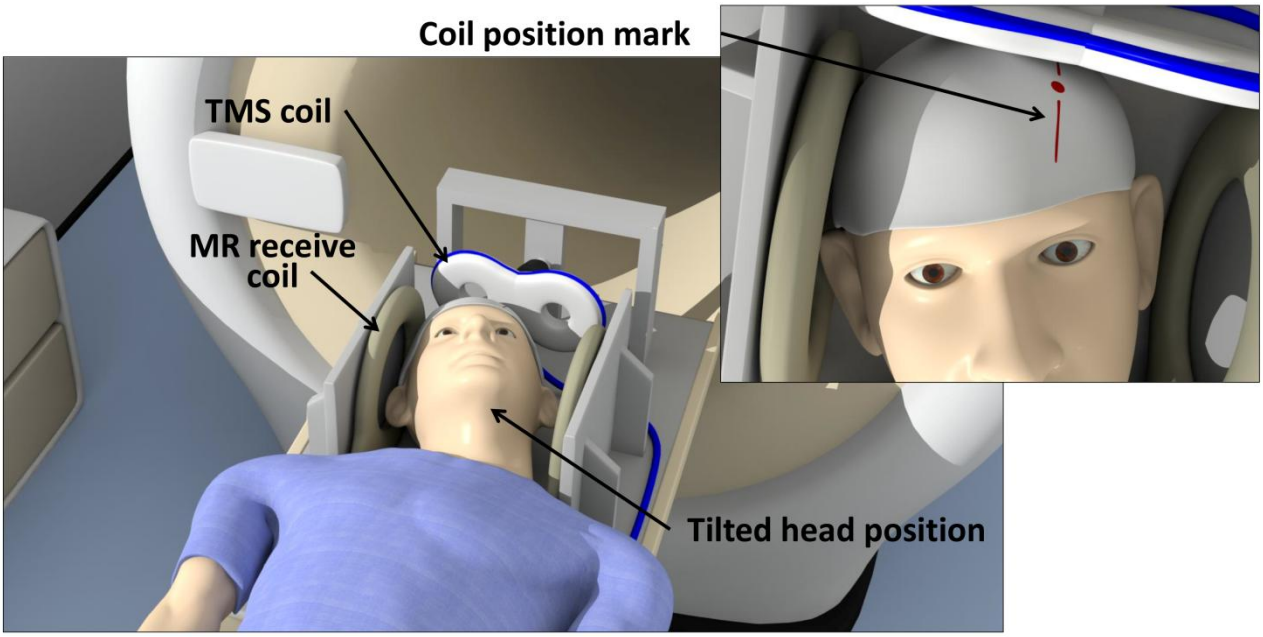

Figure 3.2 *Participant lying on the MR bed with the head positioned in between two MR receive coils and the TMS coil located over the cranium. The coil is oriented perpendicular to the static magnetic field of the MRI scanner to minimize Lorentz forces in the coil. The head is tilted in order to position the coil over the target region.*

The *a priori* analysis consists of a standard event-related GLM analysis in SPM12. The generalized linear model (GLM) includes two events: single pulses of 115% RMT and 60% RMT. The BOLD response is modeled with the canonical hemodynamic response function (HRF) and its first-order derivative. Two nuisance regressors are included in the analysis: the average BOLD signal in the white matter and the CSF. BOLD signals were filtered with a high pass filter of 80Hz before construction of the GLM. Analysis was restricted to the contrast between single TMS pulses of 115% RMT and baseline activity due to the presence of artifacts (Appendix A). The timing of these artifacts is correlated with the timing of TMS pulses of 60% RMT, complicating inference of contrast including TMS pulses of 60% RMT. Statistical images were constructed based on an F-statistic with the F-threshold at $P < 0.05$, family wise error (FWE) corrected[68].

In a *post hoc* analysis, we investigated the average hemodynamic response in the area of stimulation. The stimulation area was obtained by dilating the movement-corrected reconstruction of the TMS coil isocenter with 4 voxels, corresponding to an area with a radius of 1.6cm around the movement-corrected reconstruction of the TMS coil isocenter. The GLM was constructed with the

same regressors as in the *a priori* analysis. However, the HRF was based on a finite impulse response of 5 samples instead of the canonical HRF and its first-order derivative. The hemodynamic responses in all statistically significant voxels were averaged together to obtain an average hemodynamic response in the area of stimulation.

Results

The location of the hand area in the left M1 was successfully determined from the activation maps corresponding to voluntary thumb movements of the right hand in all participants. A summary of the findings and references to the statistical maps in the appendix (Appendix B) can be found in table 3.1. In these maps we generally observed activity in the bilateral SMA, the left putamen and the hand representation in the right cerebellum in response to voluntary movements of the right thumb (Fig. 3.3A). Occasionally, we also observed activity in the contralateral M1, the right putamen and the hand representation in the left cerebellum.

In the following sections, all indications of lateralization of activity are with respect to the hemisphere of stimulation, which is the left hemisphere. TMS was well tolerated by all participants. We investigated the contrast between TMS pulses of 100% RMT and baseline activity of the data acquired in the TMS session. A summary of the findings and references to the statistical maps in the appendix (Appendix C) can be found in table 3.2. Four participants reported TMS-induced contralateral thumb movements during the TMS session, indicated by an asterisk (*). All participants showed auditory activity in the primary auditory cortex (A1), in some cases accompanied by inferior colliculus and thalamic activity (Fig. 3.7).

The statistical map of case #7 shows TMS-induced activity in a number of areas including the bilateral M1, primary somatosensory cortex (S1) and thalamus, the ipsilateral supplementary motor area (SMA), putamen and insula and the contralateral hand area within the cerebellum (Fig. 3.3B). The TMS-induced activity correlates well with brain activity induced by voluntary movements of the right thumb (Fig. 3.3A). The TMS target was located slightly medio-anterior to the thumb area, as shown in the 3D image (Fig 3.5, case #7). The movement-corrected reconstructions of the TMS coil isocenter of all cases with respect to the functional representation of the hand in the left M1 are shown in figure 3.5. The cases in which TMS-induced thumb movement were reported showed TMS-induced activity in at least one of the regions of the motor network (M1, SMA, putamen or cerebellum) (Fig 3.4).

TMS-induced contralateral thumb movements were not reported in cases #10 and #11. These cases did not show TMS-induced activity in areas of the motor network (M1, SMA, putamen or cerebellum). The TMS coil isocenter was located within the thumb area during acquisition of the concurrent TMS-fMRI scan, also when corrected for head movements during the scan (Fig. 3.5, case #11).

Hemodynamic response in the stimulation area

The stimulation area was defined as an area with a radius of 1.6cm (4 voxels) around the movement-corrected TMS coil isocenter, resulting in a volume ranging from 1,064 to 1,724 mm^3 (266 to 431 voxels), depending on the extent of head movement during the TMS session. The amount of voxels that was significantly activated within the area of stimulation ranged from 9 to 29 voxels. The average hemodynamic responses in the stimulation area are shown in figure 3.6. In two cases (cases #8 and #11), no significantly activated voxels were present in the area of stimulation. The maximum amplitude of the hemodynamic response in the stimulation area of case #10 is lower than to the other cases.

Table 3.1 *Summary of findings on brain activity in motor regions in response to voluntary thumb movements of the right hand contrasted with baseline activity (P < 0.05, FWE corrected). Indications of lateralization refer to the left or right hemisphere. M1: primary motor cortex; SMA: supplementary motor area; Thal: thalamus; Put: putamen; Cer: hand representation in the cerebellum; Appx: Appendix.*

#	M1	SMA	Thal	Put	Cer	Appx
1	left	bi	bi	bi	right	B.1
2	left	bi	-	left	right	B.2
3	left	bi	-	-	right	B.3
4	bi	bi	bi	bi	bi	B.4
5	left	left	-	-	right	B.5
6	bi	bi	bi	bi	right	B.6

Table 3.2 *Summary of findings on TMS-induced activity in commonly activated regions for TMS pulses of 115% RMT delivered to the hand area of the left M1 contrasted with baseline activity (P < 0.05, FWE corrected). Indications of lateralization are with respect to the hemisphere of stimulation (left). An asterisk (*) indicates a session in which the participant reported TMS-induced contralateral thumb movements. M1: primary motor cortex; SMA: supplementary motor area; Thal: thalamus; Put: putamen; Cer: hand representation in the cerebellum; S1: primary somatosensory cortex; A1: primary auditory cortex; Ins: insula; Appx: Appendix.*

#	M1	SMA	Thal	Put	Cer	S1	A1	Ins	Appx
7*	bi	ipsi	bi	ipsi	contra	bi	ipsi	Ipsi	C.1
8*	ipsi	ipsi	-	-	-	-	contra	-	C.2
9*	ipsi	-	-	-	-	ipsi	ipsi	-	C.3
10	-	-	-	-	-	-	bi	bi	C.4
11	-	-	-	-	-	contra	contra	-	C.5
12*	ipsi	ipsi	-	ipsi	-	bi	bi	ipsi	C.6

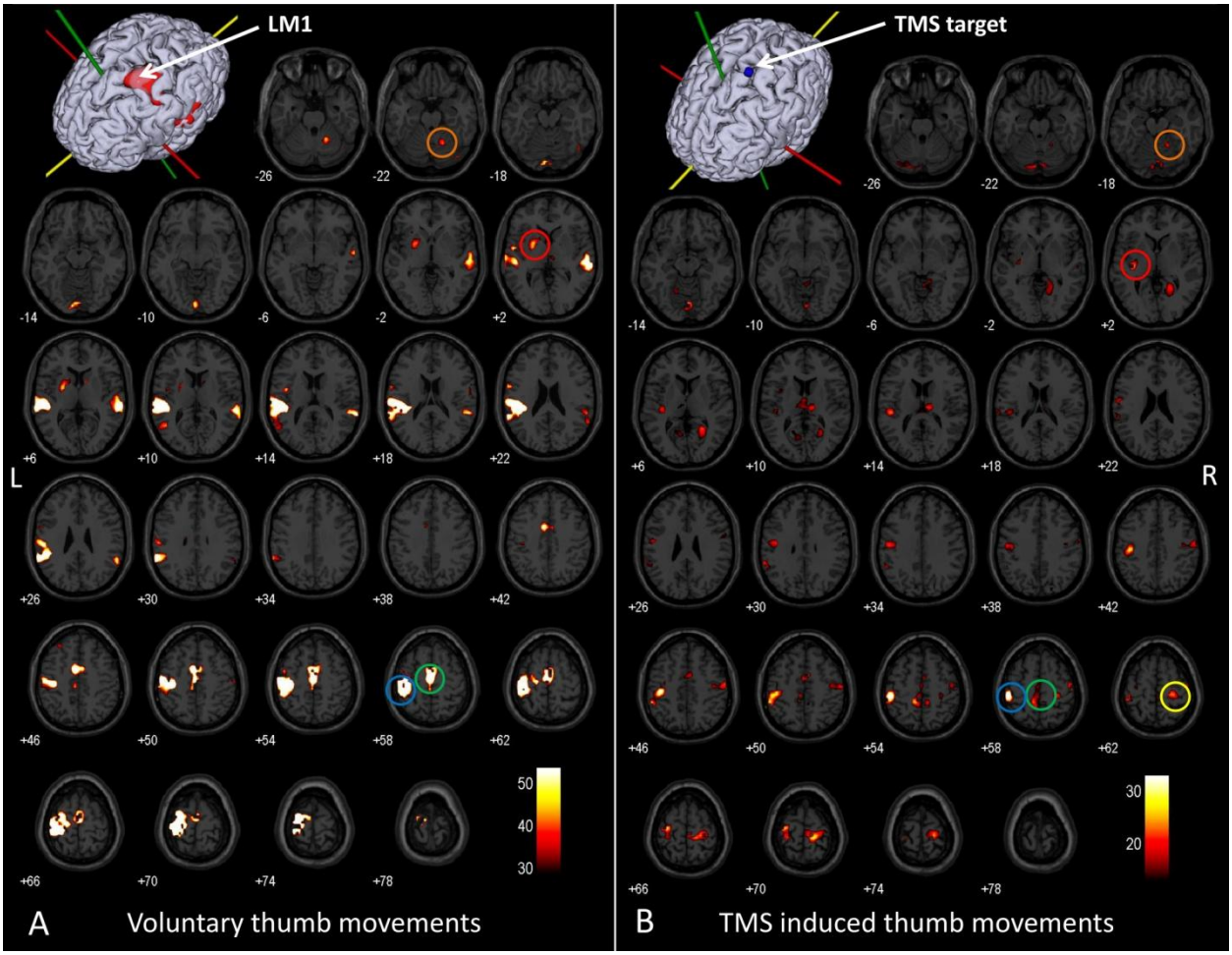

Figure 3.3A *Statistical map of voluntary thumb movements contrasted with baseline activity (P << 0.05, FWE corrected). The upper left figure shows the brain surface in 3D with the location of the hand area.* ***Figure 3.3B*** *Statistical map of TMS pulses of 115% RMT delivered to the hand area of the left M1 contrasted with baseline activity of a participant who reported thumb movements in response to TMS (P < 0.05, FWE corrected). The upper left figure shows the brain surface in 3D with the location of the TMS target. Both statistical maps show activation in the primary auditory cortex (A1). The activated regions of the motor network are encircled in color. Green: supplementary motor area (SMA); Blue: left primary motor cortex (M1); Yellow: Contralateral M1; Red: putamen; Orange: hand area in the cerebellum.*

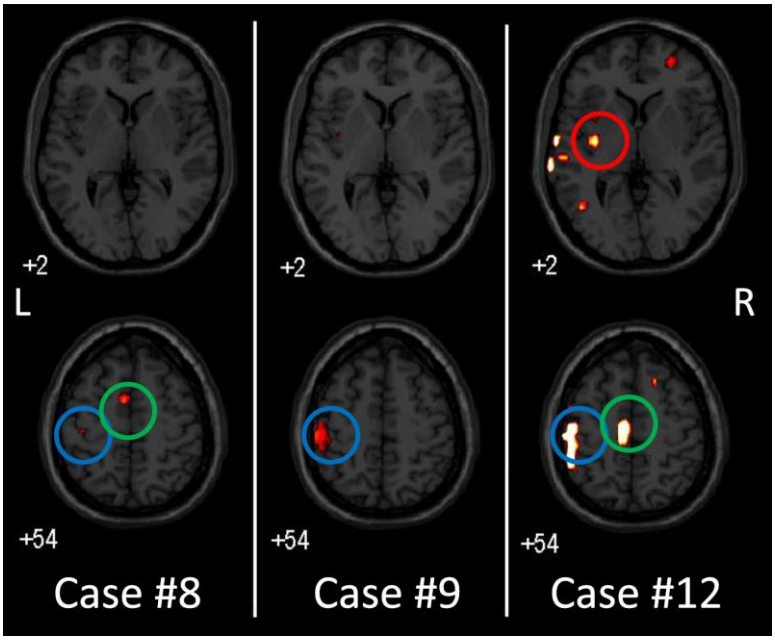

Figure 3.4 *Statistical maps of TMS pulses of 115% RMT delivered to the hard area within the left M1 contrasted with baseline activity of three participants who reported thumb movements in response to TMS (P < 0.05, FWE corrected). Motor network regions are encircled in color. Green: supplementary motor area (SMA); Blue: left primary motor cortex (M1); Red: putamen.*

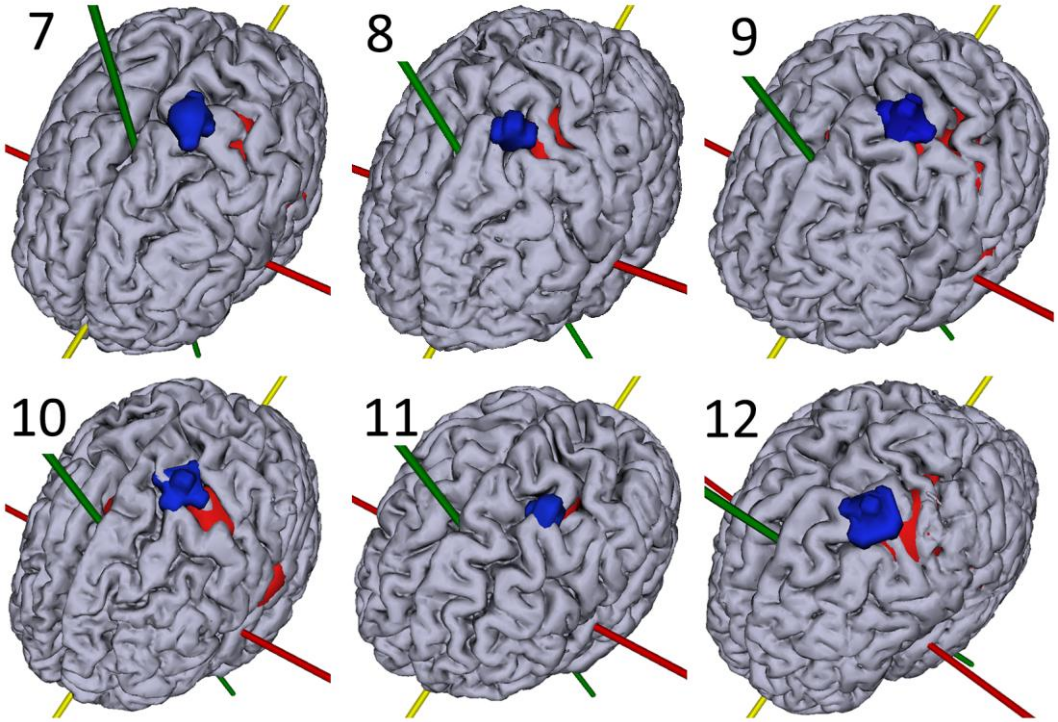

Figure 3.5 *3D brain surfaces with statistical maps of voluntary thumb movements of the right hand shown in red. The statistical maps show activity primarily in the left M1, but in some cases also in A1, S1 and the SMA. The movement-corrected reconstruction of the TMS coil isocenter is shown in blue. The number correspond to the cases in Table 3.2. M1: primary motor cortex; A1: primary auditory cortex; S1: primary somatosensory cortex; SMA: supplementary motor area.*

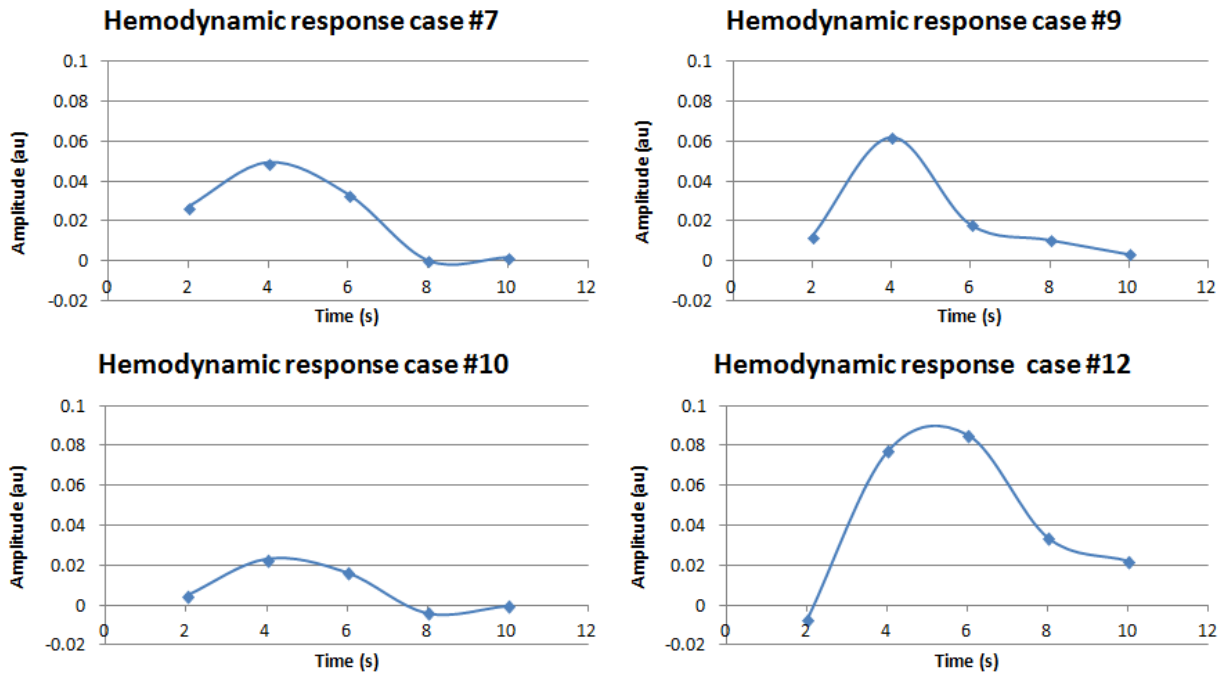

Figure 3.6 *Average hemodynamic responses in the TMS target area. The TMS pulse is delivered at time 0 and the amplitude is in arbitrary units. The case numbers refer to Table 3.2.*

Discussion

We proposed concurrent TMS-fMRI as a method to identify the networks that are activated in response to single pulses of TMS. In order to validate this method we applied single TMS pulses to the hand area within the left M1 during an fMRI recording and compared patterns of TMS-induced activity to voluntarily induced motor activity. First, we discuss TMS-induced motor activity and relate our observations to literature findings on motor networks. In subsequent sections, we discuss confounders, the absence of TMS-induced thumb movements and the effect of the MRI static magnetic field on the TMS E-field.

Motor network

Stimulation of the hand area in the left M1 induced TMS-induced network activity in a number of regions including the M1, SMA, putamen, cerebellum and the thalamus. The M1, SMA, putamen, hand area in the cerebellum and the thalamus are part of the motor network.

The SMA is associated with the initiation of movement and shown to be strongly connected to M1[69]. We also observed TMS-induced activity in the putamen, specifically in the posterior limb. In humans, the hand area in M1 projects specifically to the posterior limb of the putamen, confirming our findings[70]. We also saw TMS-induced activity in the hand area of the contralateral (with respect to the stimulation site) cerebellum. The left M1 projects to the contralateral cerebellum[71], which is in concert with our findings. Additionally, the cerebellar activity in response to voluntary thumb movements shows activity in the exact same location. Finally, we observed that TMS induces activity in the contralateral M1. We did not always observe activity in the right M1 in response to voluntary movement. The initiation of movement by the left M1 inhibits activity of the contralateral homologue, potentially inducing a negative hemodynamic response[72]. However, in our experiments, this does not induce a significant hemodynamic response except in case #12. This is similar for voluntarily-induced activity, in which we were able to capture a hemodynamic response in the contralateral M1 in a single case (case #7). This is presumably caused by insufficient statistical power.

Confounders

In addition to TMS-induced activity in regions of the motor network, we observed activity in the S1, A1 and the insula.

The activity in the A1 is related to auditory stimulation that accompanies the application of TMS (Fig. 3.7), while TMS-induced activity in S1 is related to the somatosensory stimulation that occurs when the TMS coil vibrates during pulse delivery[73]. Besides somatosensory and auditory activity, it is possible that TMS pulses of 115% RMT evoked a pain response in the brain depending on the experience of the stimulus. Pain stimuli mainly evoke brain activity in the S1 and the insula[74]. The intensity of the stimulus correlates with the strength of the activity in S1 regardless of experience of pain, while insula activity is unique to painful stimuli. Finally, painful stimuli can evoke DLPFC activity in case of conscious processing of the stimulus. We cannot reliably state that the observed insula activity is induced by the TMS E-field. However, in the absence of S1 activity, it is unlikely that neural correlates of a pain response or conscious processing of TMS stimuli are present in the data.

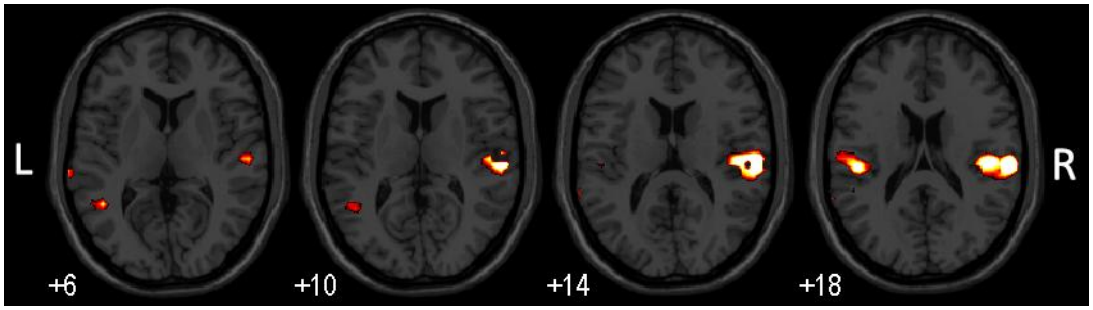

Figure 3.7 *Statistical map of TMS pulses of 115% RMT delivered to the hand area in the left M1 contrasted with baseline activity (P < 0.05, FWE corrected). Auditory activity (predominantly in the right hemisphere) induced by the clicks of the TMS coil during TMS pulse delivery. M1: primary motor cortex.*

Absence of TMS-induced thumb movements

TMS-induced thumb movements were not reported in 2 cases. For one of these cases (case #10) the amplitude of the average hemodynamic response in the area of stimulation was limited, compared to the other cases. Interestingly, the TMS coil isocenter was located slightly medial of the functional area of the hand in the left M1, similar to the cases in which TMS-induced thumb movements were reported. For the other case (case #11), the TMS coil isocenter was well positioned within the functional area of the hand, throughout the scan session (Fig 3.5, case #11). Surprisingly, we failed to detect TMS-induced activity in the motor network and TMS-induced thumb movements in both cases (cases #10 and #11) and we did not detect significantly activated voxels in the stimulation area in one case (case #11). A possibility of the absence of TMS-induced thumb movements is that the TMS E-field did not interact with the neuronal populations within the functional area of the hand, due to the local morphological complexity.

As stated previously, Kammer et al. showed that a current direction perpendicular to the orientation of the gyrus induced stronger effects compared to a parallel current direction[67]. In our experiments, the coil was oriented perpendicular to orientation of the precentral gyrus to maximize the TMS-induced effect. However, the complex morphology of the precentral gyrus and the location of the hand area within the gyrus can complicate adequate coil orientations. In one of the aforementioned cases (case #11), the thumb area was located within a section of the precentral gyrus that was oriented parallel to the TMS E-field, which is known to reduce TMS efficacy (Fig. 3.5). Whether the functional representation of the hand area within the complex morphology of the gyrus impaired the TMS-induced effect in these two cases is highly speculative, but provides a potential explanation for the absence of TMS-induced thumb movements. These findings illustrate the complexity of adequate TMS coil placement in the stimulation of a small region of a complex

morphological gyrus. In future experiments, the direction of the TMS E-field with respect to the surface of the functional area should be taken into account during coil placement, rather than the general orientation of the precentral gyrus.

MR static magnetic field interactions

In all cases in which we observed TMS-induced thumb movements and activation of the motor network, the TMS coil isocenter was located slightly medio-anterior to the hand area in the left M1 (Fig 3.5, cases #7, 8, 9 and 12). Therefore, one could argue that the isocenter of the coil does not reflect the true location of the maximum TMS E-field due to the effect of the static magnetic field (B0) of the MRI scanner on the TMS magnetic field. However, Yau et al. investigated the effects of the B0 field on the TMS magnetic field for different positions and orientations of the TMS coil within the MR bore[75]. They found that changes in coil orientation did not result in substantial TMS field variations, as long as the coil was located within the MR bore. In our experiments, the TMS coil was located well within the MR bore, limiting TMS field variations due to the MRI B0 field.

Furthermore, Fox et al. showed that TMS predominantly induces activity in the area around the sulci, rather than the area on the outer surface of the gyri[47]. Consequently, the TMS effect is stronger if the maximum E-field is induced in the sulcus, rather than in the gyrus. This could explain why we observe TMS-induced thumb movements in cases in which the TMS coil isocenter is located in the sulcus but do not observe thumb movements when the TMS coil isocenter is located in the middle of the gyrus (case #10).

Limitations and recommendations

Concurrent TMS-fMRI remains a challenging technique, which requires further improvement of the design before it can be applied more widely. A number of technical pitfalls in the application of concurrent TMS-fMRI are discussed in appendix A. In the following sections we discuss methodological limitations of our experiments and recommendations for future research. First, we discuss variability in TMS-induced activity between participants. In the following section, we propose the use of a designated EMG device to measure TMS-induced MEPs. Finally, we debate the use of a sham condition in future applications of concurrent TMS-fMRI.

Reproducibility

TMS-induced activity shows strong variability between participants, which can be explained by differences in brain morphology, functional brain topography and biochemistry, complicating group-level inference. Sources of variability in TMS-induced activity are not restricted to differences between individuals but extend to dynamic properties of brain activity[76]. The dynamic nature of brain activity also reflects in functional connectivity measurements, which exhibit changes in response to task demand[77] and learning[78], but also resting state functional connectivity varies between sessions of the same participant[79]. Thus, both conscious and subconscious neural processing of information affect network connectivity in a dynamic fashion. The dynamics of functional connectivity presumably cause variation in propagation patterns of TMS-induced activity. In case of TMS, the somatosensory and auditory components of stimulation can induce conscious processing of somatosensory, auditory and attentional information, potentially affecting propagation patterns.

The pre-existing state of neuronal populations targeted with TMS also influence the reproducibility of TMS effects. Sauseng et al. used EEG recordings to demonstrate that local oscillatory activity preceding the TMS pulse significantly affected the amplitude of the MEP. More specifically, they found a positive correlation between pre-stimulus alpha band power and MEP amplitude. Romei et al. also demonstrated that TMS effects depend on pre-existing neuronal oscillatory activity in the visual cortex[80]. Consequently, the underlying pre-existing state of the cortical neuronal populations determines local cortical excitability, regulating TMS effects.

In order to accurately investigate the reproducibility of TMS-induced activity, precise coil placement and limited head movement are required. Our results show that the TMS coil can be placed accurately and that head movement can be limited during concurrent TMS-fMRI, enabling the investigation of reproducibility of TMS-induced activity.

Assessment of motor activity

Successful application of single pulse TMS to the hand area can be verified objectively through a recording of the MEP and subjectively through a questionnaire. In addition to subjective assessment of motor activity by participants, we attempted to detect MEPs in response to TMS-induced activity with the MR-compatible ECG device, while aware of the limitations of such a device. During the intake session, voluntary thumb movements were easily detected in the EMG recordings of the same device. Unfortunately, we were not able to reliably detect TMS-induced MEPs in the EMG recordings, due to the small amplitude of the MEPs, the MR noise and the limited sampling frequency. Ideally, MEPs are recorded with a MR-compatible EMG device with sufficient sampling frequency to quantify the MEP morphology. Unfortunately, such an MR-compatible device was not available. Future applications of concurrent TMS-fMRI should include online monitoring of EMG activity with a designated EMG device in order to correlate TMS-induced MEPs with TMS-induced brain activity.

Sham condition

We saw that TMS also induces confounding brain activity through somatosensory and auditory stimulation. We analyzed the contrast of single TMS pulses of 115% RMT versus baseline activity, while aware of the limitations of this kind of contrast. Ideally, a sham TMS condition is included to filter out the somatosensory and auditory activity. Sham TMS conditions strongly reduce evoked activity in the brain while maintaining a similar auditory and somatosensory response[73][81]. Unfortunately, an event-related design with interleaved events does not allow the application of conventional sham conditions (in which the coil is rotated with respect to the head). To the best of our knowledge, a contrast between TMS pulses of 115% RMT and 60% RMT was the best sham condition in this specific situation. Unfortunately, TMS pulses of 60% RMT were temporally correlated with an artifact (appendix A). Therefore, we decided to contrast TMS pulses of 115% RMT with baseline activity. Because the neural correlates of auditory and somatosensory evoked activity are well known, inference remains reliable in the absence of a sham condition.

In future applications of concurrent TMS-fMRI, a sham condition should be included to increase the reliability of inference. A possibility is the use of an active sham coil[82]. Unfortunately, the production of Lorentz forces poses a technical challenge for the use of such a TMS coil within a static magnetic field of 3T. A more feasible alternative is the use of an offline sham condition, in which the session is reproduced while the coil is rotated with respect to the head, but the somatosensory response is maintained.

Conclusion

We proposed concurrent single pulse TMS-fMRI as a way to detect TMS-induced network activity. We showed that single pulses of TMS can be delivered precisely and safely during an fMRI recording, while accurately monitoring TMS coil placement. We found that TMS-induced motor network activity resembles voluntarily induced motor network activation. However, successful application of concurrent TMS-fMRI remains challenging. We identified several technical pitfalls in the application of this method, which require further improvements of the design in order to guarantee reliability. We recommended research on the reproducibility of TMS-induced effects, the integration of MR-compatible EMG recordings and the application of a sham condition. Once the technical challenges are overcome, the application of concurrent TMS-fMRI will further increase the understanding of the effects of TMS on the human brain. Eventually, this insight will guide the application of TMS in MDD in order to improve treatment outcome.

Chapter 4

Visualizing neural circuits with concurrent TMS-fMRI of the left DLPFC

Introduction

In chapter 1, we saw that MDD is associated with a specific neural network of dysfunctional regions and that normalization of the abnormal activity in these regions correlates with a response to treatment. In chapter 2, we introduced rTMS as a method to modulate the activity in one of these dysfunctional regions, the left DLPFC, to induce an antidepressant effect. Repetitive TMS is an increasingly popular treatment modality for patients with MDD, but little is known about network activity in response to stimulation of the left DLPFC.

We proposed concurrent TMS-fMRI as a method to visualize activation of neural networks in response to TMS in order to increase insight on how TMS interacts with neural circuits. Concurrent TMS-fMRI can visualize network activity in response to TMS pulses delivered to the left DLPFC to shed some light on the mechanism of action of rTMS treatment in MDD. Importantly, the amount of people who benefit from rTMS treatment is limited[53]. We stressed the importance of the targeting of functional regions rather than anatomical regions and the need for more understanding of how the TMS E-field interacts with neuronal populations in the cortical layer. Concurrent TMS-fMRI can increase understanding of these interactions in order to improve rTMS treatment.

In chapter 3, we showed that TMS-induced network activity can be successfully identified with concurrent TMS-fMRI. Next, we aim to visualize neural network activation in response to TMS of the left DLPFC and to put our findings in the perspective of rTMS treatment of MDD.

Methods

MRI data was acquired in 8 right-handed participants (mean age: 20.9 (18-23 years); 2 male; 6 female; mean RMT: 76.6 (58-83%)). The experimental procedure is similar to the one described in chapter 3. Deviations from the experimental procedure are described in the following sections.

TMS session

Neuronavigation was used to determine the coil position and orientation for stimulation of the left DLPFC (Fig 3.1). The location of the left DLPFC was defined anatomically as the area within the middle frontal gyrus, located 1 to 2 cm anterior of the premotor gyrus, representing parts of BA46 and BA9[83]. After successful neuronavigation, the position and orientation of the middle frontal gyrus were marked on a swimming cap. Once the participant was comfortably positioned on the MRI bed, the TMS coil was positioned over the left DLPFC with the orientation of the electrical field perpendicular to the orientation of the middle frontal gyrus.

In the first TMS session, fMRI recordings were obtained in 5 participants in which single pulses of TMS were delivered with an intensity of 100% RMT. In an additional session, fMRI recordings were acquired in 7 participants in which single pulses of TMS with an intensity of 115% RMT were interleaved with pulses with an intensity of 60% RMT. A functional MRI scan was always preceded by the acquisition of a T2-weighted scan, in which the coil position was determined with regard to the head.

Data analysis

The data acquired in the first TMS session, were analyzed based on a contrast of TMS pulses with 100% RMT versus baseline activity. From the data acquired in the second TMS session, one

dataset was excluded due to severe movement artifacts. The six remaining datasets were studied based on a contrast of TMS pulses of 115% RMT versus baseline activity.

Results

TMS was tolerated by all participants. In both TMS sessions, all participants showed activity in the primary auditory cortex (A1), in some cases accompanied by inferior colliculus and thalamic activity. All indications of lateralization of activity are with respect to the hemisphere of stimulation, which is the left hemisphere.

The data acquired in the first TMS session was contrasted with TMS pulses of 100% RMT versus baseline activity. A summary of the findings and references to the statistical maps in the appendix (Appendix C) can be found in table 4.1. The movement-corrected reconstructions of the TMS coil isocenter of the other cases were located in the dorsal end of the left DLPFC (Fig 4.1)[83][83][83][83][83]. The statistical map of case #1 shows TMS-induced activity in the frontal eye fields (FEF), middle temporal visual area (V5) and the supplementary eye fields (SEF) within the SMA (Fig. 4.2). These regions are part of an established network[84] and TMS-induced activity in these regions is observed in a number of other cases.

The data acquired in the second TMS session was used to investigate the contrast between TMS pulses of 115% RMT and baseline activity. A summary of the findings and references to the statistical maps in the appendix (Appendix D) can be found in table 4.2. In two cases, the TMS coil isocenter was not located within the left DLPFC, indicated by an asterisk (*). One dataset contains severe movement artifacts, indicated by red shading. The movement-corrected reconstructions of the TMS coil isocenter of the other cases were located on the posterior end of the left DLPFC similar to the first session (Fig 4.3). All participants show activity in the primary and secondary visual cortices (V1-2) of at least one hemisphere and three participants show TMS-induced activity in the ipsilateral cerebellum (Fig. 4.5B). The statistical map of case #12 (Table 4.2) shows TMS-induced activity in several regions including the ipsilateral DLPFC, FEF, V5 and ventral prefrontal cortex (vPFC), the contralateral cingulate cortex and parietal cortex and the bilateral SMA, thalamus, M1, S1 and V1-2 (Fig 4.4).

Finally, the contrast between TMS pulses of 115% RMT versus pulses of 60% RMT of the data acquired in the second TMS session was investigated. A summary of the findings and references to the statistical maps in the appendix (Appendix E) can be found in table 4.3. The datasets are the same as the ones described in the previous section. Cases in which the TMS coil isocenter was not located within the left DLPFC are indicated by an asterisk (*) and the dataset with severe movement artifacts is indicated by red shading. The movement-corrected reconstructions of the TMS coil isocenter are the same as in the previous section (Fig. 4.3). All participants show TMS-induced activity in the ipsilateral ventral PFC. The activity in this region is likely artifactual, more details can be found in appendix A. The statistical map of case #12 (Table 4.3) shows TMS-induced activity in the ipsilateral vPFC, DLPFC, FEF, SMA, sgACC and S1. A saggital slice illustrates TMS-induced activity in the ipsilateral vPFC and the sgACC (Fig. 4.6).

Hemodynamic response in the stimulation area

The stimulation area was defined as the area within a radius of 1.6cm (4 voxels) around the movement-corrected TMS coil isocenter, resulting in a volume ranging from 1,108 to 1,920 mm^3 (277 to 480 voxels), depending on the extent of head movement during the TMS session. The stimulation area showed significantly activated voxels in 3 out of 7 cases. The amount of voxels that was significantly activated within the area of stimulation ranged from 2 to 7 voxels. The average hemodynamic responses in the stimulation area of these cases are shown in figure 4.7.

Table 4.1 *Summary of findings on TMS-induced activity in commonly activated regions for TMS pulses of 100% RMT delivered to the left DLPFC contrasted with baseline activity (P < 0.05, FWE corrected). Indications of lateralization are with respect to the hemisphere of stimulation (left). An asterisk (*) indicates session in which the TMS coil isocenter was not located within the left DLPFC. DLPFC: dorsolateral prefrontal cortex; FEF: frontal eye fields; V5: middle temporal visual area; SMA: supplementary motor area; Thal: thalamus; V1-2: primary and secondary visual cortex; CC: cingulate cortex; S1: primary somatosensory cortex; PPC: posterior parietal cortex; Ins: insula; Appx: Appendix.*

#	DLPFC	FEF	V5	SMA	Thal	V1-2	CC	S1	PPC	Ins	Appx
1	-	bi	ispi	-	-	contra	-	-	-	-	D.1
2	-	-	ipsi	Contra	ipsi	-	-	-	-	contra	D.2
3	-	-	-	-	bi	ipsi	contra	contra	ipsi	-	D.3
4	-	-	-	-	bi	bi	-	bi	contra	ipsi	D.4
5	-	-	-	-	contra	-	-	-	-	-	D.5

Table 4.2 *Summary of findings on TMS-induced activity in commonly activated regions for TMS pulses of 115% RMT delivered to the left DLPFC contrasted with baseline activity (P < 0.05, FWE corrected). Indications of lateralization are with respect to the hemisphere of stimulation (left). An asterisk (*) indicates a session in which the TMS coil isocenter was not located within the left DLPFC. Results in red are based on data with movement artifacts. DLPFC: dorsolateral prefrontal cortex; FEF: frontal eye fields; V5: middle temporal visual area; SMA: supplementary motor area; Thal: thalamus; V1-2: primary and secondary visual cortex; CC: cingulate cortex; S1: primary somatosensory cortex; PPC: posterior parietal cortex; vPFC: ventral PFC; Appx: Appendix.*

#	DLPFC	FEF	V5	SMA	M1	V1-2	CC	S1	PPC	vPFC	Appx
6	contra	contra	bi	contra	contra	bi	contra	contra	bi	-	E.1
7*	contra	-	-	-	-	bi	contra	-	ipsi	-	E.2
8	ipsi	bi	-	bi	bi	bi	-	contra	bi	bi	E.3
9	-	contra	-	-	-	contra	-	-	ipsi	ipsi	E.4
10	-	-	ipsi	-	-	bi	ipsi	-	-	ipsi	E.5
11*	-	-	-	-	-	-	-	-	ipsi	-	E.6
12	ipsi	ipsi	-	bi	bi	bi	contra	bi	contra	ipsi	E.7

Table 4.3 *Summary of findings on TMS-induced activity in commonly activated regions for TMS pulses of 115% RMT delivered to the left DLPFC contrasted with TMS pulses of 60% RMT (P < 0.05, FWE corrected). Indications of lateralization are with respect to the hemisphere of stimulation (left). An asterisk (*) indicates a session in which the TMS coil isocenter was not located within the left DLPFC. Results in red are based on data with movement artifacts. DLPFC: dorsolateral prefrontal cortex; FEF: frontal eye fields; V5: middle temporal visual area; SMA: supplementary motor area; sgCC: subgenual anterior cingulate cortex; OFC: orbitofrontal cortex; S1: primary somatosensory cortex; PPC: posterior parietal cortex; vPFC: ventral prefrontal cortex; Appx: Appendix.*

#	DLPFC	FEF	V5	SMA	sgACC	OFC	S1	PPC	vPFC	Appx
6	-	-	-	-	-	-	-	-	ipsi	F.1
7*	bi	-	-	-	-	-	-	ipsi	ipsi	F.2
8	-	ipsi	-	ipsi	ipsi	bi	ipsi	contra	bi	F.3
9	ipsi	-	-	-	-	ipsi	ipsi	bi	ipsi	F.4
10	-	-	-	-	-	-	-	-	ipsi	F.5
11*	-	-	ipsi	-	-	-	-	-	ipsi	F.6
12	ipsi	ipsi	-	ipsi	ipsi	-	ipsi	-	ipsi	F.7

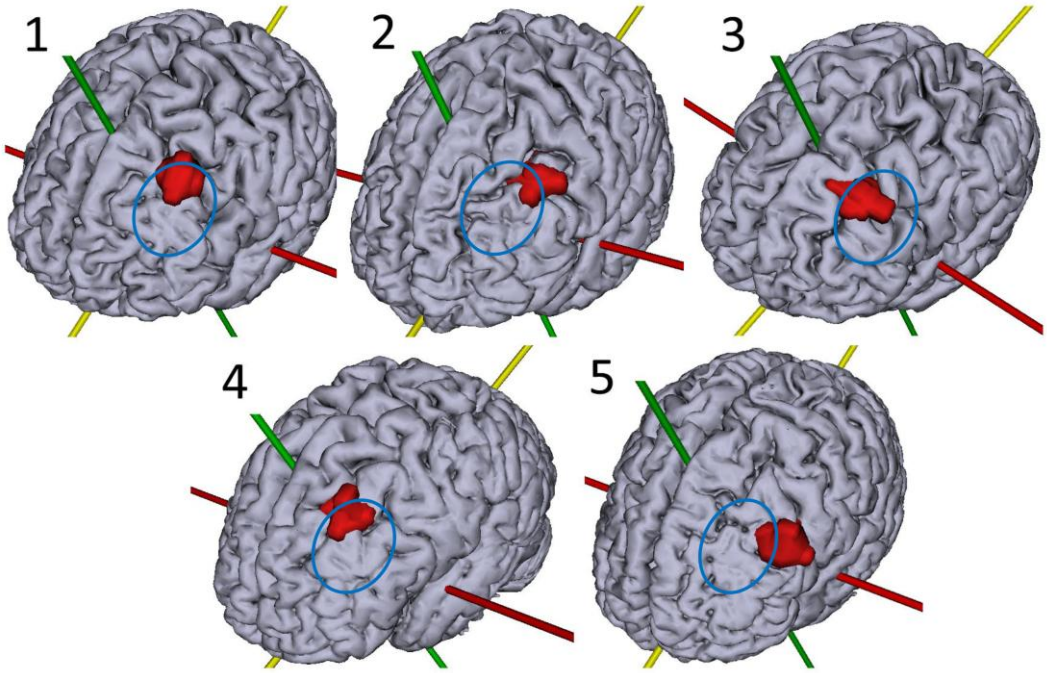

Figure 4.1 *A movement-corrected reconstruction of the isocenter projected on the corresponding cortical surface of each participant is shown in red for the first TMS session. The numbers correspond to the case numbers in Table 4.1. The DLPFC is encircled in blue. DLPFC: Dorsolateral prefrontal cortex.*

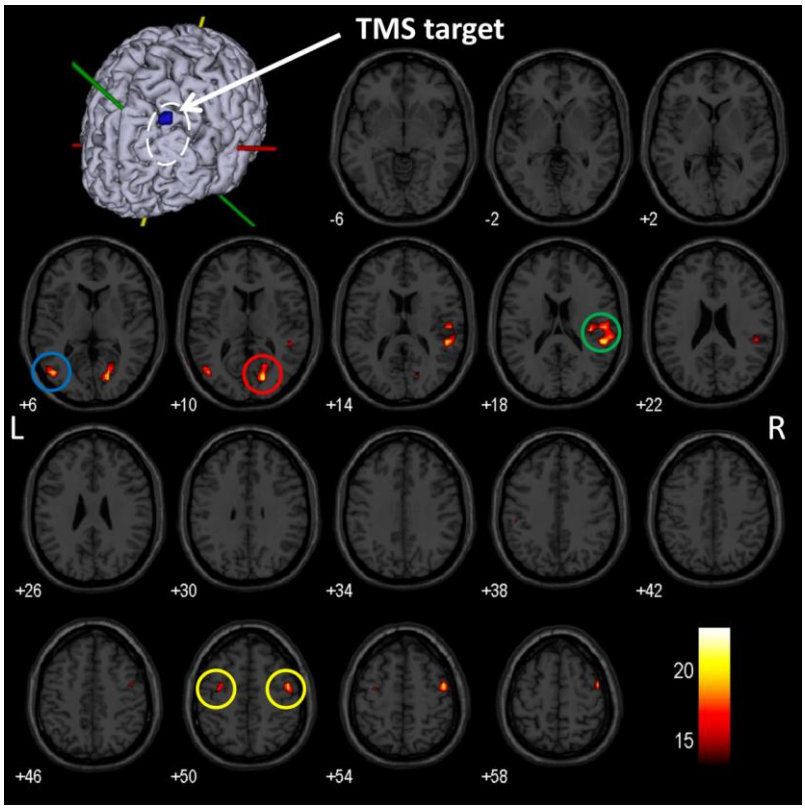

Figure 4.2 *Statistical map of TMS pulses of 100% RMT delivered to the left DLPFC contrasted with baseline activity (P < 0.05, FWE corrected). The 3D brain surface in the upper left corner shows the TMS target within the encircled left DLPFC. Activated regions are encircled in color. Yellow: Frontal eye fields (FEF); Blue: left middle temporal visual area (V5); Red: right visual association area; Green: Auditory cortex (A1). RMT: Resting motor threshold; DLPFC: Dorsolateral prefrontal cortex.*

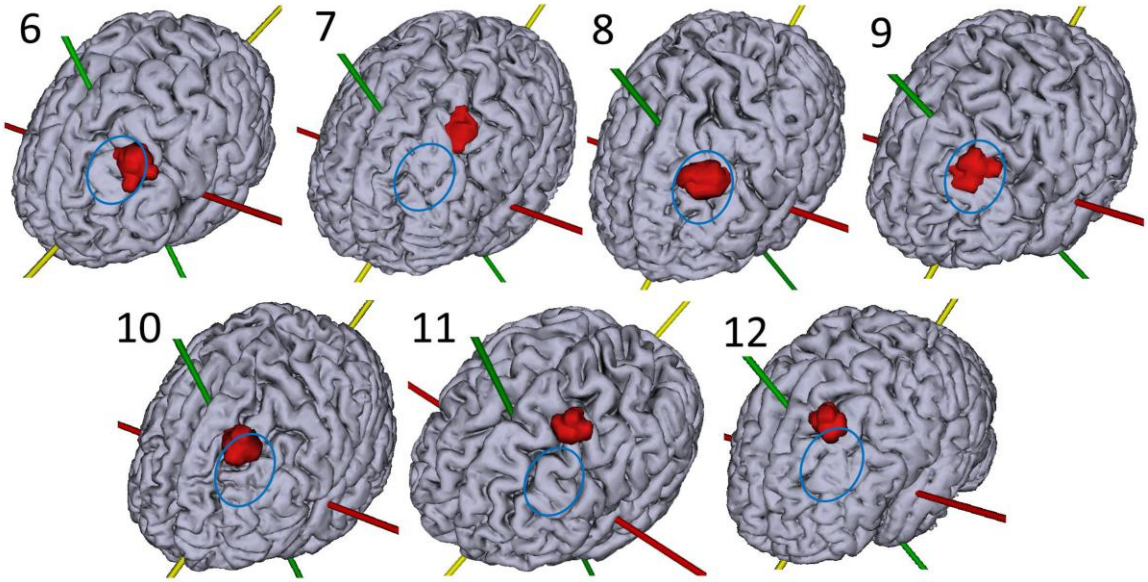

Figure 4.3 *A movement-corrected reconstruction of the isocenter projected on the corresponding brain surface of each participant is shown in red for the second TMS session. The numbers correspond to the case numbers in Table 4.2. The DLPFC is encircled in blue. DLPFC: dorsolateral prefrontal cortex.*

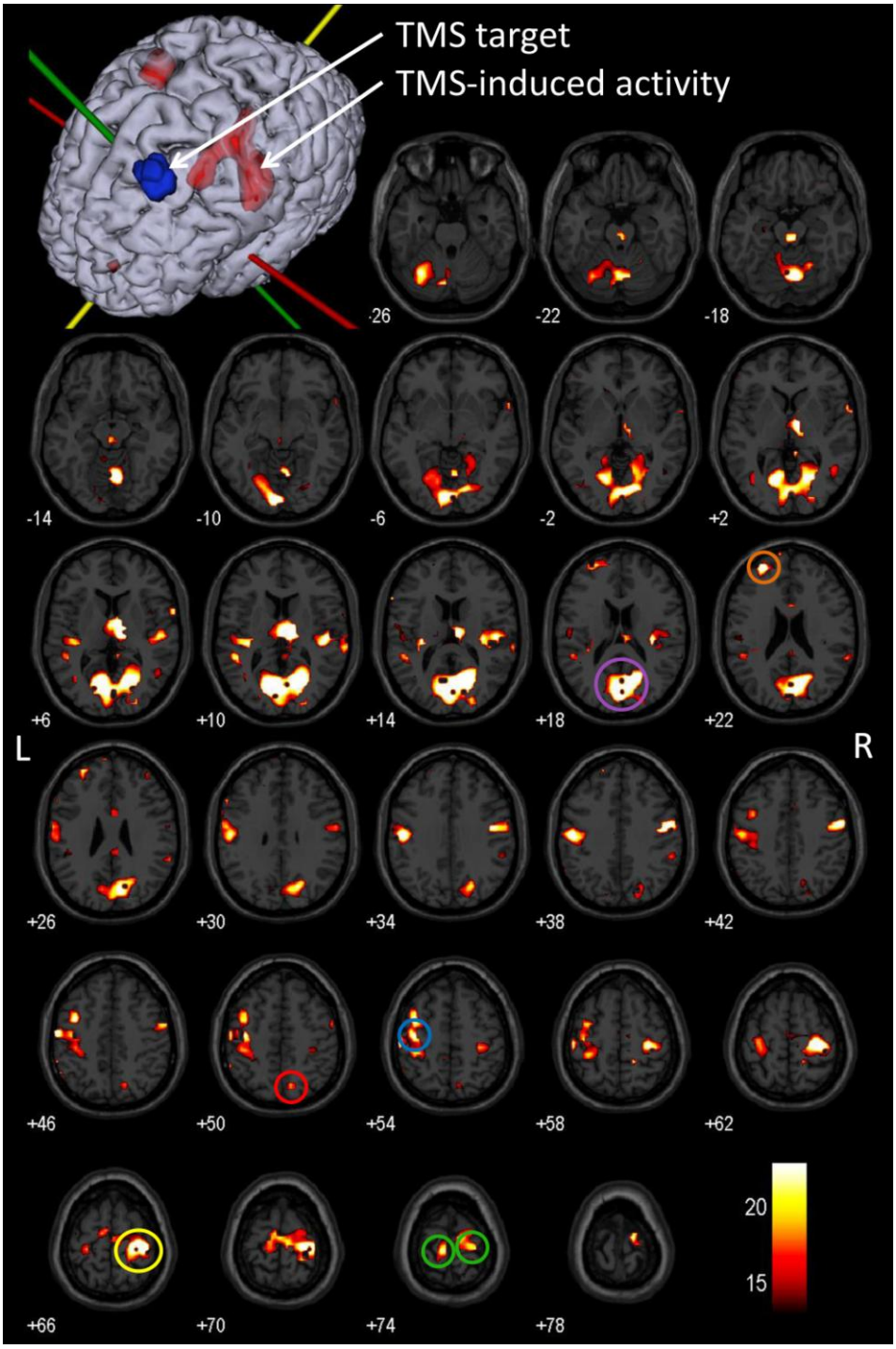

Figure 4.4 *Statistical map of TMS pulses of 115% RMT delivered to the left DLPFC contrasted with baseline activity (P < 0.05, FWE corrected). Activated regions are encircled in color. Yellow: primary somatosensory cortex (S1); Blue: frontal eye fields (FEF); Red: posterior parietal cortex (PPC); Green: primary motor cortex (M1); Purple: visual cortex (V1-2); Orange: ventral prefrontal cortex; RMT: resting motor threshold; DLPFC: dorsolateral prefrontal cortex.*

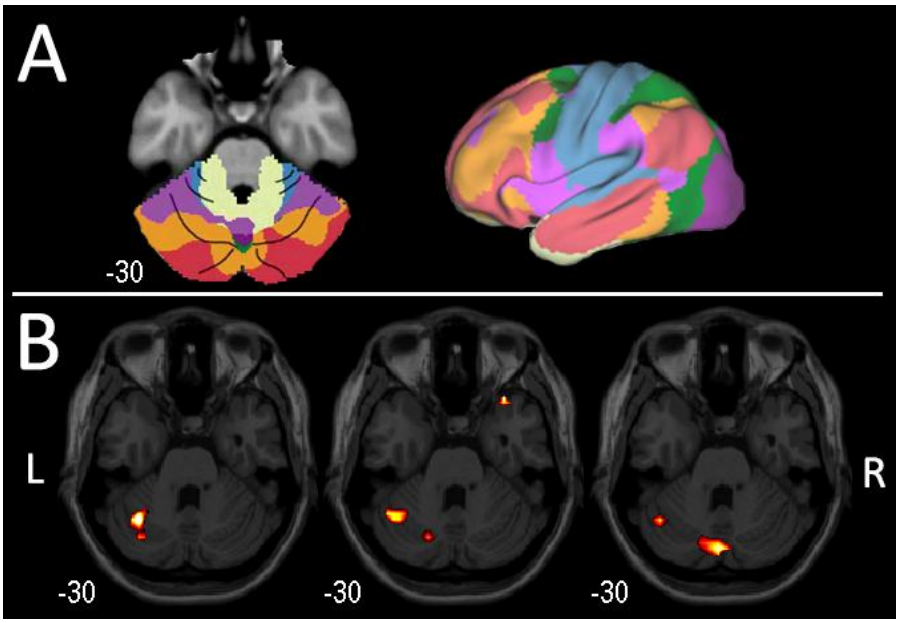

Figure 4.5A *Parcellation of the cerebellum and cerebrum based on fMRI resting state functional connectivity*[85]*. The color coding indicates regions that are functionally connected in both the cerebellum and the cerebrum. The left figure shows an axial slice of the cerebellum in MNI space.* ***Figure 4.5B*** *Statistical maps of TMS pulses of 115% RMT delivered to the left DLPFC contrasted with baseline activity for 3 different participants. The axial slices are in MNI space and correspond to axial slice of the cerebellum in figure 4.2A.*

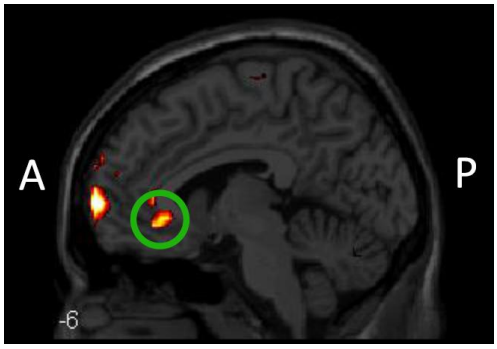

Figure 4.6 *Statistical map of TMS pulses of 115% RMT delivered to the left DLPFC contrasted with TMS pulses of 60% RMT (Sagittal view)(P < 0.05, FWE corrected). TMS-induced activity in the ipsilateral subgenual cingulate cortex (sgACC) is encircled in green.*

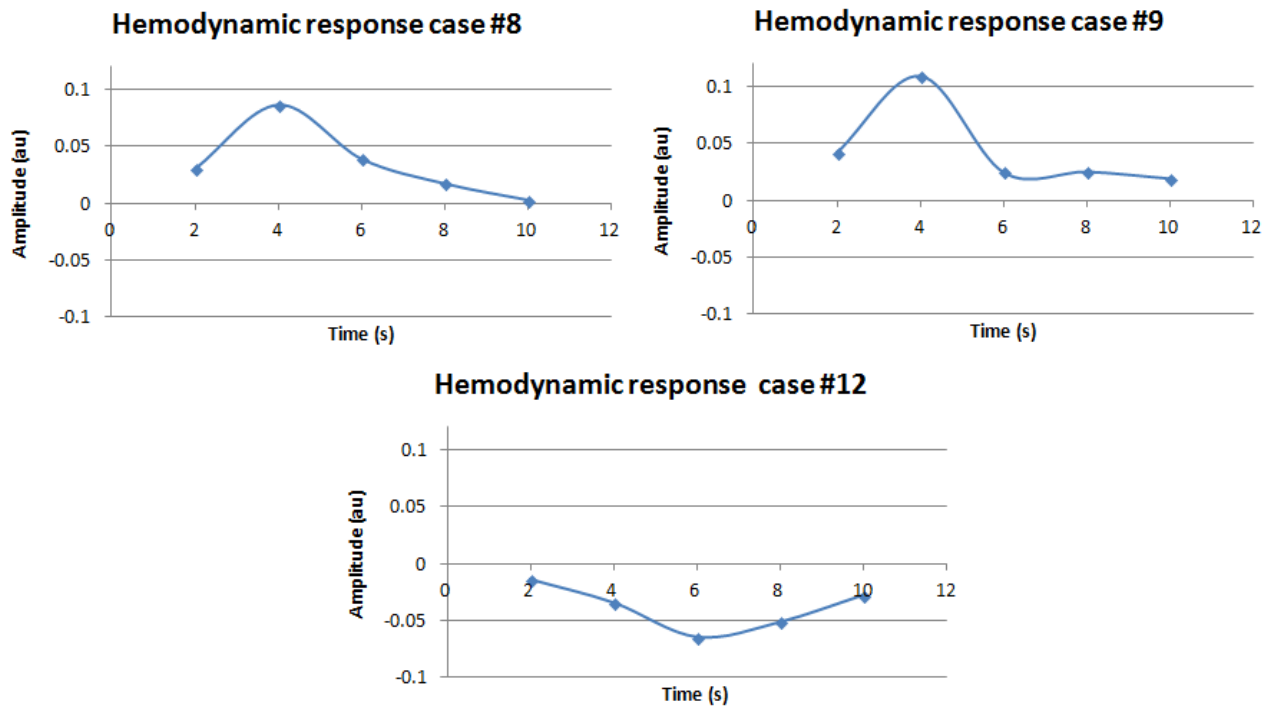

Figure 4.7 *Average hemodynamic responses in the TMS target area. The TMS pulse is delivered at time 0 and the amplitude is in arbitrary units. The case numbers refer to Table 4.2.*

Discussion

To be best of our knowledge, this is the first attempt to visualize network activity in response to single pulse TMS of the left DLPFC during an fMRI recording, in which the coil position is accurately controlled throughout the scan session. First, we elaborate on our findings in a comparison with literature findings. Finally, we discuss our findings on the hemodynamic response in the area of stimulation.

TMS-induced activity

TMS pulses of 115% RMT delivered to the left DLPFC predominantly induce brain activity in the DLPFC, FEF, V1-2, PPC, CC and the dorsal part of the cerebellum. TMS-induced activity is occasionally observed in M1, V5, and the SMA (Table 4.2). The contrast between TMS pulses of 115% RMT and 60% RMT revealed TMS-induced activity in the sgACC in addition to aforementioned activity (Table 4.3).

The FEF and V5 are associated with saccadic eye movement control in both macaques and humans[84] and have been shown to be anatomically connected in macaques[86]. Hutchison et al. investigated resting state functional connectivity of the FEF in a whole brain fMRI recording in both macaques and humans[84]. They observed strong functional connectivity with the DLPFC, SMA (especially the SEF), the PPC, V5, aspects of the CC and V1-2, which is in support of our findings. Yeo et al. created a functional parcellation of the human cerebrum based on resting state functional connectivity data, also indicating strong connectivity between the DLPFC, FEF, PPC, aspects of the CC and V5[58]. Olesen et al. provide further evidence in support of these findings[87]. Moreover, fMRI resting state functional connectivity has been shown to correlate well with diffusion tensor imaging (DTI) connectivity, indicating that functional connectivity can be translated to anatomically connected regions[88]. Our results show that propagation of the TMS-evoked potential is generally restricted to these functionally connected regions spatially, providing evidence for the validity of concurrent TMS-fMRI.

TMS-induced activity in the cerebellum is predominantly present in the left posterior lobe and is relatively consistent among participants. Buckner et al. included the cerebellum in the

functional parcellation of the human cerebrum by Yeo et al.[85]. Interestingly, they observed that the DLPFC was functionally connected to a specific region within the posterior lobe of the cerebellum in which we consistently observe TMS-induced activity. The motor areas in the cerebrum project to the contralateral cerebellum, while we observe activity in the ipsilateral cerebellum. However, it is possible that other cerebral areas, such as the DLPFC, project to the ipsilateral cerebellum. Another possibility is that TMS-induced activity propagates through the contralateral cerebral back to the ipsilateral cerebellum.

The contrast between TMS pulses of 115% RMT versus 60% RMT revealed activity in the vicinity of the coil (ventral PFC), which is presumably caused by TMS-induced field distortions which correlate with TMS pulse delivery (Appendix A). Interestingly, TMS-induced activity was observed in the sgACC in two cases (case #8 and #12), which is unlikely to be related to TMS-induced field distortions due to the distance from the coil. However, caution should be used in the interpretation of activation maps of case #8, due to the presence of movement artifacts. Neuromodulation of the sgACC is shown to be effective in the treatment of MDD[17][19] and the strength of the functional connection between the DLPFC and the sgACC is correlated with treatment outcome of rTMS treatment of the left DLPFC[60]. These findings indicate that rTMS of the left DLPFC has a neuromodulatory effect on the sgACC, providing a potential explanation for its antidepressant effect. However, it is not clear whether this functional connection is facilitated by a structural connection. Our findings show that TMS of the left DLPFC induces activity that propagates to the sgACC, providing further evidence for a functional connection between the DLPFC and the sgACC. However, we cannot definitively eliminate an artifactual origin of sgACC activity. Therefore, further research is required to investigate TMS-induced activity in the sgACC.

Local hemodynamic response

Although we observed TMS-induced activity in regions which are connected to the TMS target, we failed to detect activity directly within the area of stimulation in a substantial number of cases. In cases in which we were able to capture a hemodynamic response, the response was limited.

The electrical activity of TMS-evoked potentials is generally observed in the stimulation area in TMS-EEG recordings even in case of very small TMS E-fields[73][89]. Although, EEG recordings show the cumulative electrical activity of a much larger region than fMRI, one would expect to detect a hemodynamic response in the area of stimulation in fMRI recordings. The TMS E-field excites cortical neurons with sufficient magnitude to induce observable evoked electrical activity in EEG, but does not result in a detectable hemodynamic response. A possible explanation is that the hemodynamic response is induced by an increased energy demand, which is predominantly driven by synaptic activity rather than spiking activity[90]. We therefore argue that in some cases, the TMS E-field bypasses synaptic transmission, reducing the hemodynamic response. In these cases, the TMS E-field presumably polarizes the descending white matter tracts, inducing an evoked potential that travels along the white matter tracts to arrive at a distant synapse. Subsequently, the synaptic activity induces a hemodynamic response which can be detected in the BOLD signal.

However, Fox et al. did observe changes in cerebral blood flow in the vicinity of the TMS coil isocenter using TMS-PET[47] and others have observed TMS-induced activity in the stimulation area in concurrent TMS-fMRI[91]. Another possibility is that the response of neuronal populations in the area of stimulation is not consistent enough to be detected by fMRI analyses. These inconsistencies lower the temporal correlation of the BOLD response in the voxel with the TMS events, resulting in lower statistical power. These inconsistencies can result from changes in local excitability due previous TMS pulses and head movement during scanning. In contrast, distant TMS-induced activity always propagates through the same white matter tracts and is therefore more consistent. Thus, the correlation with the TMS events is stronger, resulting in higher statistical power.

Limitations and recommendations

We discuss the methodological limitations of the experimental procedure in the following section. The technical limitations are discussed in appendix A. First, we discuss the variability of TMS-induced activity and propose a way to control for inter-participant variability. Finally, we debate the current golden standard in determining TMS intensity.

Variability of TMS-induced network activity

We observed substantial variability in TMS-induced activity between participants. One of the sources of variability of TMS-induced activity is the diversity in TMS targets. In cases #7 and #11, the TMS coil isocenter was not located in the DLPFC, but in the premotor cortex. The network connectivity of the DLPFC and the premotor cortex are significantly different. Therefore, the TMS-induced network activity is different. However, TMS-induced activity also shows substantial variability between cases in which the TMS coil isocenter was located precisely within the neuroanatomical borders of the DLPFC during the entire session (cases #6, #9 and #10). Thus, the variability of TMS-induced network activity is also present in sessions with limited head movement and well-controlled coil placement, which is a major limitation of concurrent TMS-fMRI.

The DLPFC is an anatomical region enclosed by anatomical landmarks such as the superior and inferior frontal sulcus. However, the DLPFC consists of multiple different functional regions, which are not necessarily enclosed by anatomical landmarks. BA9 and BA46 are different functional regions located within the DLPFC. However, BA9 has different white matter projections than BA46. Thus, TMS pulses delivered to BA9 follow different propagation patterns than TMS pulses that are delivered to BA46. Unfortunately, these functional regions show strong inter-participant variability, especially in the prefrontal cortex[58][57]. In order to control for variability in functional regions between participants, a personalized map of functional regions is required to guide TMS pulse delivery.

Resting state MRI functional connectivity can be used to create a parcellation of functionally connected regions, which has been shown to relate well to underlying structural connectivity[92][93]. Fox et al. demonstrated the relevance of these functional regions for rTMS of the DLPFC, specifically. They showed that stimulation of regions with a stronger functional connection to sgACC produced better treatment outcome compared regions with weak connectivity[60]. Furthermore, resting state functional connectivity can be used to directly correlate TMS-induced activity with functionally connected regions. In this way, it is possible to control for the differences in network connectivity between participants. Vink et al. applied such an approach in EEG recordings and showed that the propagation of TMS-induced activity correlated with some measures of EEG resting state functional connectivity[94]. However, it is debatable whether their observations translate directly to resting state functional connectivity in fMRI.

TMS intensity

We used a standardized procedure for RMT assessment to determine a personalized TMS intensity for each participant. The RMT is currently the golden standard in TMS applications[42]. However, the RMT is based on the cortical excitability of the primary motor cortex, rather than the cortical excitability of the left DLPFC. It is well established that the cortical excitability of a specific brain region depends on the pre-existing oscillatory activity of this region[51][52][80]. It is highly unlikely that the oscillatory activity in M1 resembles the rhythmic activity in the left DLPFC, rendering a similar cortical excitability of both regions unlikely.

Conclusion

We set out to visualize network activity in response to TMS of the left DLPFC with concurrent TMS-fMRI. We saw that stimulation of the left DLPFC induces network activity in a number of brain regions that are part of a network commonly associated with regulation of saccadic eye movements. Interestingly, we observed activity in the sgACC, providing evidence for a functional connection

between the DLPFC and the sgACC, potentially facilitating neuromodulatory effects of rTMS treatment of the DLPFC. However, the observed network activity is strongly variable between participants. The strong variability of TMS-induced activity presumably arises from the complex morphology and functional topography of the human brain. Furthermore, the way in which the TMS E-field interacts with the complex brain morphology and the dynamic nature of functional network connectivity further increase variability of TMS-induced network activity.

Conclusion

Major depressive disorder is a highly complex disorder that severely affects mood and pleasure in day to day activities. It is an intractable disorder that is accompanied by a complex network of dysfunctional regions. Repetitive TMS modulates the activity in one of these dysfunctional regions, the left DLPFC, to induce an antidepressant effect. However, the number of patients who benefit from rTMS treatment is limited. In order to improve TMS treatment, more understanding of the complex interaction of the TMS E-field and the neuronal populations in the cortical layer is required. Additionally, network activation in response to stimulation of the left DLPFC can provide more insight into the mechanism of action of rTMS treatment in MDD. We proposed concurrent TMS-fMRI as a method to visualize the effects of TMS.

We set out to investigate the reliability of concurrent TMS-fMRI in the identification of neural networks by stimulating the motor network and comparing TMS-induced network activity with voluntarily induced motor network activation. We demonstrated that single pulses of TMS can be delivered safely and accurately during an fMRI recording in order to visualize TMS-induced brain activity and that voluntarily induced activation of the motor network correlates well with TMS-induced motor activity. Further investigation of TMS-induced motor activity can benefit from the integration of EMG recordings in order to correlate MEPs to TMS-induced brain activity. We attempted a creative approach to detect MEPs during concurrent TMS-fMRI and concluded that a designated MR-compatible EMG device is required in order to compare both measures qualitatively.

The application of concurrent TMS-fMRI remains challenging and further improvements have to be made in order to use it reliably. One of these improvements is of technical nature. We saw that the flow of current through the TMS coil during image acquisition is detrimental for image quality and the reliability of inference. A concurrent TMS-fMRI setup should include a robust relay that completely blocks the flow of current during image acquisition and accurate timing of both TMS pulse delivery and TMS machine output adjustment. Furthermore, proper grounding of the TMS coil to the Faraday cage is essential for decent image quality.

We also investigated network activity in response to TMS of the left DLPFC and attempted to put our observations in the perspective of rTMS treatment of MDD. We saw that stimulation of the left DLPFC induces network activity in a number of brain regions that are part of a network commonly associated with regulation of saccadic eye movements. Interestingly, we also observed TMS-induced activity in the sgACC. This provides evidence for a functional connection between the DLPFC and the sgACC, potentially facilitating neuromodulatory effects of rTMS treatment of the DLPFC. However, we also saw substantial variability in TMS-induced activity between participants. This is a major challenge for concurrent TMS-fMRI research. Variability arises from the intractable interaction between the TMS E-field and the complex morphology of the underlying cortical surface. We know that the orientation and location of the TMS E-field with respect to the functional area in the cortical layer determines TMS efficacy to a large extent. The representation of functional regions within anatomical landmarks is another contributor to inconsistencies in TMS-induced activity. Therefore, targeting of functional regions rather than structural regions can increase the consistency of TMS-induced network activity. Sources of variability in TMS-induced network activity are not restricted to differences between participants due to the dynamic nature of functional network connectivity. Additionally, the oscillatory activity of target neuronal populations and the biochemistry of the brain at the time of stimulation significantly affect the effects of TMS. Therefore, the reproducibility of network activity in response to TMS should be investigated in future applications of concurrent TMS-fMRI.

Finally, we proposed to guide the design of patient-specific head models with concurrent TMS-fMRI data. Unfortunately, the design of personalized head models faces some major challenges. One of these challenges is the acquisition of volumetric meshes of different tissue types from a structural scan, which are required for the simulation of the TMS E-field in the brain.

In conclusion, concurrent TMS-fMRI can offer valuable information on the effects of TMS on neural networks. However, both methodological and technical developments are required before it can be used to improve rTMS treatment of MDD through guiding of the design of personalized head models.

Appendix A

Technical aspects of concurrent TMS-fMRI

A setup for concurrent TMS-fMRI

Concurrent TMS-fMRI attempts to record the hemodynamic response of the brain to TMS. This is achieved by the delivery of TMS pulses to the brain of the participant during the acquisition of a functional MRI scan (Fig. 3.2). The TMS device is located in the control room and is connected to the TMS coil inside the scanner room. The TMS coil, consisting of two circular windings of copper wire, is located over the patients head inside the MR bore. During image acquisition, following Faraday's law of induction, eddy currents are induced in the windings of copper wire. To avoid the flow of eddy currents, a relay is included in the circuit, which is grounded to the Faraday cage. A simplified schematic of the setup is shown in figure A.1. The TMS coil is positioned perpendicular to direction of the B0 field to minimize the production of Lorentz forces during TMS pulse delivery. The fixed orientation of the TMS coil requires flexible positioning of the participant's head in order to stimulate different brain regions.

As discussed previously, TMS uses electromagnetic induction to induce an electrical field inside the brain. The magnetic field induced by the TMS coil causes temporary inhomogeneities in the B0 field of the MRI scanner. Delivery of a TMS pulse during the application of the RF pulse or during MR readout causes distorted images (Fig. A.2). Fig. A.2A shows a reference image without TMS pulse delivery. Fig. A.2B and Fig. A.2C show the effect of TMS pulse delivery during the 180 refocusing pulse and during MR readout of a spin echo sequence on the image. Consequently, it is of importance to deliver the TMS pulse outside the window of image acquisition (refocusing pulse and readout). Therefore, a period of 300ms is included after the acquisition phase, in which the TMS pulse is delivered (Fig. A.3).

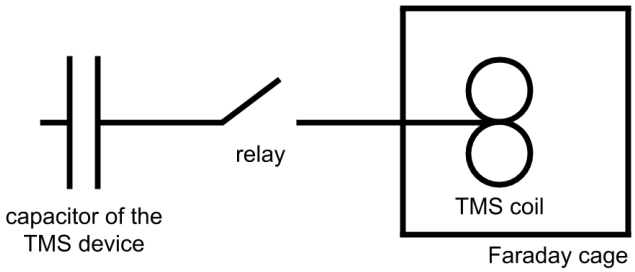

Figure A.2 *Simplified schematic overview of the electrical circuit.*

Noise

As mentioned in the previous section, the connection between the TMS device and the TMS coil contains a relay, which is grounded to the Faraday cage to avoid RF leakage (Fig. A.3). The relay is located inside the MR control room, with the connection to the TMS coil leading through the Faraday cage into the MR room. The grounding of the TMS coil to the Faraday cage is extremely important in maintaining the homogeneity of the MRI B0 field and guaranteeing image quality (Fig A.4B). If the TMS coil is not correctly grounded to the Faraday cage, the cable leading to the TMS device serves as an antenna that picks up radiofrequency noise in the control room and transports it to the MR bore, disturbing the homogeneity of the MRI B0 field and introducing noise into the images (Fig A.4A).

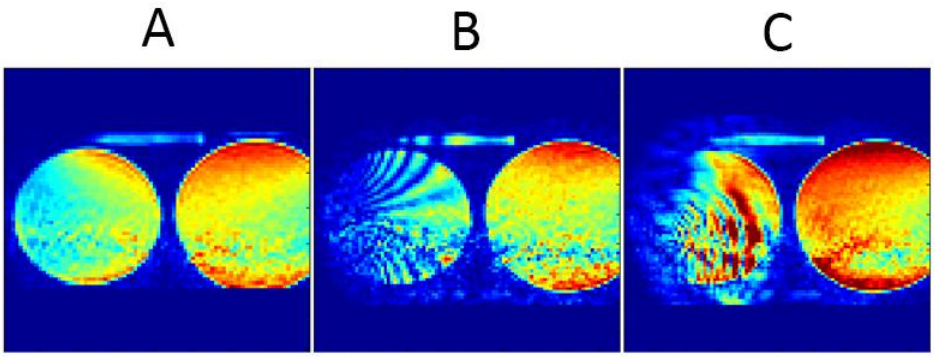

Figure A.2A *A reference image without TMS pulse delivery. The gradient in the circular phantom is caused by the sensitivity of the MR receive coils.* ***Figure A.2B*** *The effect of TMS pulse delivery during the 180 refocusing pulse.* ***Figure A.2C*** *The effect of TMS pulse delivery during MR readout.*

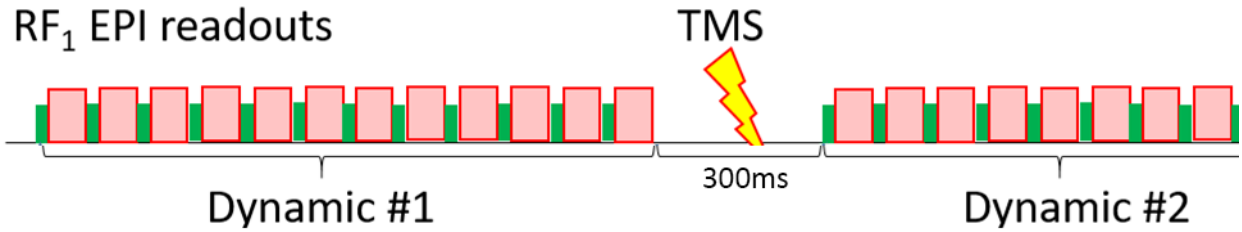

Figure A.3 *TMS pulses are delivered in the 300ms window in between EPI readouts.*

TMS-related artifacts

As discussed previously, the application of TMS during an EPI sequence requires accurate timing in order to avoid TMS-induced artifacts in the EPI volumes. Therefore, TMS is applied during the 300ms after image acquisition. During experiments in which a constant RMT percentage is delivered, the EPI volumes are completely clean of artifacts. However, during experiments in which the RMT percentage is interleaved between 60% RMT and 115% RMT, severe distortions can be observed in some of the reconstructed images (Fig. A.5A). The volumes with these artifacts can be identified in the mean BOLD signal in the vicinity of the TMS coil, as strong deflections from the baseline, with a width of a single dynamic.

As stated previously, the intensity of the TMS pulse is interleaved manually between 60% RMT and 115% RMT in between TMS pulse delivery. The intensity of the TMS pulse is changed, i.e. the TMS machine output is changed, by modifying the load on the internal capacitor of the TMS device. This causes small current leakage to the TMS coil due to polarization effects inside the relay. It is important to note that the exact mechanism by which small currents are induced in the TMS coil is not completely clear. The leakage of current causes small perturbations in the magnetic field near the TMS coil. These local magnetic field distortions cause artifacts during acquisition of slices in the vicinity of the coil. These artifacts can also be seen as deflections in the BOLD signal in the voxels affected by the magnetic field perturbations.

As stated previously, the artifacts are visible in individual slices, which are acquired during the adjustment of the TMS machine output. To detect the distorted slices, the average BOLD signal in the grey matter was calculated for each slice, resulting in 30 average BOLD signals of 500 samples. A distorted slice could be identified as a positive or negative peak in the BOLD signal, depending on the exact nature of the distortion. The distorted slices were corrected through temporal interpolation (Fig. A.5B). Unfortunately, subtle distortions were also present in the data. These subtle deflections were consistently seen in the window after delivery of TMS pulses of 60% RMT, when the TMS machine output is manually increased to 115% RMT (Fig. A.6). The consistent nature of these subtle artifacts complicates the inference of the contrasts including TMS pulses of 60% RMT. For example, a huge cluster of activity can be observed in the vicinity of the coil for contrasts including TMS pulses

of 60% RMT, while this cluster is completely absent in the 115% RMT versus baseline contrast (Fig. A.7).

To better assess this origin of these artifacts, we performed a few experiments on a phantom, in which periods with a varying TMS machine output, were interleaved with periods with a constant TMS machine output. We only observed the artifacts in periods in which the TMS machine output varied. This confirms our hypothesis that current leaks from the TMS machine to the TMS coil. Based on these observations, we believe that to avoid these artifacts, the TMS machine output intensity should be changed outside the MR-acquisition window, i.e. in the 300ms interval after the EPI train and before the MRI RF excitation pulse of the subsequent dynamic. Unfortunately, this goes beyond human precision and therefore should be performed automatically. This should be included in future applications of concurrent TMS-fMRI experiments.

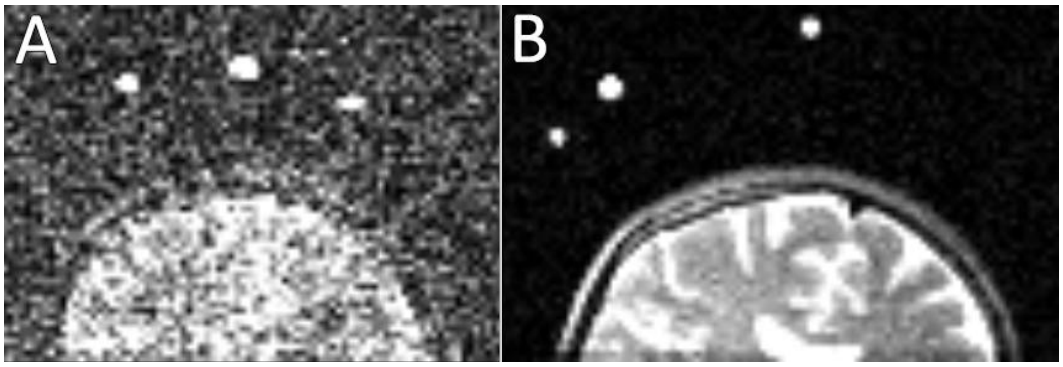

Figure A.4A *A noisy T2-weighted scan with coil probes due to improper grounding of the TMS coil to the Faraday cage.* ***Figure A.4B*** *A normal T2-weighted scan with coil probes.*

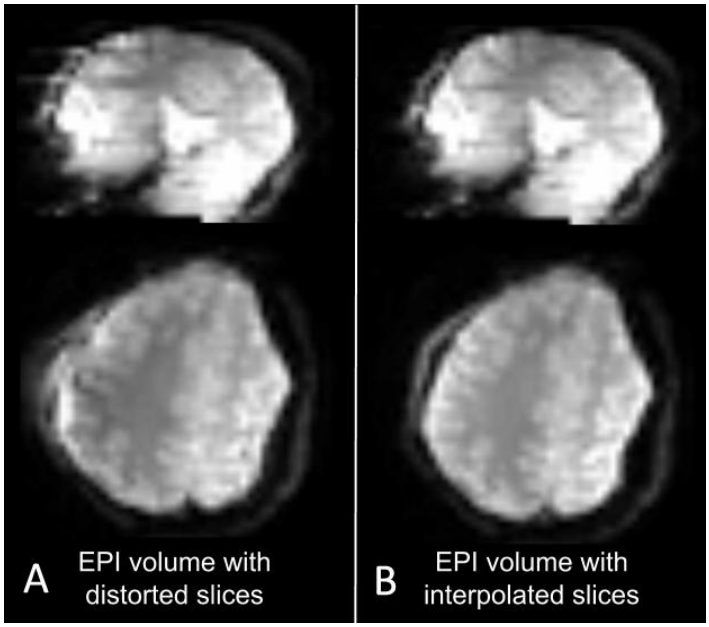

Figure A.5A *Image distortions in a 2 different slices of an EPI volume acquired during the interleaved scheme.* ***Figure A.5B*** *Reconstructed EPI volume based on the temporal interpolation of the two distorted slices.*

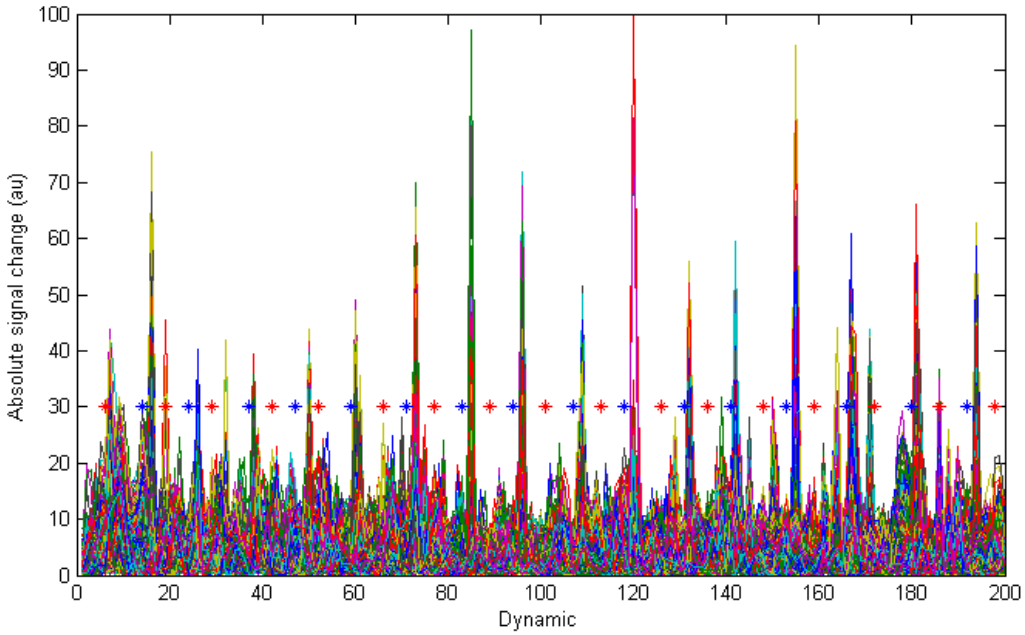

Figure A.6 *Absolute deviations from the baseline BOLD signal of all voxels that show a significant TMS-induced response for TMS pulses of 115% RMT versus TMS pulses of 60% RMT. The blue and red stars indicate the timing of 60% RMT and 115% RMT TMS pulses, respectively. High amplitude peaks can be observed consistently after delivery of TMS pulses of 60% RMT.*

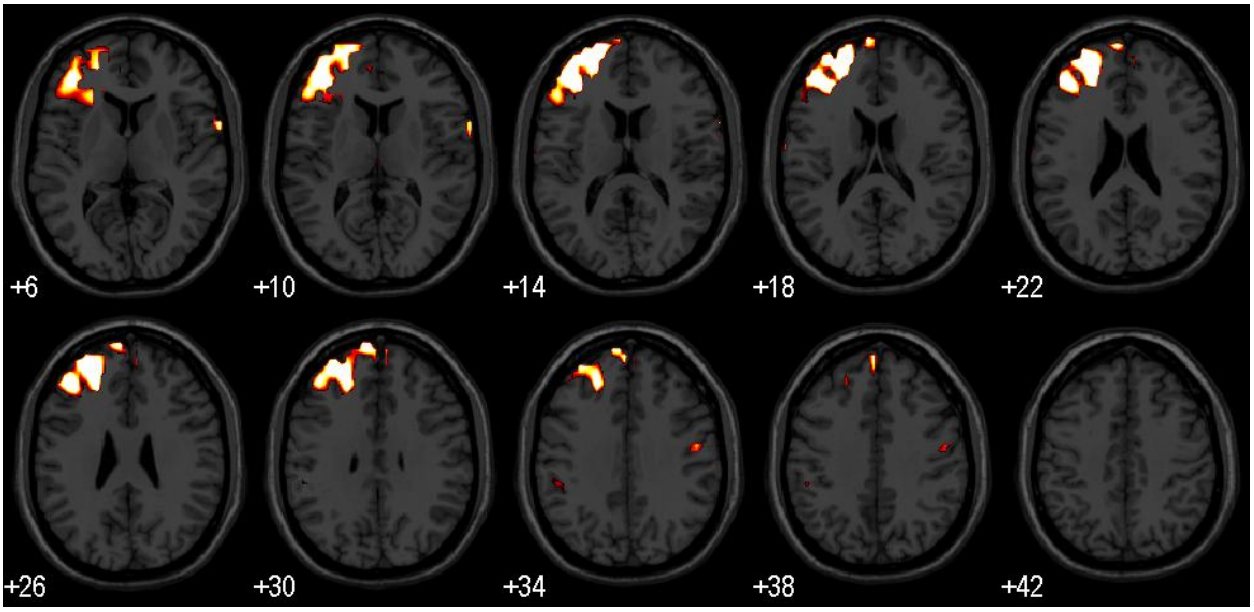

Figure A.7 *Statistical map of TMS pulses of 115% RMT delivered to the left DLPFC versus 60% RMT. A huge cluster of activity can be observed in the vicinity of the coil, while activity is almost absent in the rest of the brain. DLPFC: dorsolateral prefrontal cortex.*

Appendices B to F

Appendices B to F are part of a digital copy attached to the main thesis. The appendix figures (without captions) can also be accessed digitally through the following links.

Follow the following link to access the figures of appendix B:
https://drive.google.com/open?id=0B7FraBNj_9qNYzVzQU9peHJ2cTg

Follow the following link to access the figures of appendix C:
https://drive.google.com/open?id=0B7FraBNj_9qNYzVzQU9peHJ2cTg

Follow the following link to access the figures of appendix D:
https://drive.google.com/open?id=0B7FraBNj_9qNdWZ3dXV4UVNrMUU

Follow the following link to access the figures of appendix D:
https://drive.google.com/open?id=0B7FraBNj_9qNUVBrbTE4VTRZeFE

Follow the following link to access the figures of appendix F:
https://drive.google.com/open?id=0B7FraBNj_9qNWWxFOGpVOVVlc0U

References

[1] A. P. Association and others, *Diagnostic and statistical manual of mental disorders (DSM-5{®})*. American Psychiatric Pub, 2013.

[2] M. Hamilton, "A rating scale for depression," *J. Neurol. Neurosurg. Psychiatry*, vol. 23, no. 1, pp. 56–62, 1960.

[3] A. J. Ferrari, A. J. Somerville, A. J. Baxter, R. Norman, S. B. Patten, T. Vos, and H. A. Whiteford, "Global variation in the prevalence and incidence of major depressive disorder: a systematic review of the epidemiological literature."

[4] R. S. Mcintyre, M.-J. Filteau, L. Martin, S. Patry, A. Carvalho, D. S. Cha, M. Barakat, and M. Miguelez, "Treatment-resistant depression: Definitions, review of the evidence, and algorithmic approach," 2013.

[5] D. S. Hasin, R. D. Goodwin, F. S. Stinson, and B. F. Grant, "Epidemiology of major depressive disorder: results from the National Epidemiologic Survey on Alcoholism and Related Conditions," *Arch. Gen. Psychiatry*, vol. 62, no. 10, pp. 1097–1106, 2005.

[6] E. I. Fried and R. M. Nesse, "Depression is not a consistent syndrome: an investigation of unique symptom patterns in the STAR* D study," *J. Affect. Disord.*, vol. 172, pp. 96–102, 2015.

[7] A. Little, "Treatment-resistant depression," *Am. Fam. Physician*, vol. 80, no. 2, pp. 167–172, 2009.

[8] L. Pessoa and P. R. Hof, "From Paul Broca's great limbic lobe to the limbic system," *J. Comp. Neurol.*, vol. 523, no. 17, pp. 2495–2500, 2015.

[9] J. W. Papez, "A proposed mechanism of emotion," *Arch. Neurol. Psychiatry*, vol. 38, no. 4, pp. 725–743, 1937.

[10] R. J. R. Blair, J. S. Morris, C. D. Frith, D. I. Perrett, and R. J. Dolan, "Dissociable neural responses to facial expressions of sadness and anger," *Brain*, vol. 122, no. 5, pp. 883–893, 1999.

[11] G. Bush, P. Luu, and M. I. Posner, "Cognitive and emotional influences in anterior cingulate cortex," *Trends.Cogn Sci.*, vol. 4, no. 6, pp. 215–222, 2000.

[12] W. C. Drevets, J. L. Price, J. R. Simpson Jr., R. D. Todd, T. Reich, M. Vannier, and M. E. Raichle, "Subgenual prefrontal cortex abnormalities in mood disorders," *Nature*, vol. 386, no. 6627. pp. 824–827, 1997.

[13] K. N. Botteron, M. E. Raichle, W. C. Drevets, A. C. Heath, and R. D. Todd, "Volumetric reduction in left subgenual prefrontal cortex in early onset depression," *Biol. Psychiatry*, vol. 51, no. 4, pp. 342–344, 2002.

[14] W. C. Drevets, N. Ryan, W. Bogers, B. Birmaher, D. Axelson, and R. Dahl, "Subgenual prefrontal cortex volume decreased in healthy humans at high familial risk for mood disorders," *Soc Neurosci Abs*, vol. 799, p. 18, 2004.

[15] P. Videbech, "PET measurements of brain glucose metabolism and blood flow in major depressive disorder: a critical review," *Acta Psychiatr. Scand.*, vol. 101, no. 1, pp. 11–20, 2000.

[16] H. S. Mayberg, S. K. Brannan, J. L. Tekell, J. A. Silva, R. K. Mahurin, S. Mcginnis, and P. A. Jerabek, "Regional Metabolic Effects of Fluoxetine in Major Depression: Serial Changes and Relationship to Clinical Response."

[17] H. S. Mayberg, A. M. Lozano, V. Voon, H. E. McNeely, D. Seminowicz, C. Hamani, J. M. Schwalb, and S. H. Kennedy, "Deep brain stimulation for treatment-resistant depression," *Neuron*, vol. 45, no. 5, pp. 651–660, 2005.

[18] S. H. Kennedy, K. R. Evans, S. Krüger, H. S. Mayberg, J. H. Meyer, S. McCann, A. I. Arifuzzman, S. Houle, and F. J. Vaccarino, "Changes in Regional Brain Glucose Metabolism Measured With Positron Emission Tomography After Paroxetine Treatment of Major Depression," *Am. J. Psychiatry*, vol. 158, no. 6, pp. 899–905, 2001.

[19] P. E. Holtzheimer, “Subcallosal Cingulate Deep Brain Stimulation for Treatment-Resistant Unipolar and Bipolar Depression,” *Arch. Gen. Psychiatry*, vol. 69, no. 2, p. 150, 2012.
[20] H. Damasio, T. Grabowski, R. Frank, A. M. Galaburda, and A. R. Damasio, “The return of Phineas Gage: Clues about the brain from the skull of a famous patient,” *Science*, vol. 264, no. 5162. pp. 1102–1105, 1994.
[21] M. Koenigs and J. Grafman, “The functional neuroanatomy of depression: Distinct roles for ventromedial and dorsolateral prefrontal cortex,” *Behav. Brain Res.*, vol. 201, no. 2, pp. 239–243, 2009.
[22] B. L. Miller and J. L. Cummings, *The human frontal lobes: Functions and disorders*. Guilford press, 2007.
[23] M. S. Korgaonkar, S. M. Grieve, A. Etkin, S. H. Koslow, and L. M. Williams, “Using standardized fMRI protocols to identify patterns of prefrontal circuit dysregulation that are common and specific to cognitive and emotional tasks in major depressive disorder : First wave results from the iSPOT-D study ,” *Neuropsychopharmacology*, vol. 38, no. 5, pp. 863–871, 2013.
[24] A. L. Brody, S. Saxena, M. A. Mandelkern, L. A. Fairbanks, M. L. Ho, and L. R. Baxter, “Brain metabolic changes associated with symptom factor improvement in major depressive disorder,” *Biol. Psychiatry*, vol. 50, no. 3, pp. 171–178, 2001.
[25] M. Koenigs, E. D. Huey, M. Calamia, V. Raymont, D. Tranel, and J. Grafman, “Distinct regions of prefrontal cortex mediate resistance and vulnerability to depression.,” *J. Neurosci.*, vol. 28, no. 47, pp. 12341–8, 2008.
[26] E. A. Phelps and J. E. LeDoux, “Contributions of the amygdala to emotion processing: From animal models to human behavior,” *Neuron*, vol. 48, no. 2, pp. 175–187, 2005.
[27] J. P. Hamilton, M. Siemer, and I. H. Gotlib, “Amygdala volume in major depressive disorder: a meta-analysis of magnetic resonance imaging studies.,” *Mol. Psychiatry*, vol. 13, no. 11, pp. 993–1000, 2008.
[28] J. P. Hamilton, M. Siemer, and I. H. Gotlib, “Amygdala volume in major depressive disorder: a meta-analysis of magnetic resonance imaging studies.,” *Mol. Psychiatry*, vol. 13, no. 11, pp. 993–1000, 2008.
[29] B. Chen, D. Dowlatshahi, G. M. MacQueen, J. F. Wang, and L. T. Young, “Increased hippocampal BDNF immunoreactivity in subjects treated with antidepressant medication,” *Biol. Psychiatry*, vol. 50, no. 4, pp. 260–265, 2001.
[30] W. C. Drevets, W. Bogers, and M. E. Raichle, “Functional anatomical correlates of antidepressant drug treatment assessed using PET measures of regional glucose metabolism,” *Eur. Neuropsychopharmacol.*, vol. 12, no. 6, pp. 527–544, 2002.
[31] W. C. Drevets, T. O. Videen, J. L. Price, S. H. Preskorn, S. T. Carmichael, and M. E. Raichle, “A functional anatomical study of unipolar depression,” *J. Neurosci.*, vol. 12, no. 9, pp. 3628–3641, 1992.
[32] D. A. Pizzagalli, D. Iosifescu, L. A. Hallett, K. G. Ratner, and M. Fava, “Reduced hedonic capacity in major depressive disorder: Evidence from a probabilistic reward task,” *J. Psychiatr. Res.*, 2008.
[33] J. P. O’Doherty, “Reward representations and reward-related learning in the human brain: insights from neuroimaging,” *Curr. Opin. Neurobiol.*, vol. 14, no. 6, pp. 769–776, 2004.
[34] H. Johansen-Berg, D. A. Gutman, T. E. J. Behrens, P. M. Matthews, M. F. S. Rushworth, E. Katz, A. M. Lozano, and H. S. Mayberg, “Anatomical connectivity of the subgenual cingulate region targeted with deep brain stimulation for treatment-resistant depression,” *Cereb. Cortex*, vol. 18, no. 6, pp. 1374–1383, 2008.
[35] S. R. Sesack and A. a Grace, “Cortico-Basal Ganglia reward network: microcircuitry.,” *Neuropsychopharmacology*, vol. 35, no. 1, pp. 27–47, 2010.
[36] P. Videbech, “PET measurements of brain glucose metabolism and blood flow in major depressive disorder: a critical review,” *Acta Psychiatr. Scand.*, vol. 101, no. 1, pp. 11–20, 2000.

[37] D. A. Pizzagalli, A. J. Holmes, A. G. Daniel Dillon, E. L. Goetz, B. L. Jeffrey Birk, B. Ryan Bogdan, A. D. Darin Dougherty, D. V Iosifescu, S. L. Rauch, and M. Fava, "Reduced Caudate and Nucleus Accumbens Response to Rewards in Unmedicated Individuals With Major Depressive Disorder," *Am J Psychiatry*, vol. 1666, 2009.

[38] M. J. Smoski, J. Felder, J. Bizzell, S. R. Green, M. Ernst, T. R. Lynch, and G. S. Dichter, "fMRI of alterations in reward selection, anticipation, and feedback in major depressive disorder," *J. Affect. Disord.*, 2009.

[39] T. E. Schlaepfer, M. X. Cohen, C. Frick, M. Kosel, D. Brodesser, N. Axmacher, A. Y. Joe, M. Kreft, D. Lenartz, and V. Sturm, "Deep brain stimulation to reward circuitry alleviates anhedonia in refractory major depression.," *Neuropsychopharmacology*, vol. 33, no. 2, pp. 368–77, 2008.

[40] D. A. Malone, D. D. Dougherty, A. R. Rezai, L. L. Carpenter, G. M. Friehs, E. N. Eskandar, S. L. Rauch, S. A. Rasmussen, A. G. Machado, C. S. Kubu, A. R. Tyrka, L. H. Price, P. H. Stypulkowski, J. E. Giftakis, M. T. Rise, P. F. Malloy, S. P. Salloway, and B. D. Greenberg, "Deep Brain Stimulation of the Ventral Capsule/Ventral Striatum for Treatment-Resistant Depression," *Biol. Psychiatry*, 2009.

[41] R. D. Weiner, H. J. Rogers, J. R. T. Davidson, and L. R. Squire, "Effects of stimulus parameters on cognitive side effects," *Ann. N. Y. Acad. Sci.*, vol. 462, no. 1, pp. 315–325, 1986.

[42] S. Rossi, M. Hallett, P. M. Rossini, A. Pascual-Leone, G. Avanzini, S. Bestmann, A. Berardelli, C. Brewer, T. Canli, R. Cantello, R. Chen, J. Classen, M. Demitrack, V. Di Lazzaro, C. M. Epstein, M. S. George, F. Fregni, R. Ilmoniemi, R. Jalinous, B. Karp, J. P. Lefaucheur, S. Lisanby, S. Meunier, C. Miniussi, P. Miranda, F. Padberg, W. Paulus, A. Peterchev, C. Porteri, M. Provost, A. Quartarone, A. Rotenberg, J. Rothwell, J. Ruohonen, H. Siebner, G. Thut, J. Valls-Sol??, V. Walsh, Y. Ugawa, A. Zangen, and U. Ziemann, "Safety, ethical considerations, and application guidelines for the use of transcranial magnetic stimulation in clinical practice and research," *Clin. Neurophysiol.*, vol. 120, no. 12, pp. 2008–2039, 2009.

[43] E. A. Allen, B. N. Pasley, T. Duong, and R. D. Freeman, "Transcranial magnetic stimulation elicits coupled neural and hemodynamic consequences," *Science (80-.).*, vol. 317, no. 5846, pp. 1918–1921, 2007.

[44] P. B. Fitzgerald, S. Fountain, and Z. J. Daskalakis, "A comprehensive review of the effects of rTMS on motor cortical excitability and inhibition," *Clin. Neurophysiol.*, vol. 117, no. 12, pp. 2584–2596, 2006.

[45] D. J. L. G. Schutter and J. van Honk, "A standardized motor threshold estimation procedure for transcranial magnetic stimulation research.," *J. ECT*, vol. 22, no. 3, pp. 176–178, 2006.

[46] A. Rahman, D. Reato, M. Arlotti, F. Gasca, A. Datta, L. C. Parra, and M. Bikson, "Cellular effects of acute direct current stimulation: somatic and synaptic terminal effects.," *J. Physiol.*, vol. 591, no. Pt 10, pp. 2563–78, 2013.

[47] P. T. Fox, S. Narayana, N. Tandon, H. Sandoval, S. P. Fox, P. Kochunov, and J. L. Lancaster, "Column-Based Model of Electric Field Excitation of Cerebral Cortex," *Hum. Brain Mapp.*, vol. 22, no. 1, pp. 1–14, 2004.

[48] A. M. Janssen, T. F. Oostendorp, and D. F. Stegeman, "The coil orientation dependency of the electric field induced by TMS for M1 and other brain areas.," *J. Neuroeng. Rehabil.*, vol. 12, no. 1, p. 47, 2015.

[49] S. Kähkönen, J. Wilenius, V. V Nikulin, M. Ollikainen, and R. J. Ilmoniemi, "Alcohol reduces prefrontal cortical excitability in humans: a combined TMS and EEG study," *Neuropsychopharmacology*, vol. 28, no. 4, p. 747, 2003.

[50] L. Fadiga, L. Fogassi, G. Pavesi, and G. Rizzolatti, "Motor facilitation during action observation: a magnetic stimulation study," *J. Neurophysiol.*, vol. 73, no. 6, pp. 2608–2611, 1995.

[51] P. Sauseng, W. Klimesch, C. Gerloff, and F. C. Hummel, "Spontaneous locally restricted EEG alpha activity determines cortical excitability in the motor cortex," *Neuropsychologia*, vol. 47, no. 1, pp. 284–288, 2009.

[52] G. Thut, D. Veniero, V. Romei, C. Miniussi, P. Schyns, and J. Gross, “Rhythmic TMS causes local entrainment of natural oscillatory signatures,” *Curr. Biol.*, vol. 21, no. 14, pp. 1176–1185, 2011.

[53] J. P. O’Reardon, H. B. Solvason, P. G. Janicak, S. Sampson, K. E. Isenberg, Z. Nahas, W. M. McDonald, D. Avery, P. B. Fitzgerald, C. Loo, M. A. Demitrack, M. S. George, and H. A. Sackeim, “Efficacy and Safety of Transcranial Magnetic Stimulation in the Acute Treatment of Major Depression: A Multisite Randomized Controlled Trial,” *Biol. Psychiatry*, vol. 62, no. 11, pp. 1208–1216, 2007.

[54] K. R. Connolly, A. Helmer, M. A. Cristancho, P. Cristancho, and J. P. O’Reardon, “Effectiveness of transcranial magnetic stimulation in clinical practice post-FDA approval in the United States: results observed with the first 100 consecutive cases of depression at an academic medical center.,” *J. Clin. Psychiatry*, vol. 73, no. 4, pp. e567--73, 2012.

[55] P. Holtzheimer, W. McDonald, M. Mufti, M. Kelley, S. Quinn, G. Corso, and C. M. Epstein, “Accelerated repetitive transcranial magnetic stimulation (aTMS) for treatment-resistant depression,” *Depress Anxiety*, vol. 27, no. 10, pp. 960–963, 2010.

[56] P. B. Fitzgerald, K. Hoy, S. Mcqueen, J. J. Maller, S. Herring, R. Segrave, M. Bailey, G. Been, J. Kulkarni, and Z. J. Daskalakis, “A Randomized Trial of rTMS Targeted with MRI Based Neuro-Navigation in Treatment-Resistant Depression,” *Neuropsychopharmacology*, vol. 34, 2009.

[57] H. L. Sophia Mueller, danhong Wang, Michael D. Fox, B.T. Thomas Yeo, Jorge Sepulcre, Mert R. Sabuncu, Rebecca Shafee, Jie Lu, “Individual Variability in Functional Connectivity Architecture of the Human Brain,” *Neuron*, vol. 18, no. 9, pp. 1199–1216, 2013.

[58] B. T. T. Yeo, F. M. Krienen, J. Sepulcre, M. R. Sabuncu, D. Lashkari, M. Hollinshead, J. L. Roffman, J. W. Smoller, L. Zollei, J. R. Polimeni, B. Fischl, H. Liu, and R. L. Buckner, “The organization of the human cerebral cortex estimated by intrinsic functional connectivity,” *J. Neurophysiol.*, vol. 106, pp. 1125–1165, 2011.

[59] A. T. Sack, R. Cohen Kadosh, T. Schuhmann, M. Moerel, V. Walsh, and R. Goebel, “Optimizing Functional Accuracy of TMS in Cognitive Studies: A Comparison of Methods,” *J. Cogn. Neurosci.*, vol. 21, no. 2, pp. 207–221, 2009.

[60] M. D. Fox, R. L. Buckner, M. P. White, M. D. Greicius, and A. Pascual-Leone, “Efficacy of transcranial magnetic stimulation targets for depression is related to intrinsic functional connectivity with the subgenual cingulate,” *Biol. Psychiatry*, vol. 72, no. 7, pp. 595–603, 2012.

[61] C. Baeken, D. Marinazzo, G.-R. Wu, P. Van Schuerbeek, J. De Mey, I. Marchetti, M.-A. Vanderhasselt, J. Remue, R. Luypaert, and R. De Raedt, “Accelerated HF-rTMS in treatment-resistant unipolar depression: Insights from subgenual anterior cingulate functional connectivity.,” *World J. Biol. Psychiatry*, vol. 32, no. 0, pp. 1–12, 2014.

[62] H. J. Hopman, S. F. W. Neggers, L. C. W. Lam, A. D. P. Mak, and S. S. M. Chan, “Preliminary results: resting-state fMRI correlations between left dorsolateral prefrontal cortex and subgenual cingulate and the relationship with repetitive transcranial magnetic stimulation treatment response,” *Brain Stimul. Basic, Transl. Clin. Res. Neuromodulation*, vol. 10, no. 2, p. 403, Apr. 2017.

[63] C. C. Teneback, B. Ziad Nahas, A. M. Speer, M. Molloy, R. E. MSN Laurie Stallings, P. M. Kenneth Spicer, S. Craig Risch, and M. S. George, “Changes in Prefrontal Cortex and Paralimbic Activity in Depression Following Two Weeks of Daily Left Prefrontal TMS,” *J Neuropsychiatry Clin Neurosci*, vol. 114, 1999.

[64] X. M. Zheng, “Regional cerebral blood flow changes in drug-resistant depressed patients following treatment with transcranial magnetic stimulation: A statistical parametric mapping analysis,” *Psychiatry Res. - Neuroimaging*, 2000.

[65] M. J. Lan, B. T. Chhetry, C. Liston, J. J. Mann, and M. Dubin, “Transcranial Magnetic Stimulation of Left Dorsolateral Prefrontal Cortex Induces Brain Morphological Changes in Regions Associated with a Treatment Resistant Major Depressive Episode: An Exploratory Analysis,” *Brain Stimul.*, vol. 9, pp. 577–583, 2016.

[66] R. De Raedt, L. Leyman, C. Baeken, P. Van Schuerbeek, R. Luypaert, M. A. Vanderhasselt, and U. Dannlowski, “Neurocognitive effects of HF-rTMS over the dorsolateral prefrontal cortex on the attentional processing of emotional information in healthy women: An event-related fMRI study,” *Biol. Psychol.*, 2010.
[67] T. Kammer, M. Vorwerg, and B. Herrnberger, “Anisotropy in the visual cortex investigated by neuronavigated transcranial magnetic stimulation,” *Neuroimage*, vol. 36, no. 2, pp. 313–321, 2007.
[68] W. D. Penny, K. J. Friston, J. T. Ashburner, S. J. Kiebel, and T. E. Nichols, *Statistical parametric mapping: the analysis of functional brain images*. Academic press, 2011.
[69] G. Goldberg, “Supplementary motor area structure and function: review and hypotheses,” *Behav. Brain Sci.*, vol. 8, no. 4, pp. 567–588, 1985.
[70] S. F. W. Neggers, B. B. Zandbelt, M. S. Schall, and J. D. Schall, “Comparative diffusion tractography of corticostriatal motor pathways reveals differences between humans and macaques,” *J. Neurophysiol.*, vol. 113, no. 7, pp. 2164–2172, 2015.
[71] E. Manni and L. Petrosini, “A century of cerebellar somatotopy: a debated representation.,” *Nat. Rev. Neurosci.*, vol. 5, no. 3, pp. 241–9, 2004.
[72] A. Ferbert, A. Priori, J. C. Rothwell, B. L. Day, J. G. Colebatch, and C. D. Marsden, “Interhemispheric inhibition of the human motor cortex.,” *J. Physiol.*, vol. 453, no. D, pp. 525–46, 1992.
[73] S. H. Lisanby, D. Gutman, B. Luber, C. Schroeder, and H. A. Sackeim, “Sham TMS: Intracerebral measurement of the induced electrical field and the induction of motor-evoked potentials,” *Biol. Psychiatry*, vol. 49, no. 5, pp. 460–463, 2001.
[74] K. Bornhövd, M. Quante, V. Glauche, B. Bromm, C. Weiller, C. Büchel, K. Bornhovd, M. Quante, V. Glauche, B. Bromm, C. Weiller, and C. Buchel, “Painful stimuli evoke different stimulus-response functions in the amygdala, prefrontal, insula and somatosensory cortex: a single-trial fMRI study.,” *Brain*, vol. 125, no. Pt 6, pp. 1326–1336, 2002.
[75] J. M. Yau, R. Jalinous, G. L. Cantarero, and J. E. Desmond, “Static field influences on transcranial magnetic stimulation: Considerations for TMS in the scanner environment,” *Brain Stimul.*, vol. 7, no. 3, pp. 388–393, 2014.
[76] C. der Malsburg, W. A. Phillips, and W. Singer, *Dynamic coordination in the brain: from neurons to mind*. MIT Press, 2010.
[77] A. Fornito, B. J. Harrison, A. Zalesky, and J. S. Simons, “Competitive and cooperative dynamics of large-scale brain functional networks supporting recollection,” *Proc. Natl. Acad. Sci.*, vol. 109, no. 31, pp. 12788–12793, 2012.
[78] D. S. Bassett, N. F. Wymbs, M. A. Porter, P. J. Mucha, J. M. Carlson, and S. T. Grafton, “Dynamic reconfiguration of human brain networks during learning,” *Proc. Natl. Acad. Sci.*, vol. 108, no. 18, pp. 7641–7646, 2011.
[79] T. Meindl, S. Teipel, R. Elmouden, S. Mueller, W. Koch, O. Dietrich, U. Coates, M. Reiser, and C. Glaser, “Test--retest reproducibility of the default-mode network in healthy individuals,” *Hum. Brain Mapp.*, vol. 31, no. 2, pp. 237–246, 2010.
[80] V. Romei, V. Brodbeck, C. Michel, A. Amedi, A. Pascual-Leone, and G. Thut, “Spontaneous fluctuations in posterior alpha-band EEG activity reflect variability in excitability of human visual areas,” *Cereb. cortex*, vol. 18, no. 9, pp. 2010–2018, 2008.
[81] C. K. Loo, J. L. Taylor, S. C. Gandevia, B. N. McDarmont, P. B. Mitchell, and P. S. Sachdev, “Transcranial magnetic stimulation (TMS) in controlled treatment studies: Are some ‘sham’ forms active?,” *Biol. Psychiatry*, vol. 47, no. 4, pp. 325–331, 2000.
[82] F. Hoeft, D. A. Wu, A. Hernandez, G. H. Glover, and S. Shimojo, “Electroncally switchable sham transcranial magnetic stimulation (TMS) system,” *PLoS One*, vol. 3, no. 4, 2008.
[83] R. Ahdab, S. S. Ayache, P. Brugières, C. Goujon, and J.-P. Lefaucheur, “Comparison of ‘standard’ and ‘navigated’ procedures of TMS coil positioning over motor, premotor and prefrontal targets in patients with chronic pain and depression,” *Neurophysiol. Clin.*

Neurophysiol., vol. 40, no. 1, pp. 27–36, 2010.
[84] R. M. Hutchison, J. P. Gallivan, J. C. Culham, J. S. Gati, R. S. Menon, and S. Everling, "Functional connectivity of the frontal eye fields in humans and macaque monkeys investigated with resting-state fMRI," *J. Neurophysiol.*, vol. 107, no. 9, pp. 2463–2474, 2012.
[85] R. L. Buckner, F. M. Krienen, A. Castellanos, J. C. Diaz, and B. T. T. Yeo, "The organization of the human cerebellum estimated by intrinsic functional connectivity," *J Neurophysiol*, vol. 106, pp. 2322–2345, 2011.
[86] G. B. Stanton, C. J. Bruce, and M. E. Goldberg, "Topography of projections to posterior cortical areas from the macaque frontal eye fields," *J. Comp. Neurol.*, vol. 353, no. 2, pp. 291–305, 1995.
[87] P. J. Olesen, Z. Nagy, H. Westerberg, and T. Klingberg, "Combined analysis of DTI and fMRI data reveals a joint maturation of white and grey matter in a fronto-parietal network," *Cogn. Brain Res.*, vol. 18, no. 1, pp. 48–57, 2003.
[88] P. Skudlarski, K. Jagannathan, V. D. Calhoun, M. Hampson, B. A. Skudlarska, and G. Pearlson, "Measuring brain connectivity: Diffusion tensor imaging validates resting state temporal correlations," *Neuroimage*, vol. 43, no. 3, pp. 554–561, 2008.
[89] C. Bonato, C. Miniussi, and P. M. Rossini, "Transcranial magnetic stimulation and cortical evoked potentials: A TMS/EEG co-registration study," *Clin. Neurophysiol.*, vol. 117, no. 8, pp. 1699–1707, 2006.
[90] R. B. Buxton, K. Uludağ, D. J. Dubowitz, and T. T. Liu, "Modeling the hemodynamic response to brain activation," *Neuroimage*, vol. 23, no. SUPPL. 1, pp. 220–233, 2004.
[91] S. Bestmann, C. C. Ruff, F. Blankenburg, N. Weiskopf, J. Driver, and J. C. Rothwell, "Mapping causal interregional influences with concurrent TMS--fMRI," *Exp. brain Res.*, vol. 191, no. 4, pp. 383–402, 2008.
[92] M. D. Greicius, K. Supekar, V. Menon, and R. F. Dougherty, "Resting-state functional connectivity reflects structural connectivity in the default mode network," *Cereb. Cortex*, vol. 19, no. 1, pp. 72–78, 2009.
[93] C. J. Honey, C. J. Honey, O. Sporns, O. Sporns, L. Cammoun, L. Cammoun, X. Gigandet, X. Gigandet, J. P. Thiran, J. P. Thiran, R. Meuli, R. Meuli, P. Hagmann, and P. Hagmann, "Predicting human resting-state functional connectivity from structural connectivity.," *Proc. Natl. Acad. Sci. U. S. A.*, vol. 106, no. 6, pp. 2035–40, 2009.
[94] J. J. T. Vink, M. B. Westover, A. Pascual-Leone, and M. M. Shafi, "EEG functional connectivity predicts propagation of TMS-evoked potentials," *Brain Stimul. Basic, Transl. Clin. Res. Neuromodulation*, vol. 10, no. 2, p. 516, 2017.

Appendix B

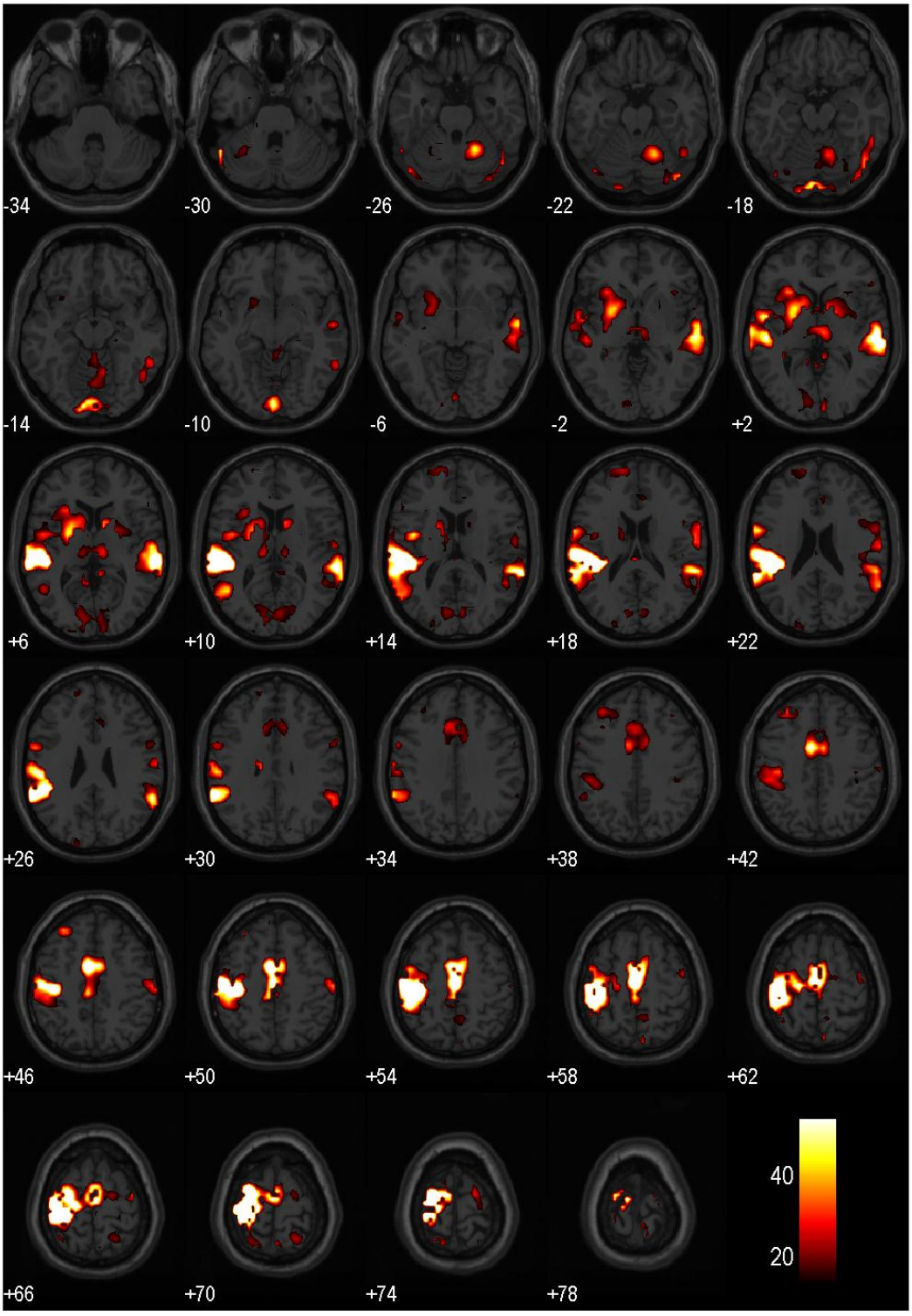

Figure B.1 *Statistical map of voluntary thumb movements of the right hand contrasted with baseline activity (P < 0.05, FWE corrected).*

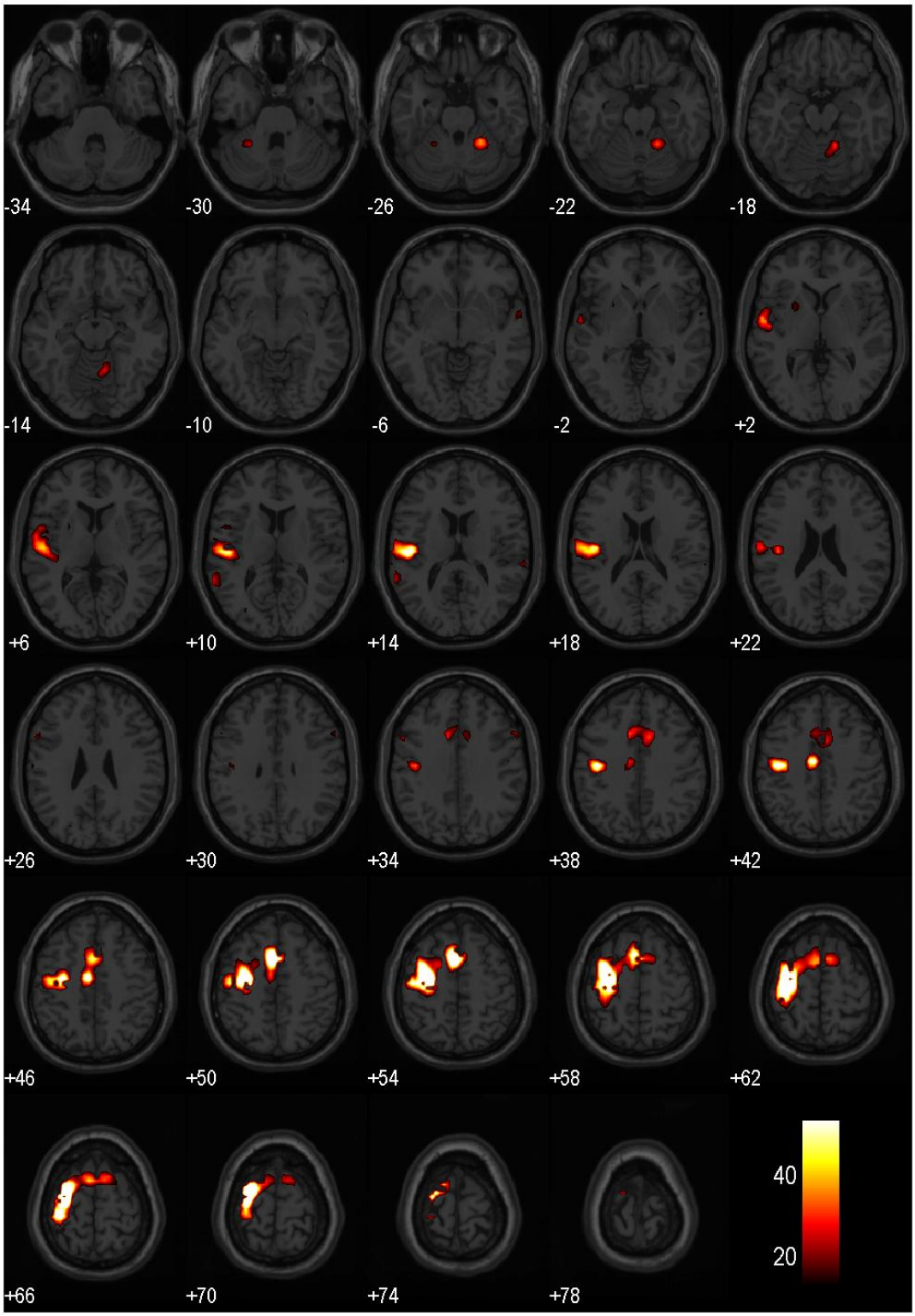

Figure B.2 *Statistical map of voluntary thumb movements of the right hand contrasted with baseline activity (P < 0.05, FWE corrected).*

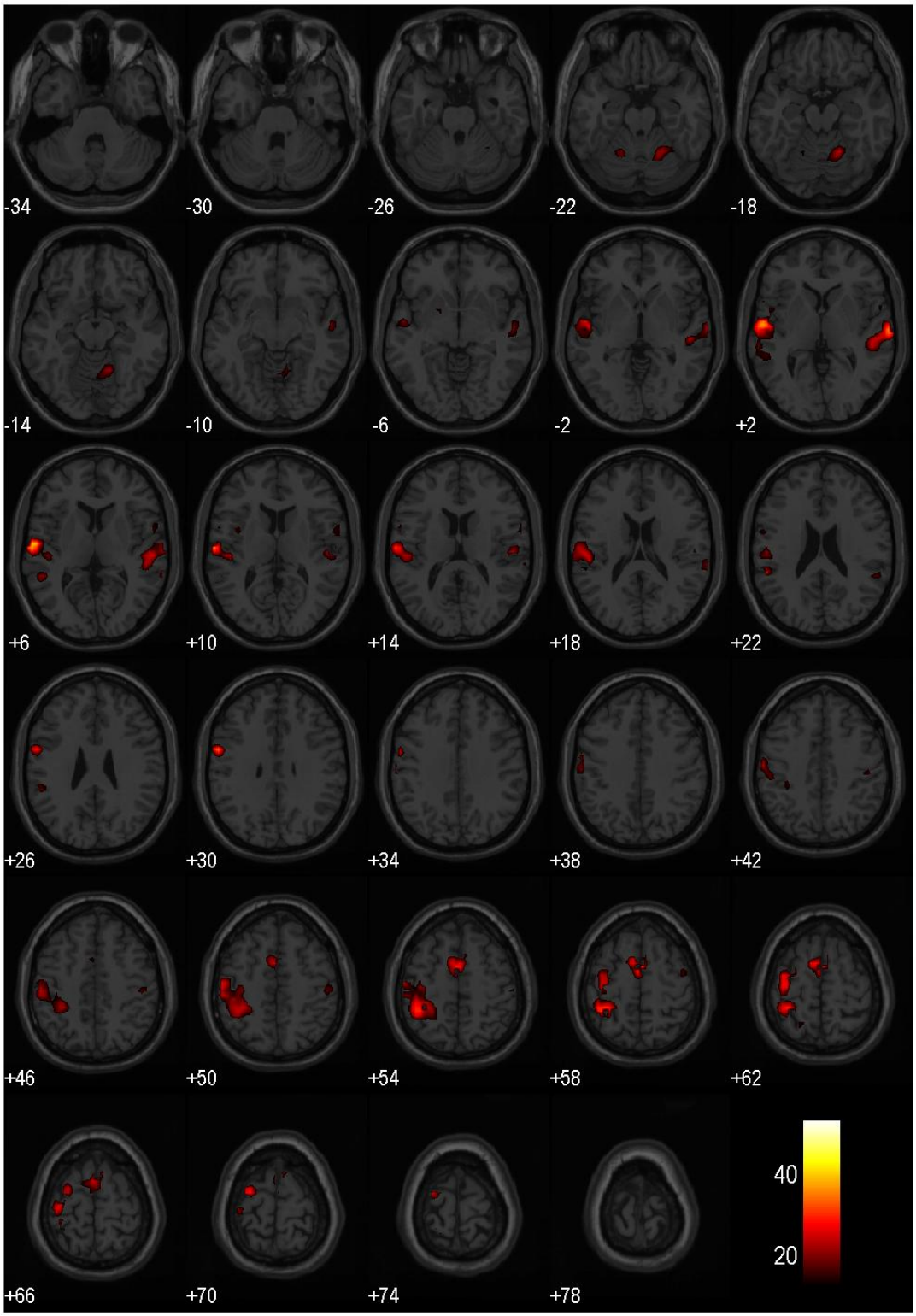

Figure B.3 *Statistical map of voluntary thumb movements of the right hand contrasted with baseline activity (P < 0.05, FWE corrected).*

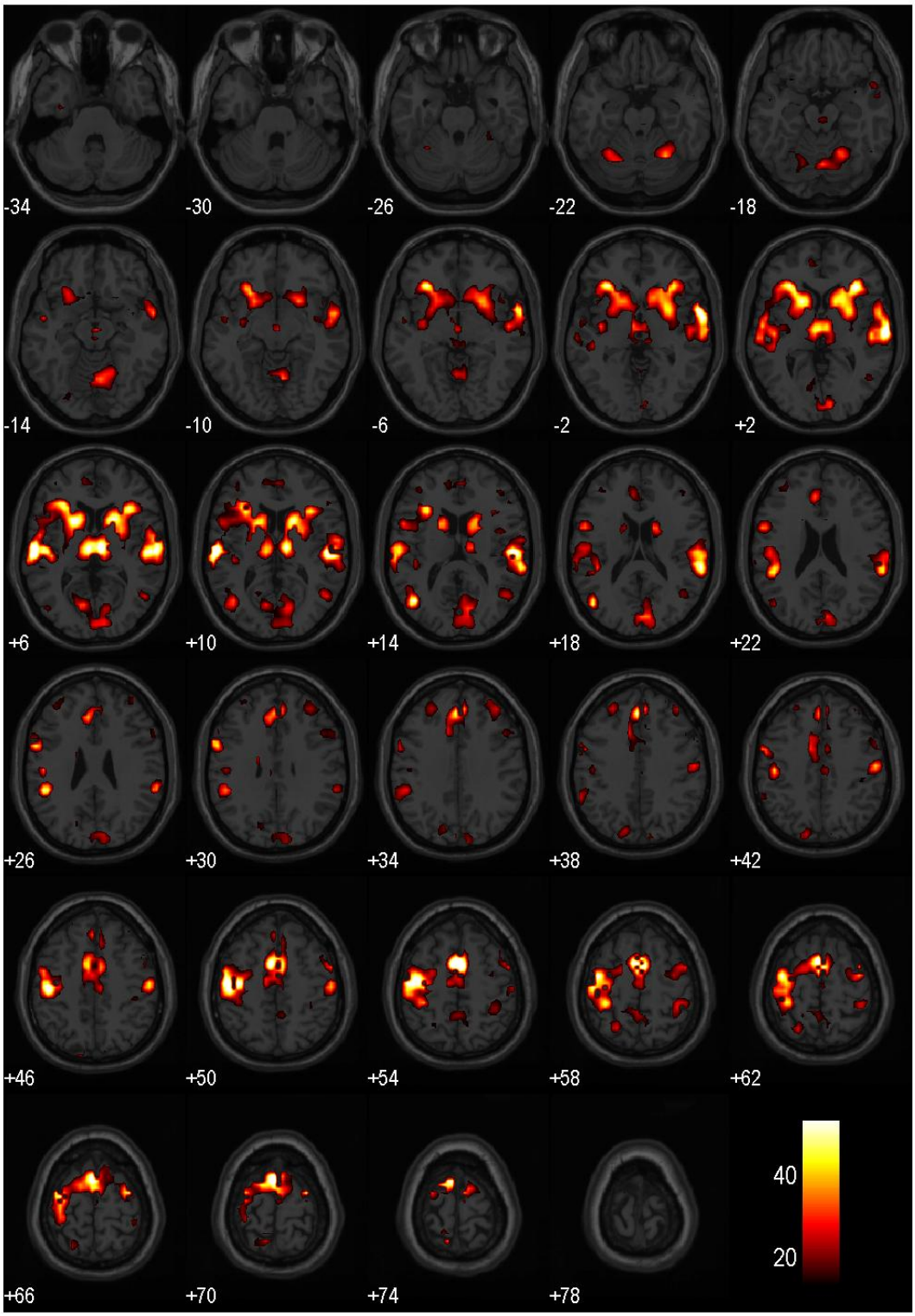

Figure B.4 *Statistical map of voluntary thumb movements of the right hand contrasted with baseline activity (P < 0.05, FWE corrected).*

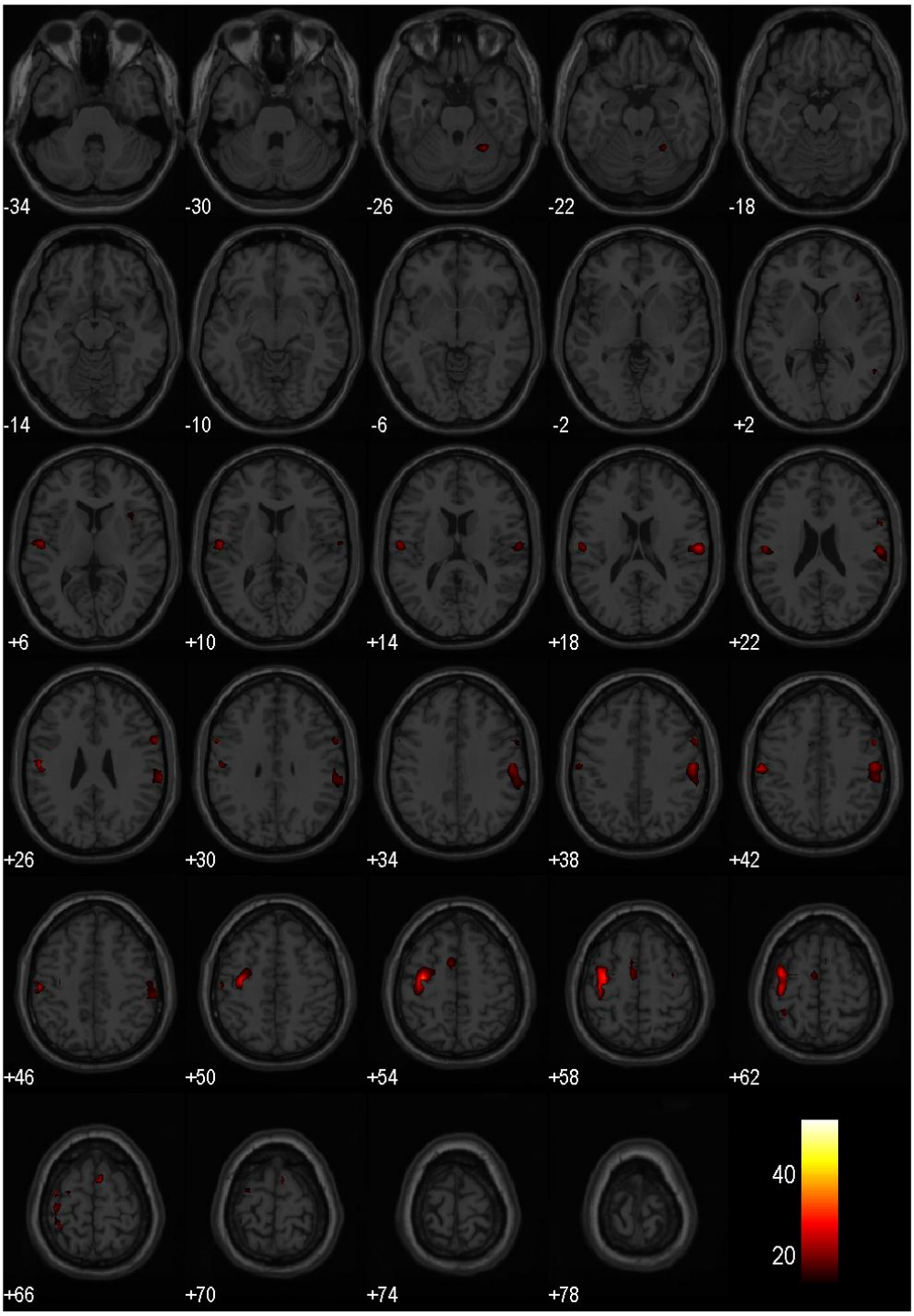

Figure B.5 *Statistical map of voluntary thumb movements of the right hand contrasted with baseline activity (P < 0.05, FWE corrected).*

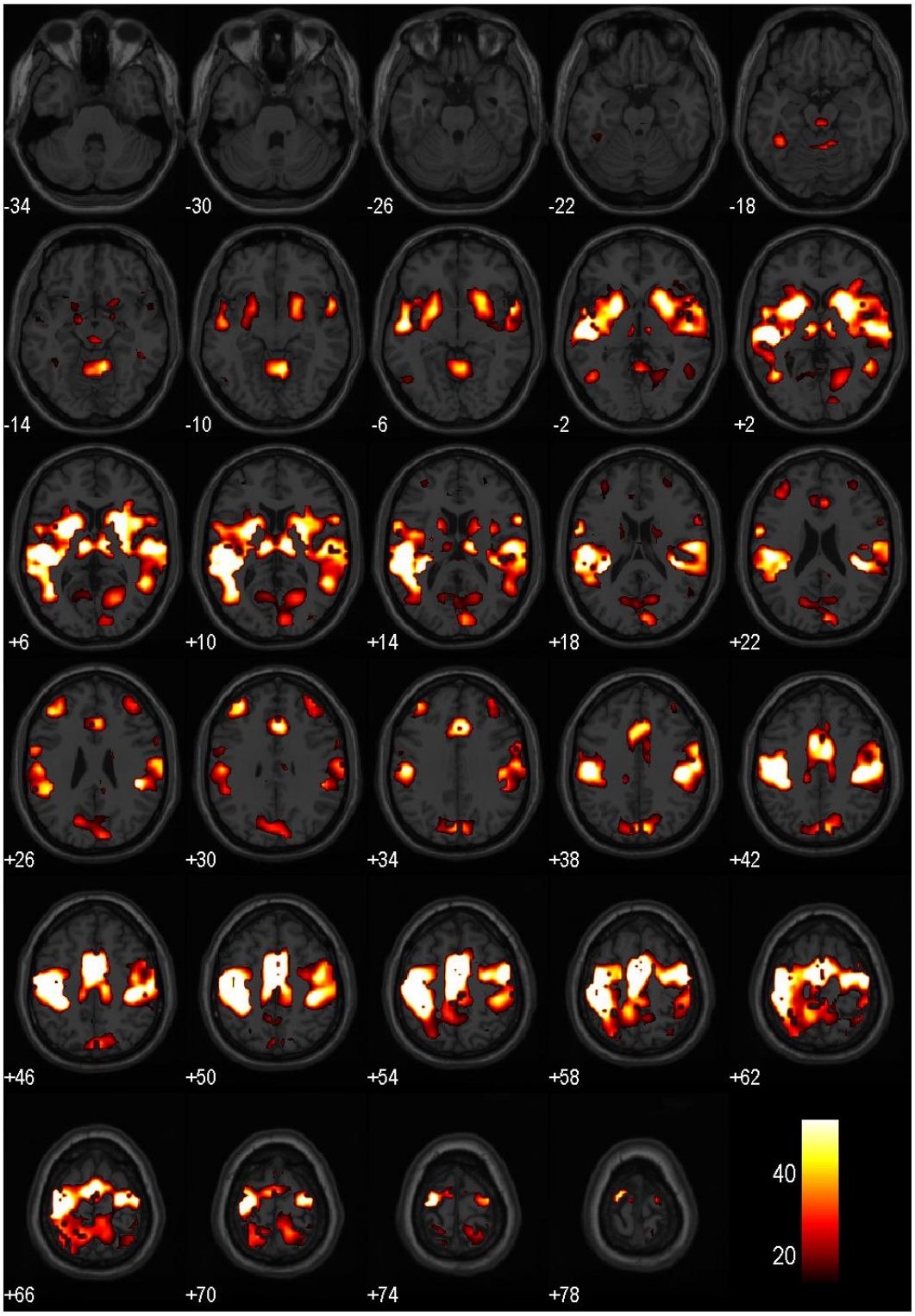

Figure B.6 *Statistical map of voluntary thumb movements of the right hand contrasted with baseline activity (P < 0.05, FWE corrected).*

Appendix C

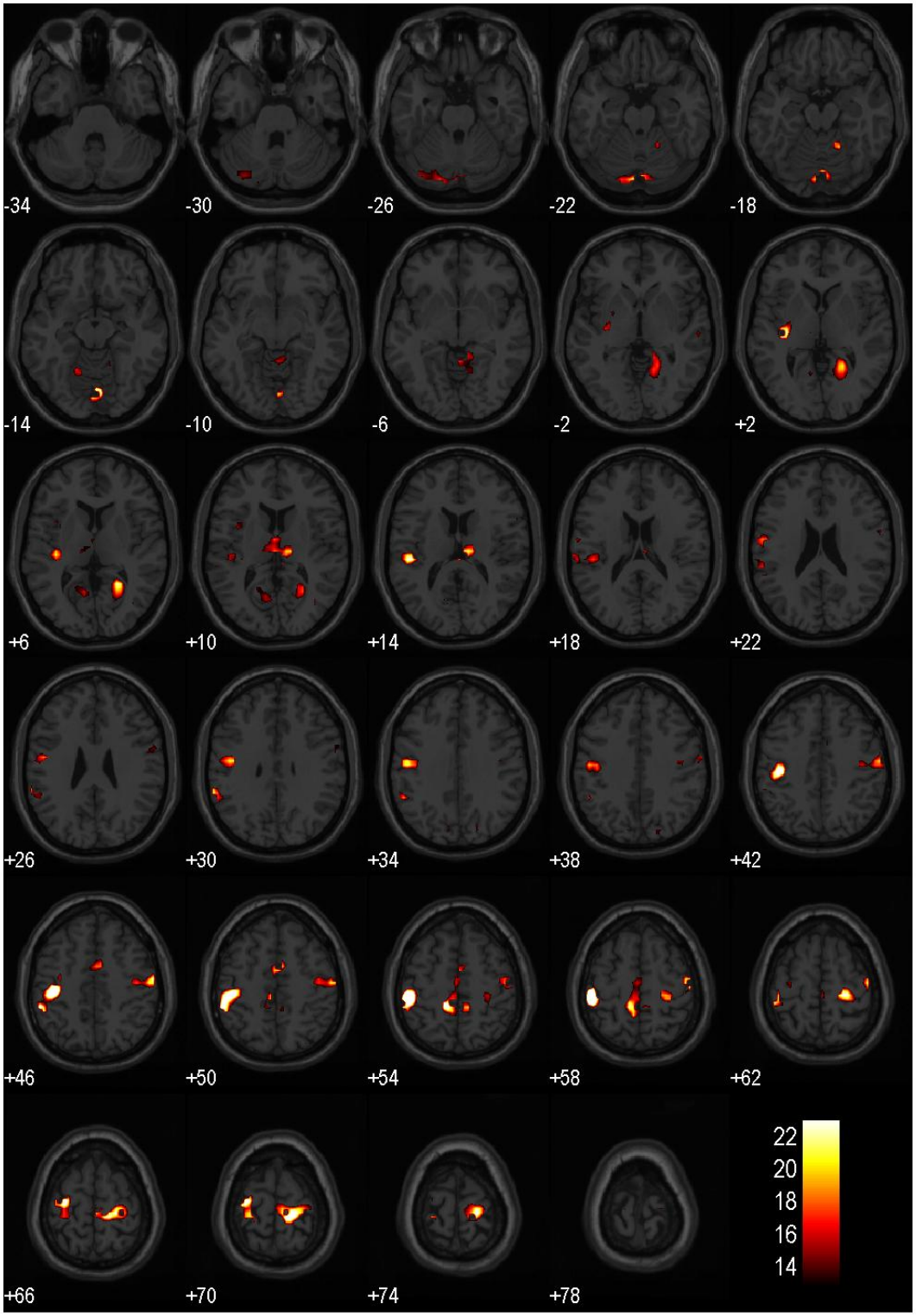

Figure C.1 *Statistical map of TMS pulses of 115% RMT delivered to the hand area within the left M1 contrasted with baseline activity (P < 0.05, FWE corrected). The participant reported TMS-induced thumb movements. M1: primary motor cortex.*

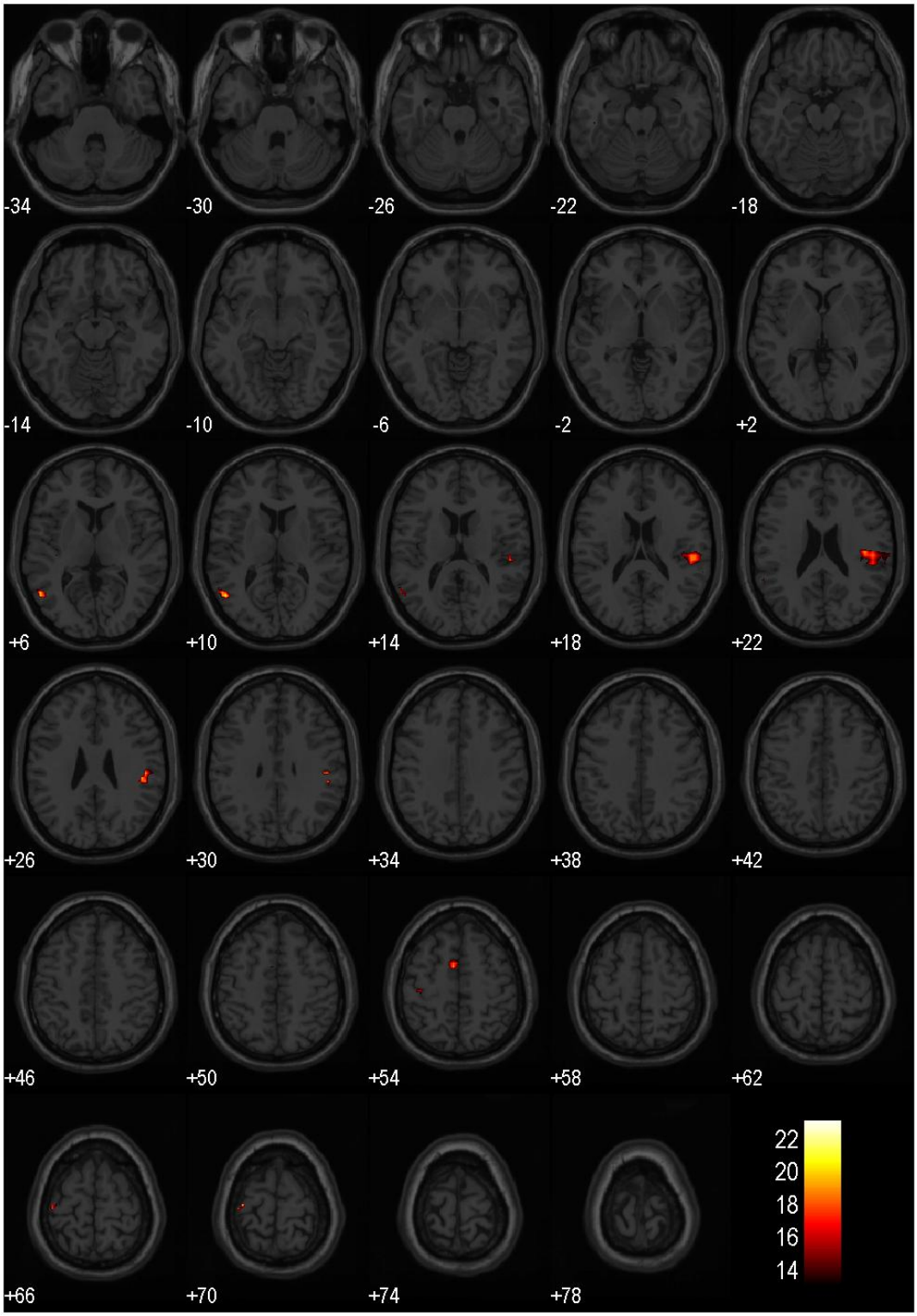

Figure C.2 *Statistical map of TMS pulses of 115% RMT delivered to the hand area within the left M1 contrasted with baseline activity (P < 0.05, FWE corrected). The participant reported TMS-induced thumb movements. M1: primary motor cortex.*

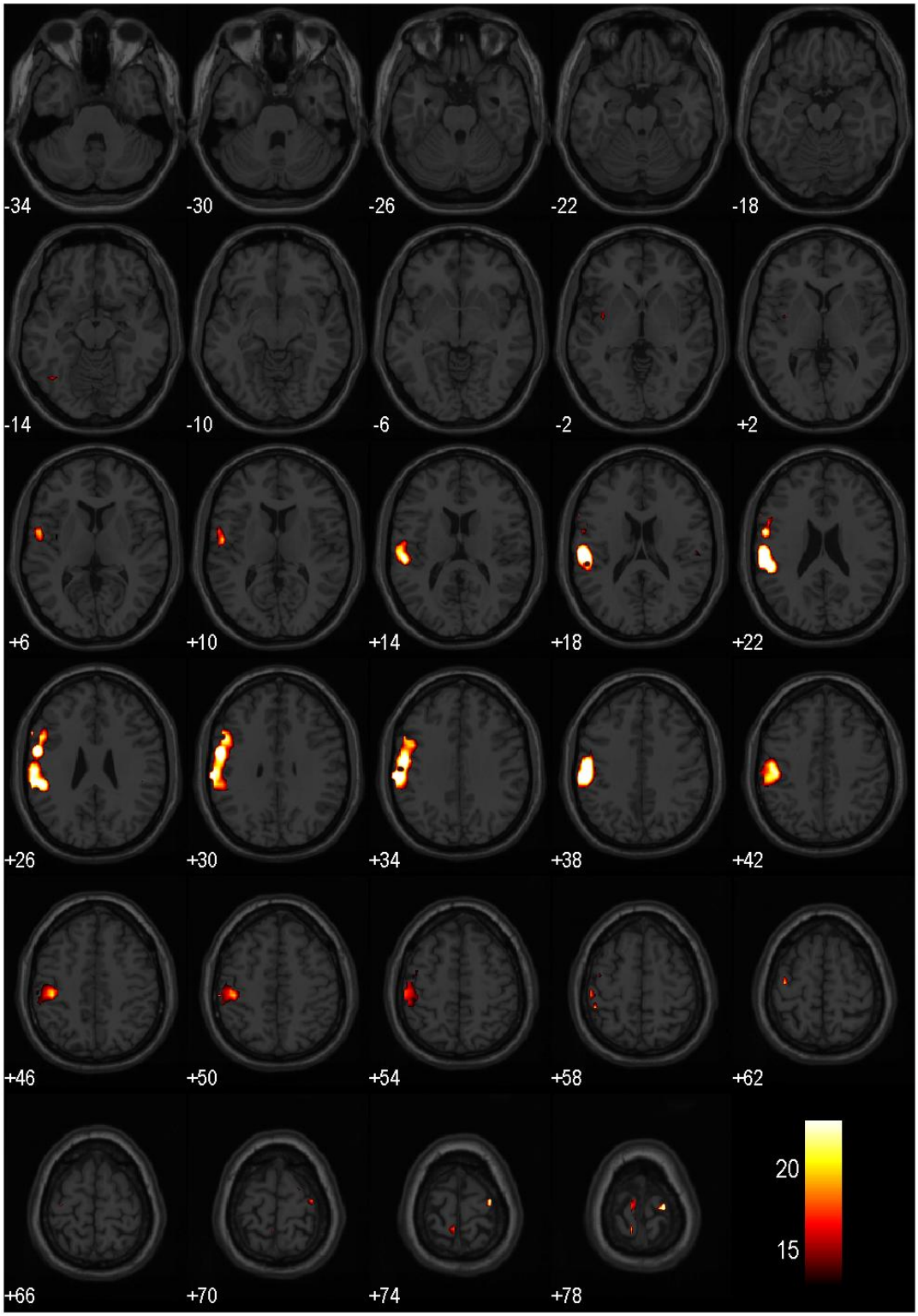

Figure C.3 *Statistical map of TMS pulses of 115% RMT delivered to the hand area within the left M1 contrasted with baseline activity (P < 0.05, FWE corrected). The participant reported TMS-induced thumb movements. M1: primary motor cortex.*

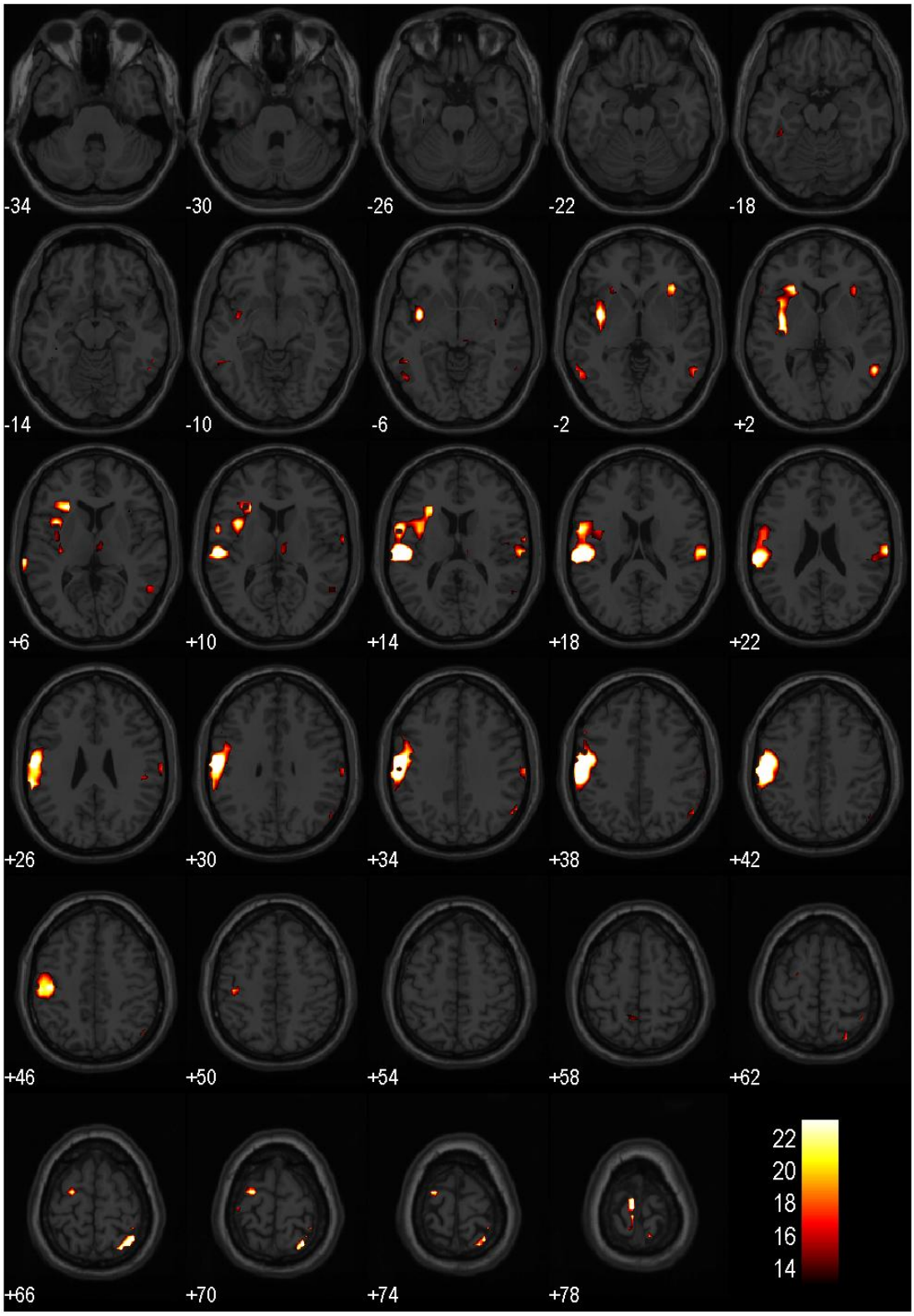

Figure C.4 *Statistical map of TMS pulses of 115% RMT delivered to the hand area within the left M1 contrasted with baseline activity (P < 0.05, FWE corrected). The participant did* ***not*** *report TMS-induced thumb movements. M1: primary motor cortex.*

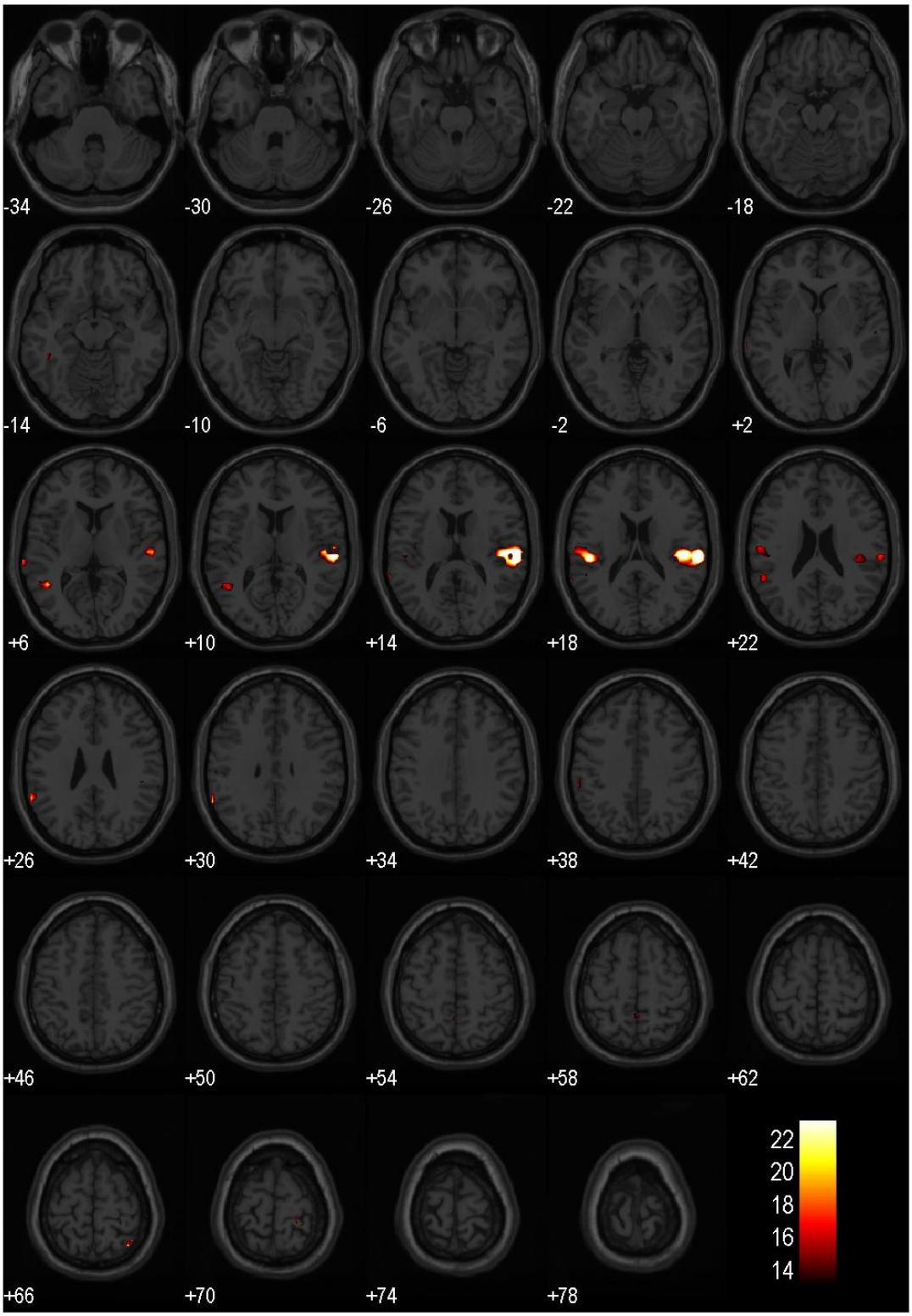

Figure C.5 *Statistical map of TMS pulses of 115% RMT delivered to the hand area within the left M1 contrasted with baseline activity (P < 0.05, FWE corrected). The participant did* ***not*** *report TMS-induced thumb movements. M1: primary motor cortex.*

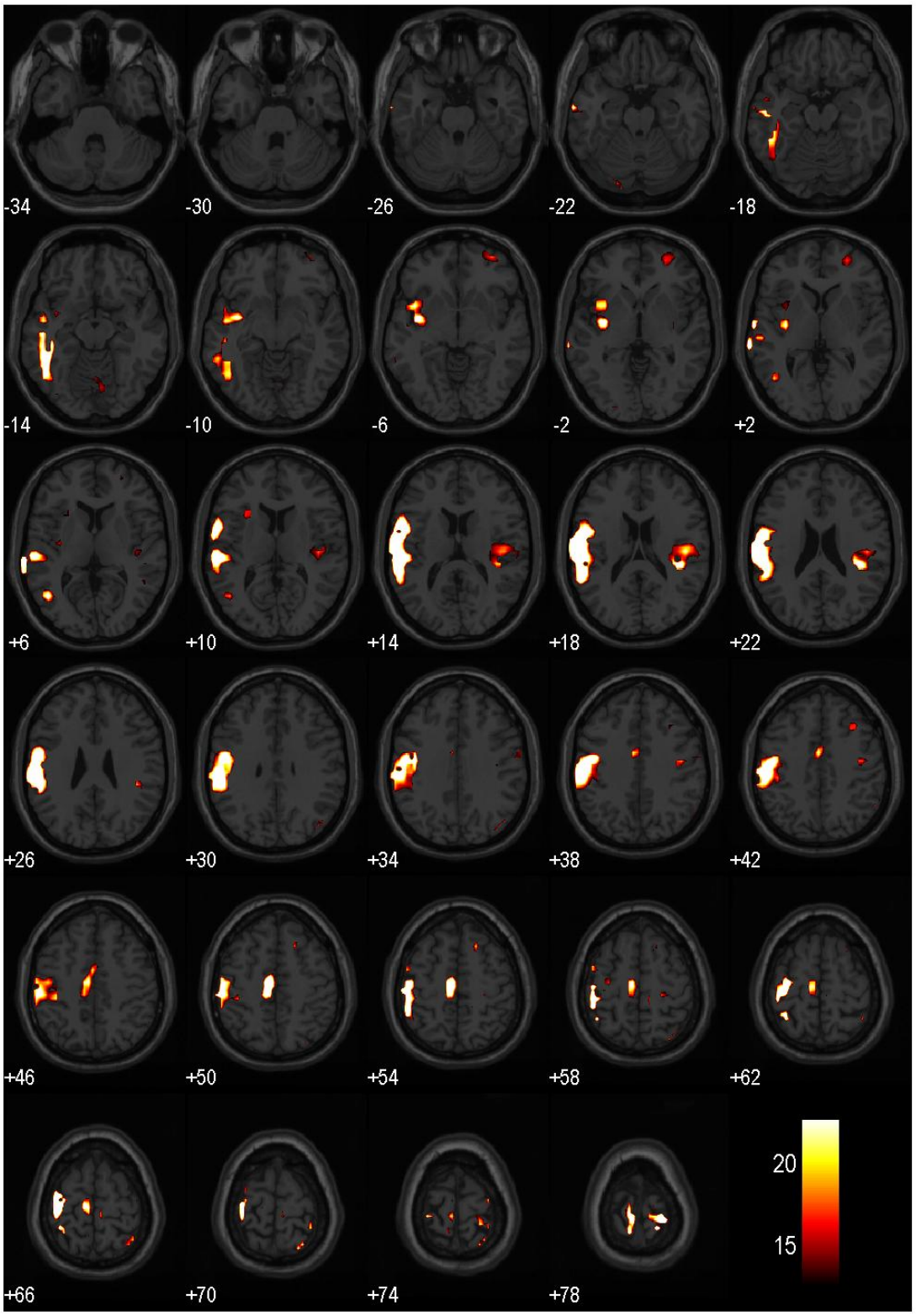

Figure C.6 *Statistical map of TMS pulses of 115% RMT delivered to the hand area within the left M1 contrasted with baseline activity (P < 0.05, FWE corrected). The participant reported TMS-induced thumb movements. M1: primary motor cortex.*

Appendix D

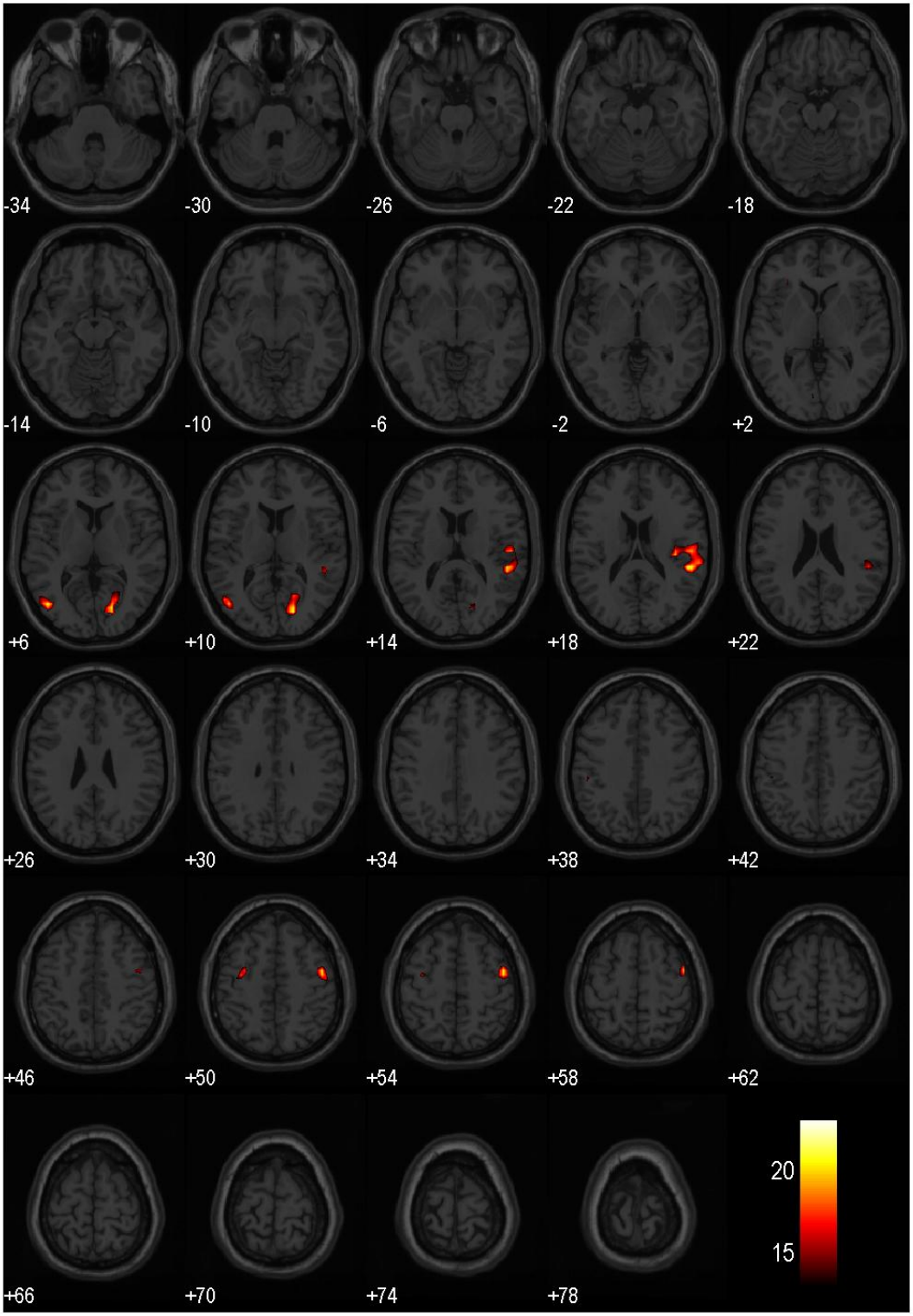

Figure D.1 *Statistical map of TMS pulses of 100% RMT delivered to the left DLPFC contrasted with baseline activity (P < 0.05, FWE corrected). The TMS coil isocenter was located* ***inside*** *the left DLPFC. DLPFC: dorsolateral prefrontal cortex.*

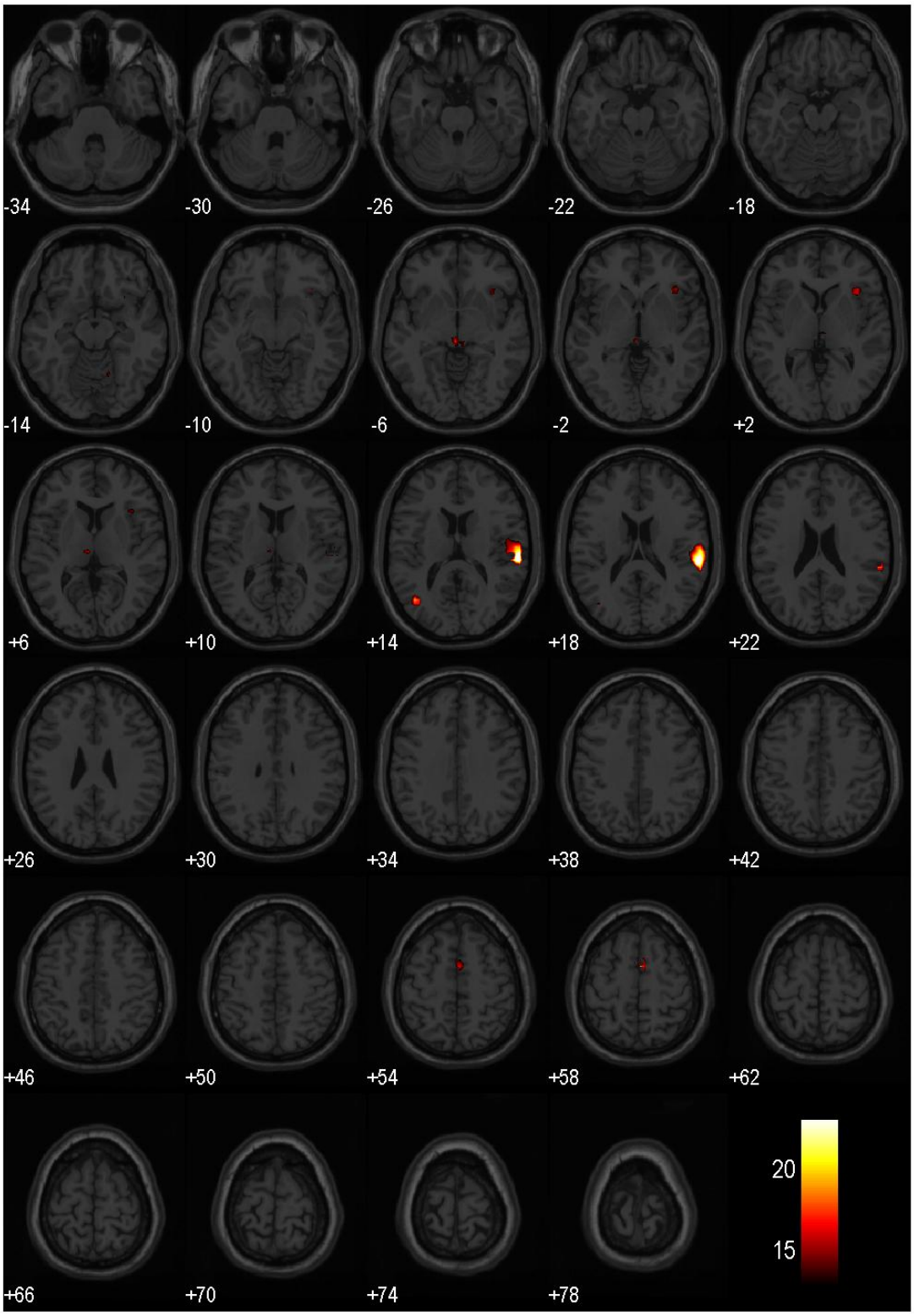

Figure D.2 *Statistical map of TMS pulses of 100% RMT delivered to the left DLPFC contrasted with baseline activity (P < 0.05, FWE corrected). The TMS coil isocenter was located* ***outside*** *the left DLPFC. DLPFC: dorsolateral prefrontal cortex.*

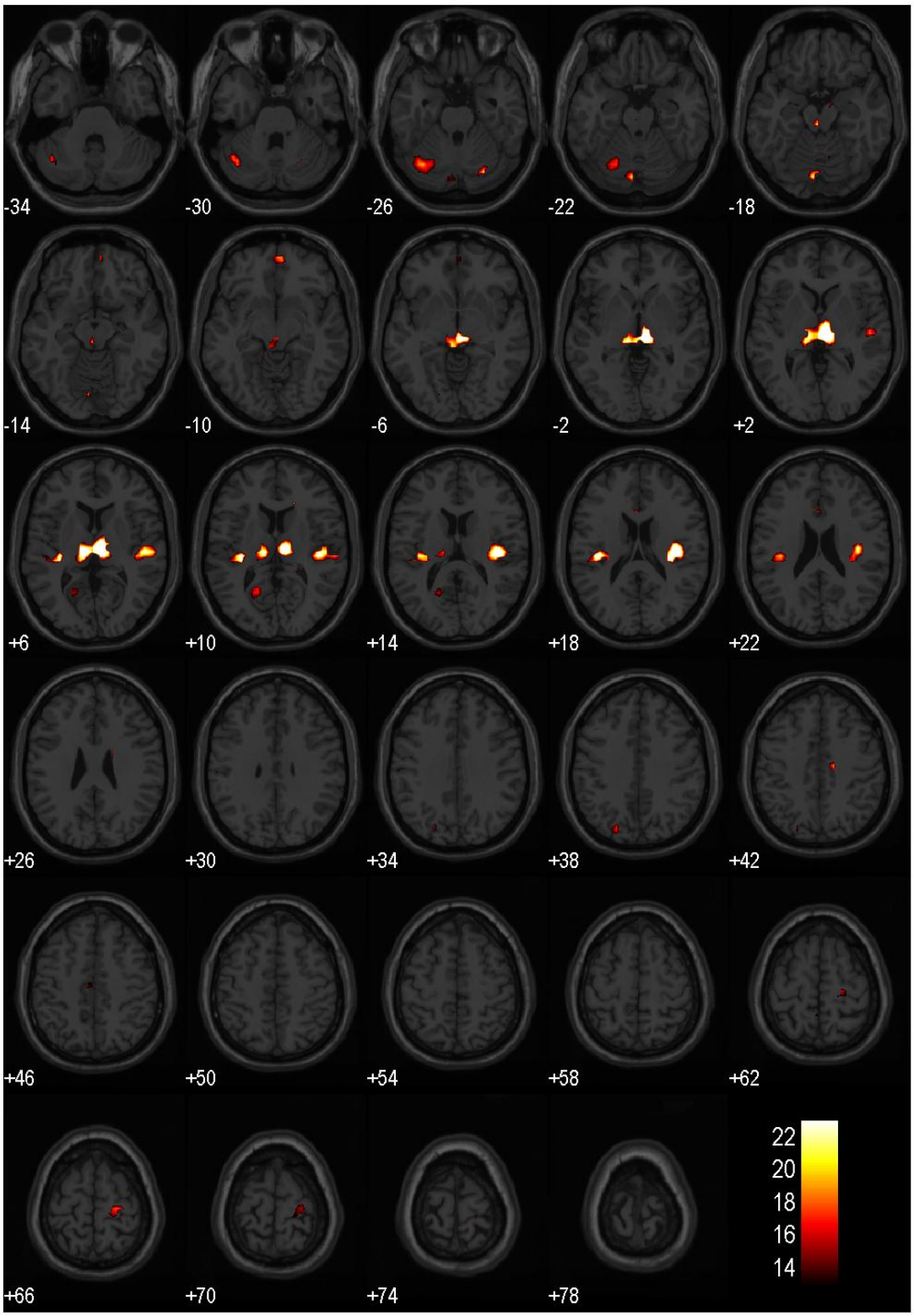

Figure D.3 *Statistical map of TMS pulses of 100% RMT delivered to the left DLPFC contrasted with baseline activity (P < 0.05, FWE corrected). The TMS coil isocenter was located* ***inside*** *the left DLPFC. DLPFC: dorsolateral prefrontal cortex.*

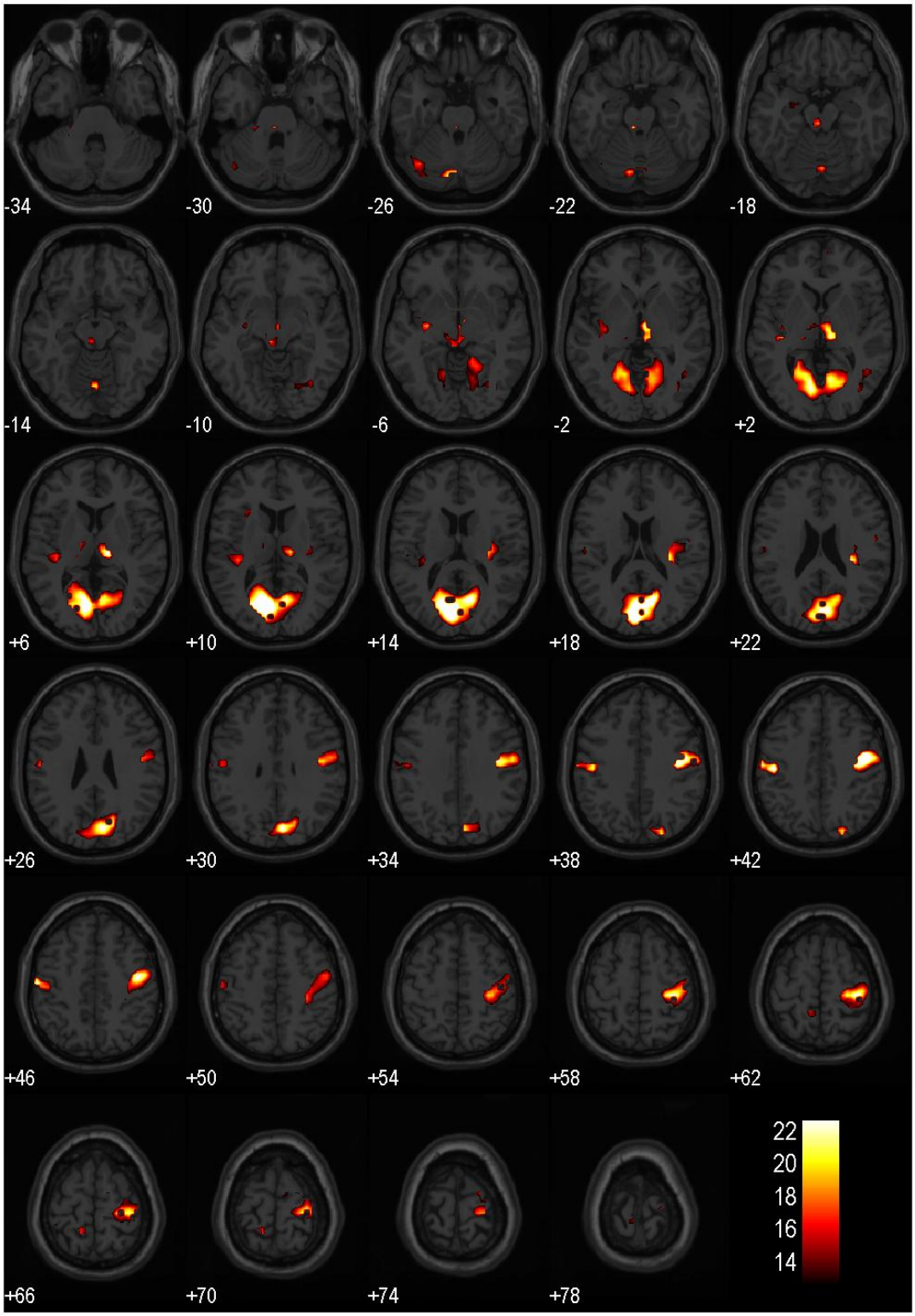

Figure D.4 *Statistical map of TMS pulses of 100% RMT delivered to the left DLPFC contrasted with baseline activity (P < 0.05, FWE corrected). The TMS coil isocenter was located* ***inside*** *the left DLPFC. DLPFC: dorsolateral prefrontal cortex.*

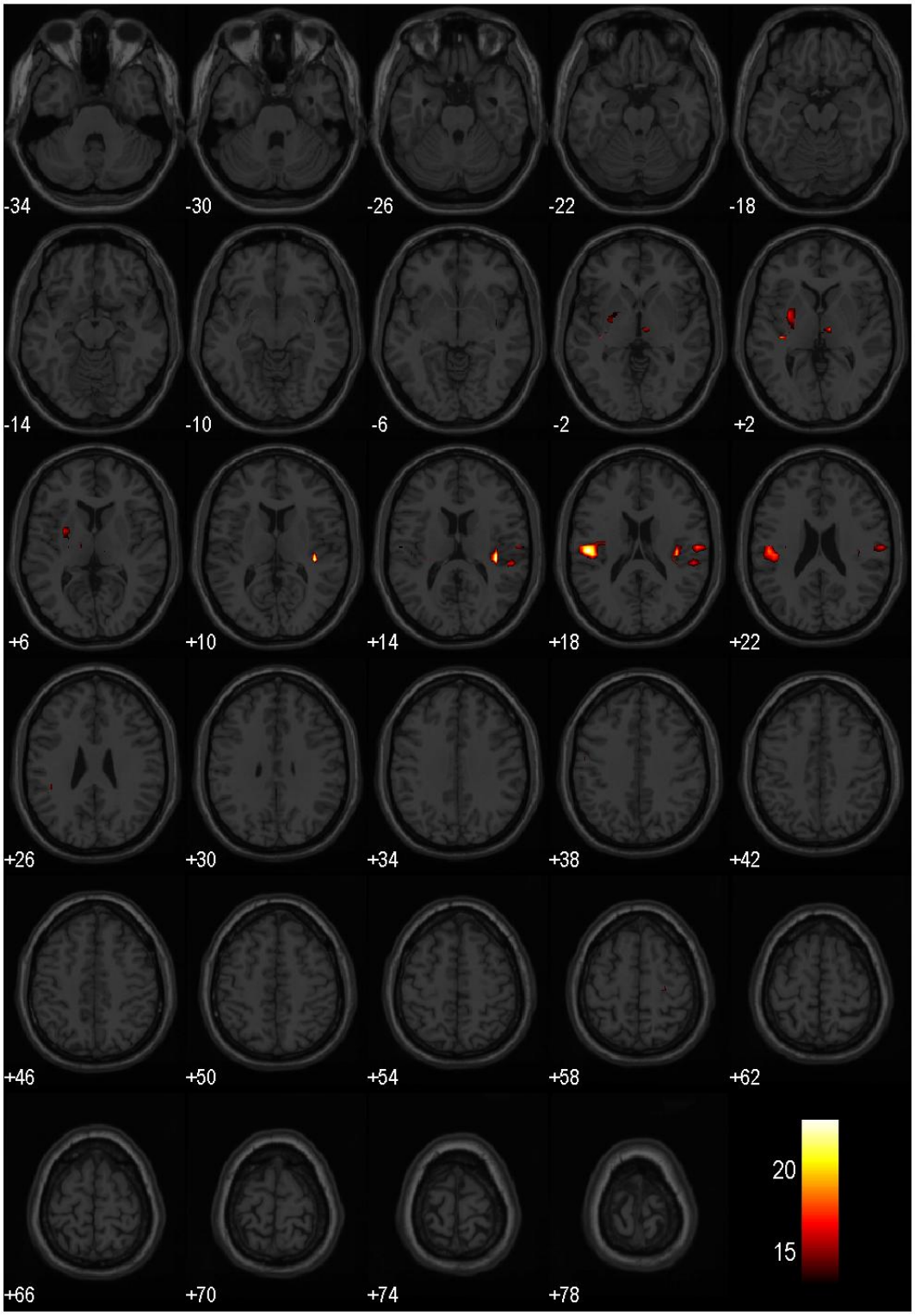

Figure D.5 *Statistical map of TMS pulses of 100% RMT delivered to the left DLPFC contrasted with baseline activity (P < 0.05, FWE corrected). The TMS coil isocenter was located* ***outside*** *the left DLPFC. DLPFC: dorsolateral prefrontal cortex.*

Appendix E

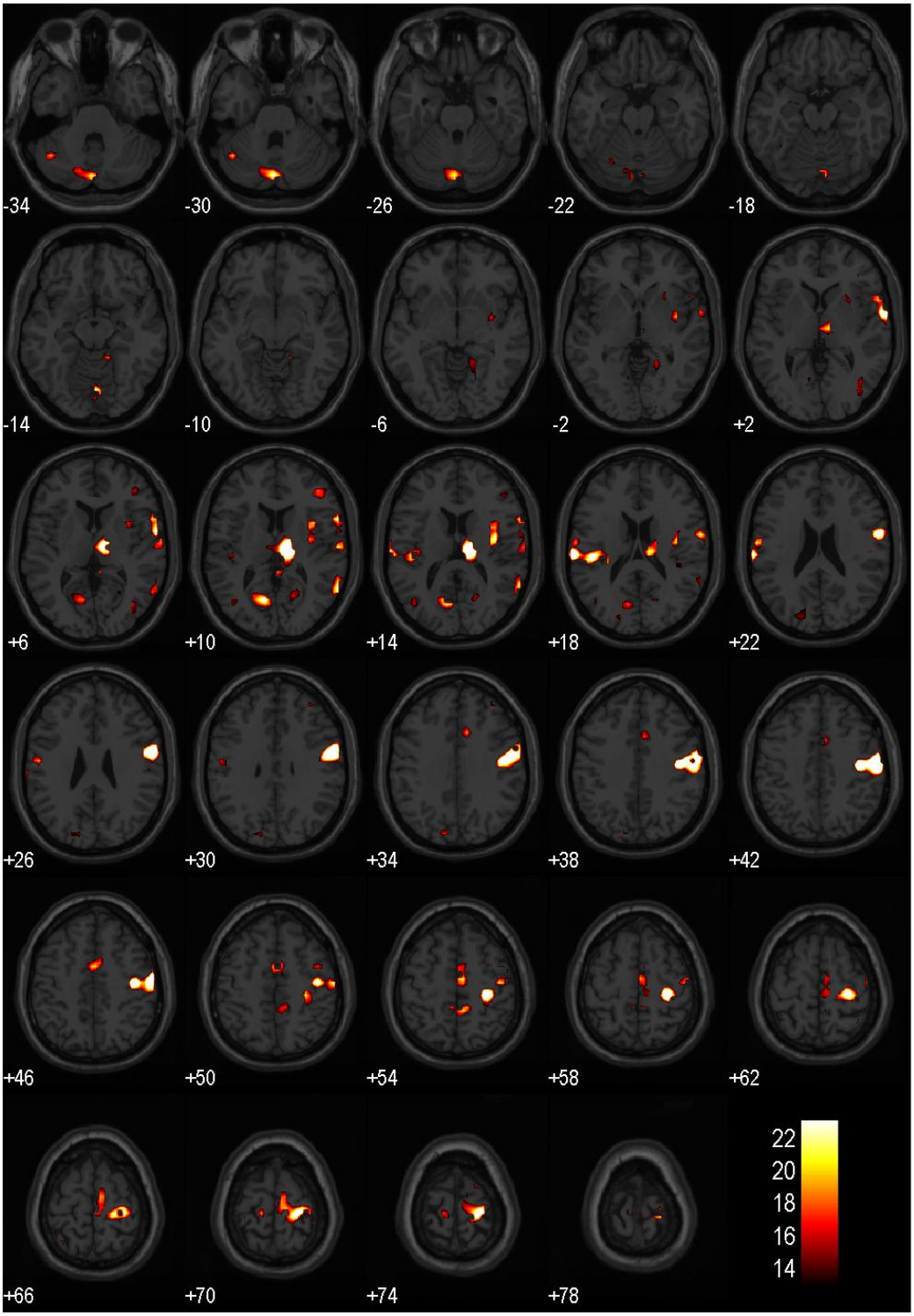

Figure E.1 *Statistical map of TMS pulses of 115% RMT delivered to the left DLPFC contrasted with baseline activity (P < 0.05, FWE corrected). The TMS coil isocenter was located* ***inside*** *the left DLPFC. DLPFC: dorsolateral prefrontal cortex.*

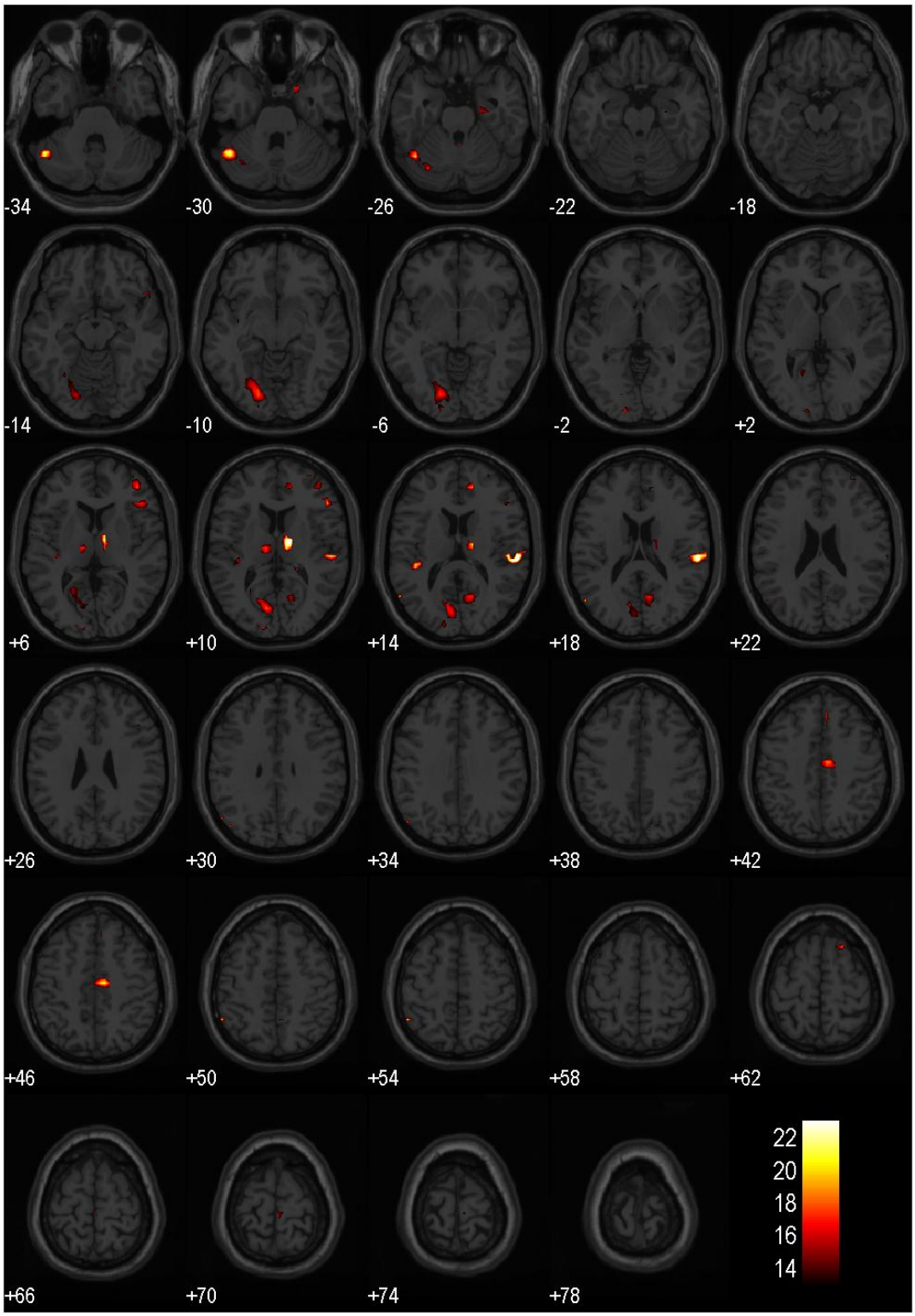

Figure E.2 *Statistical map of TMS pulses of 115% RMT delivered to the left DLPFC contrasted with baseline activity (P < 0.05, FWE corrected). The TMS coil isocenter was located* ***outside*** *the left DLPFC. DLPFC: dorsolateral prefrontal cortex.*

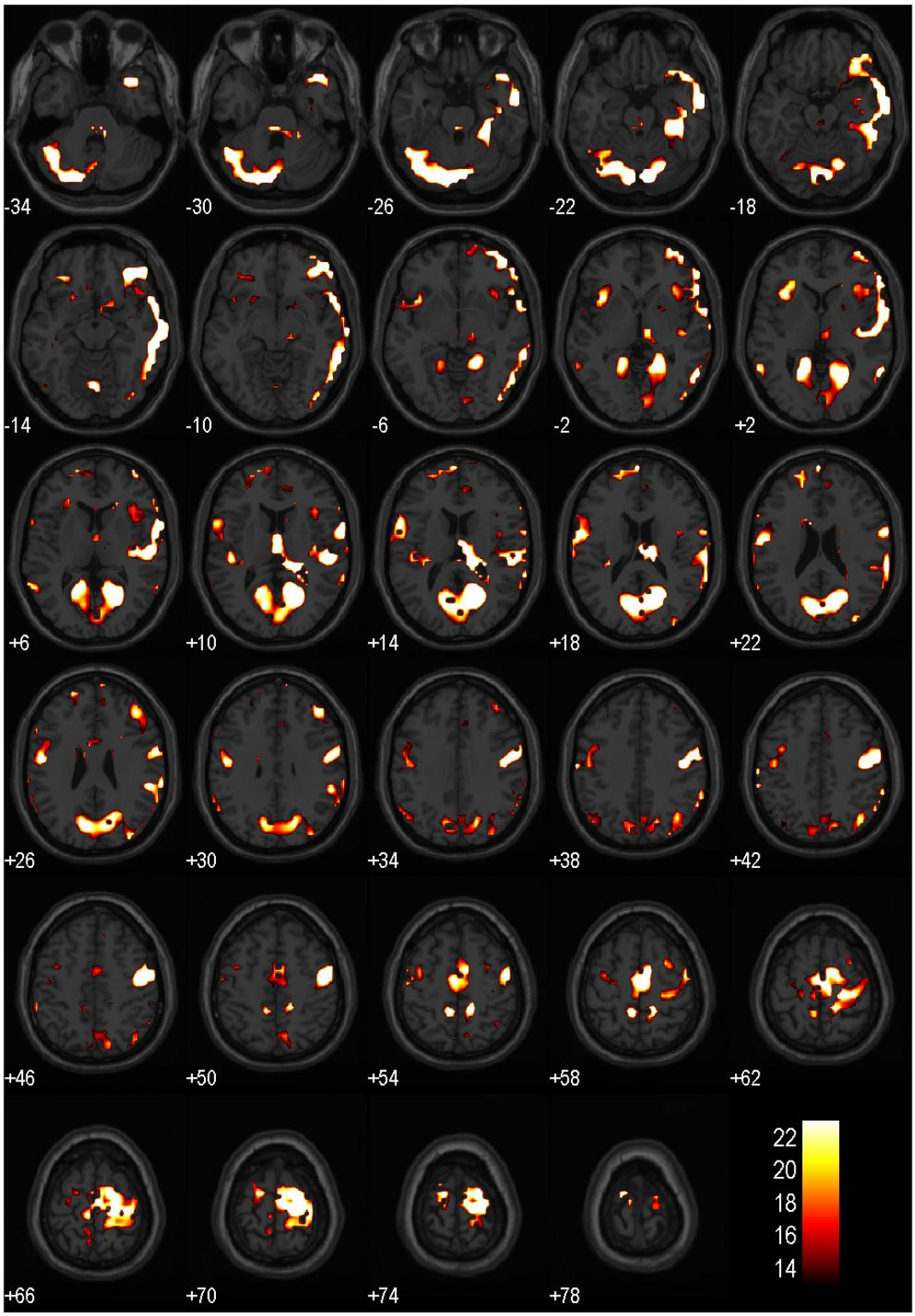

Figure E.3 *Statistical map of TMS pulses of 115% RMT delivered to the left DLPFC contrasted with baseline activity (P < 0.05, FWE corrected). The statistical map shows movement artefacts. The TMS coil isocenter was located* ***inside*** *the left DLPFC. DLPFC: dorsolateral prefrontal cortex.*

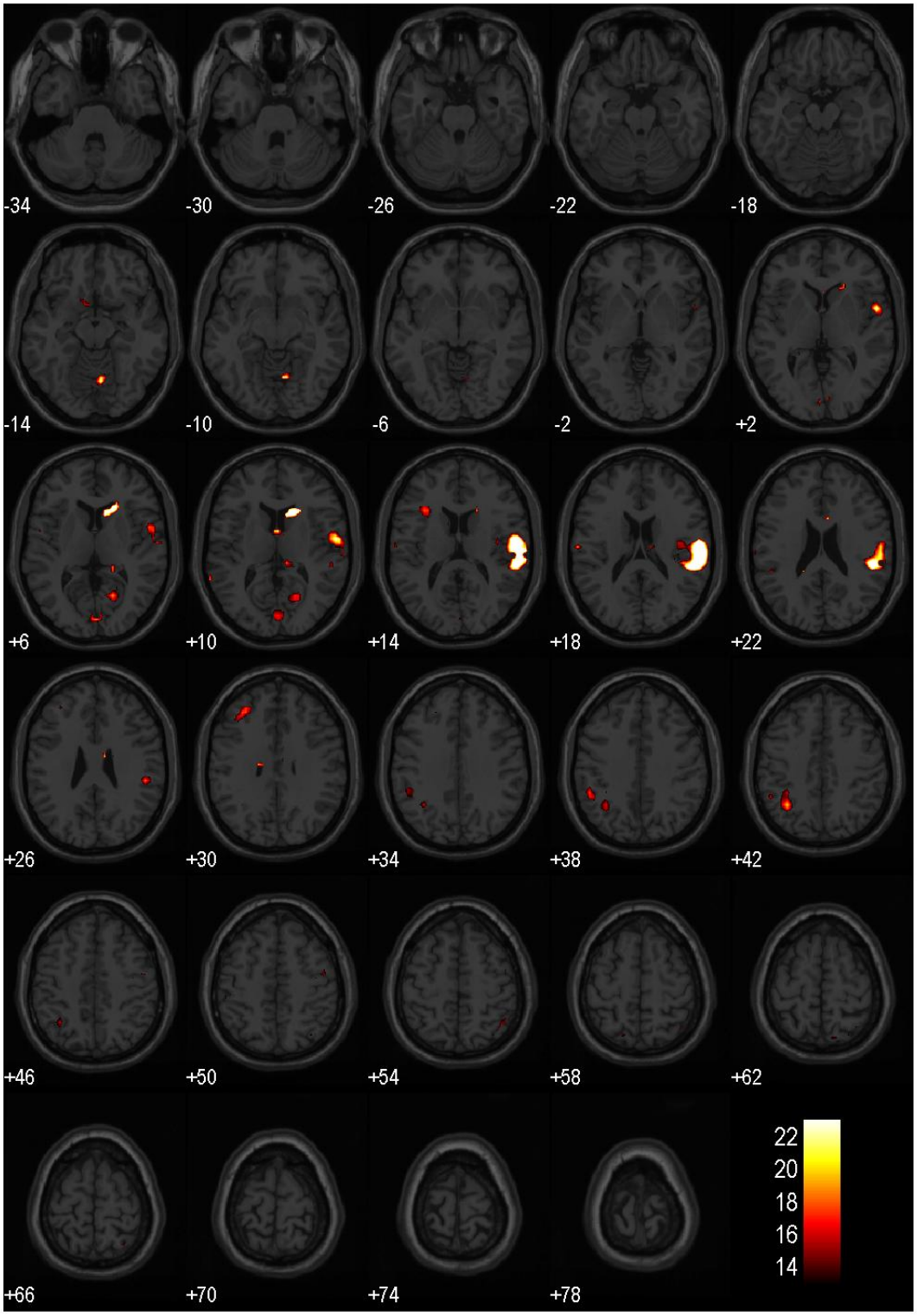

Figure E.4 *Statistical map of TMS pulses of 115% RMT delivered to the left DLPFC contrasted with baseline activity (P < 0.05, FWE corrected). The TMS coil isocenter was located* ***inside*** *the left DLPFC. DLPFC: dorsolateral prefrontal cortex.*

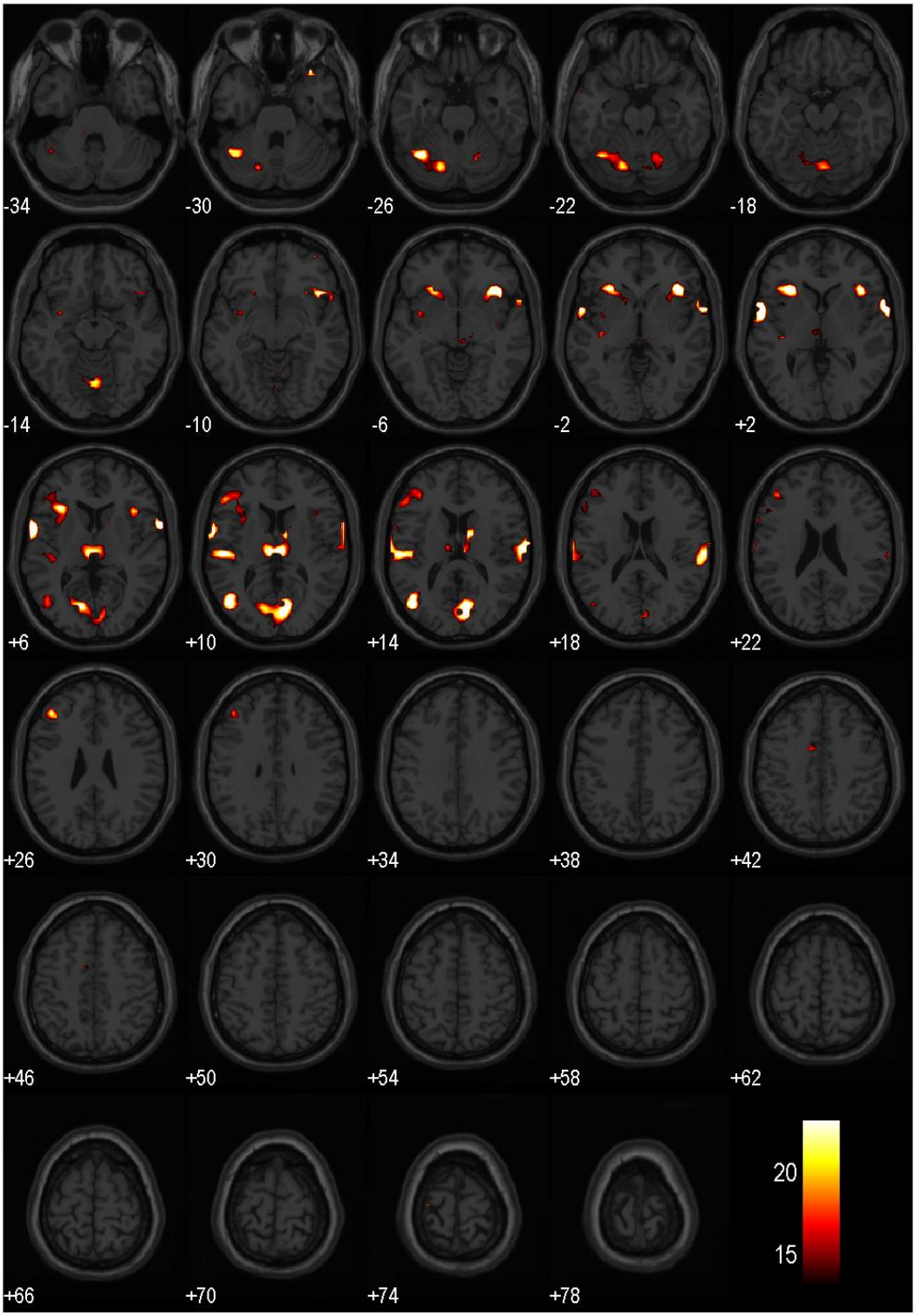

Figure E.5 *Statistical map of TMS pulses of 115% RMT delivered to the left DLPFC contrasted with baseline activity (P < 0.05, FWE corrected). The TMS coil isocenter was located* ***inside*** *the left DLPFC. DLPFC: dorsolateral prefrontal cortex.*

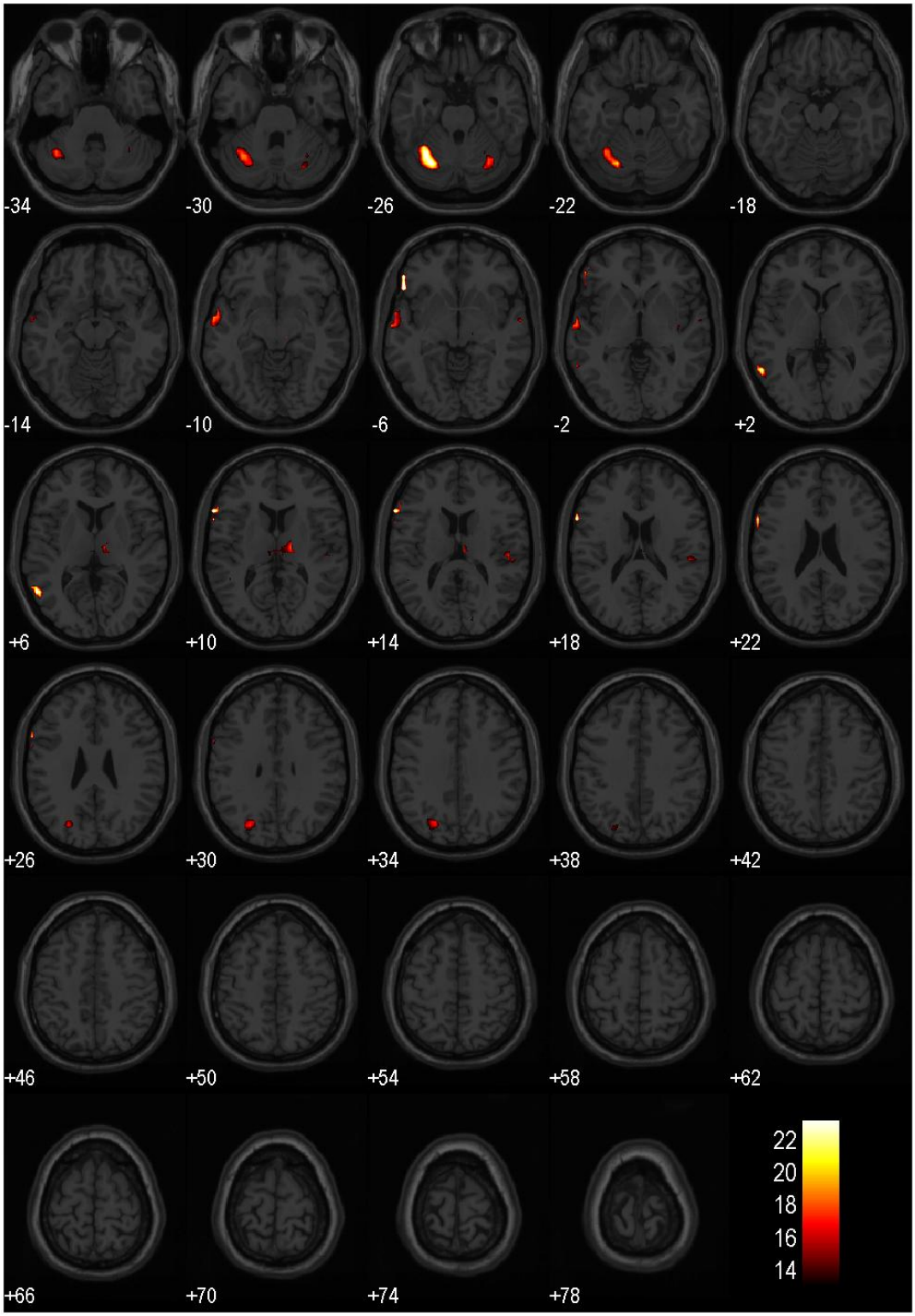

Figure E.6 *Statistical map of TMS pulses of 115% RMT delivered to the left DLPFC contrasted with baseline activity (P < 0.05, FWE corrected). The TMS coil isocenter was located* ***outside*** *the left DLPFC. DLPFC: dorsolateral prefrontal cortex.*

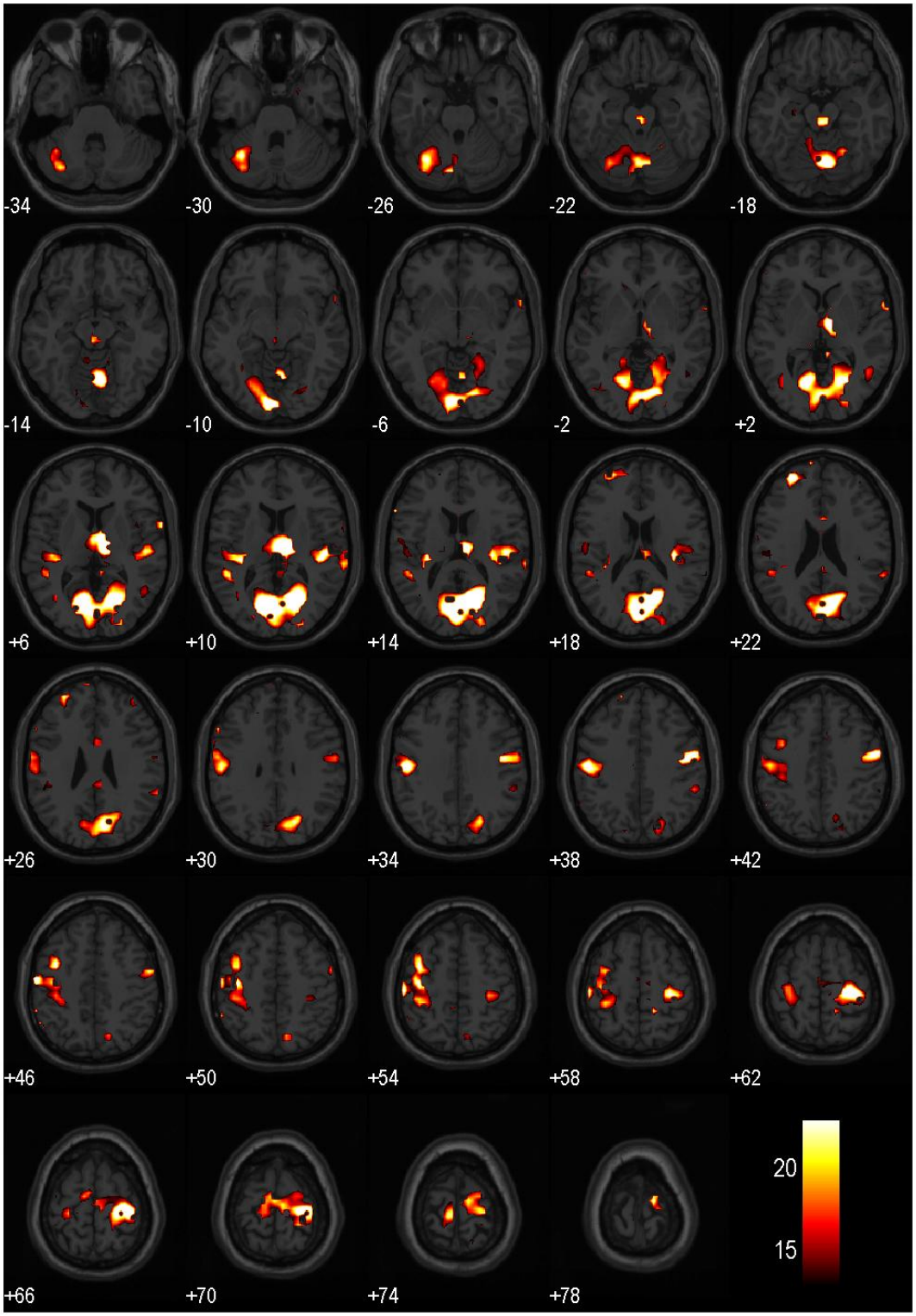

Figure E.7 *Statistical map of TMS pulses of 115% RMT delivered to the left DLPFC contrasted with baseline activity (P < 0.05, FWE corrected). The TMS coil isocenter was located* ***inside*** *the left DLPFC. DLPFC: dorsolateral prefrontal cortex.*

Appendix F

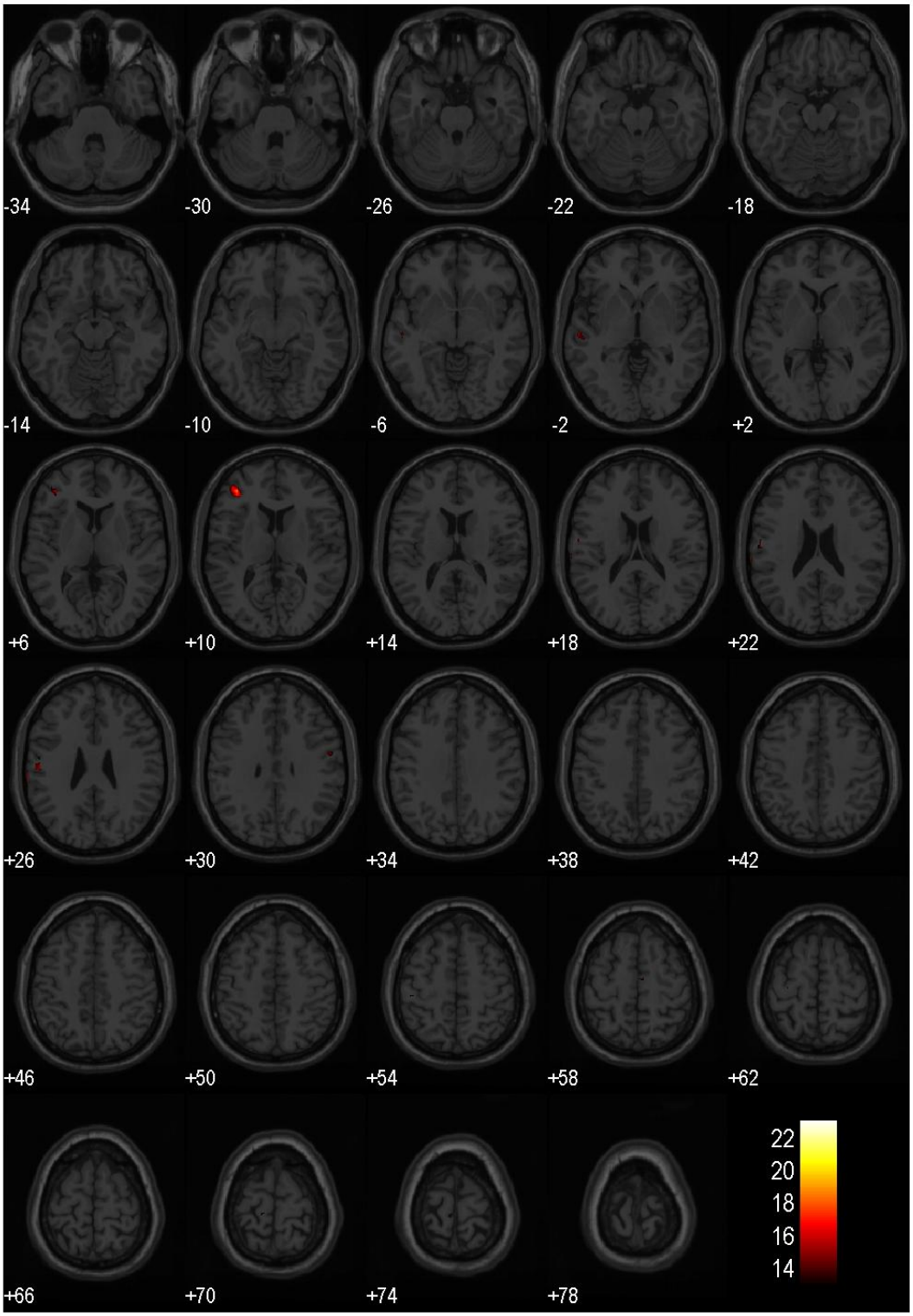

Figure F.1 *Statistical map of TMS pulses of 115% RMT delivered to the left DLPFC contrasted with TMS pulses of 60% RMT (P < 0.05, FWE corrected). The TMS coil isocenter was located* ***inside*** *the left DLPFC. DLPFC: dorsolateral prefrontal cortex.*

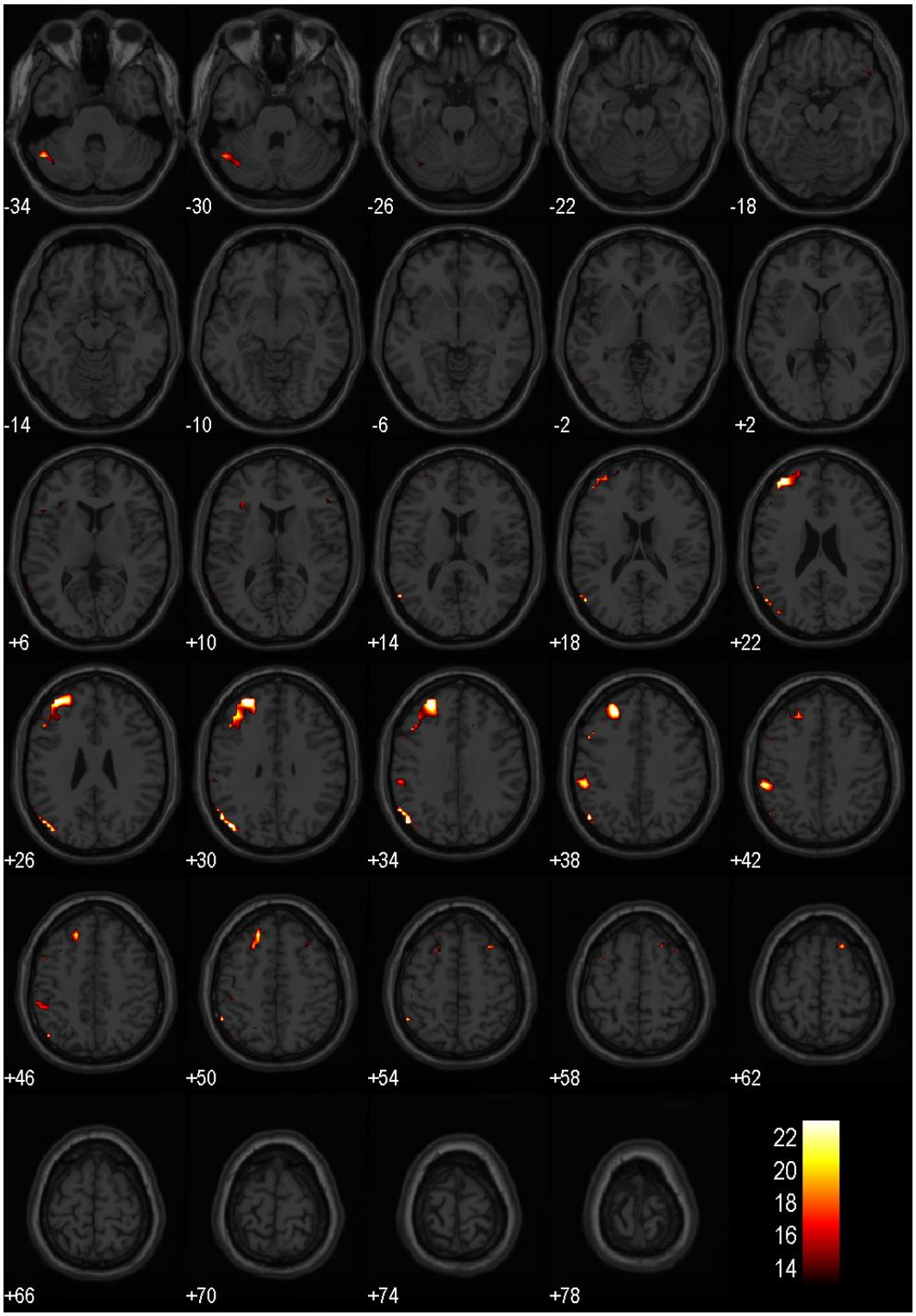

Figure F.2 *Statistical map of TMS pulses of 115% RMT delivered to the left DLPFC contrasted with TMS pulses of 60% RMT (P < 0.05, FWE corrected). The TMS coil isocenter was located* ***outside*** *the left DLPFC. DLPFC: dorsolateral prefrontal cortex.*

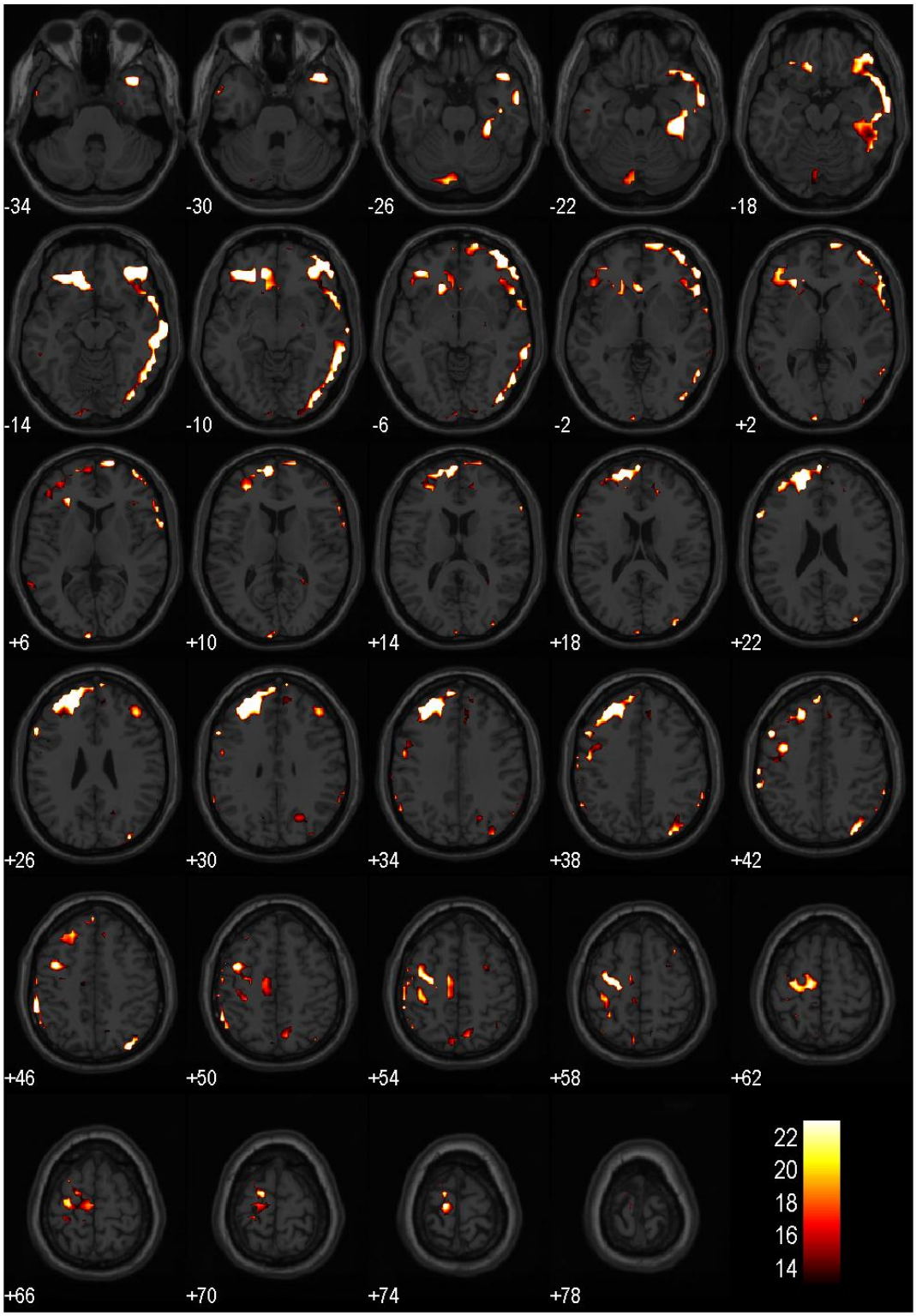

Figure F.3 *Statistical map of TMS pulses of 115% RMT delivered to the left DLPFC contrasted with TMS pulses of 60% RMT (P < 0.05, FWE corrected). The statistical map shows movement artefacts. The TMS coil isocenter was located* ***inside*** *the left DLPFC. DLPFC: dorsolateral prefrontal cortex.*

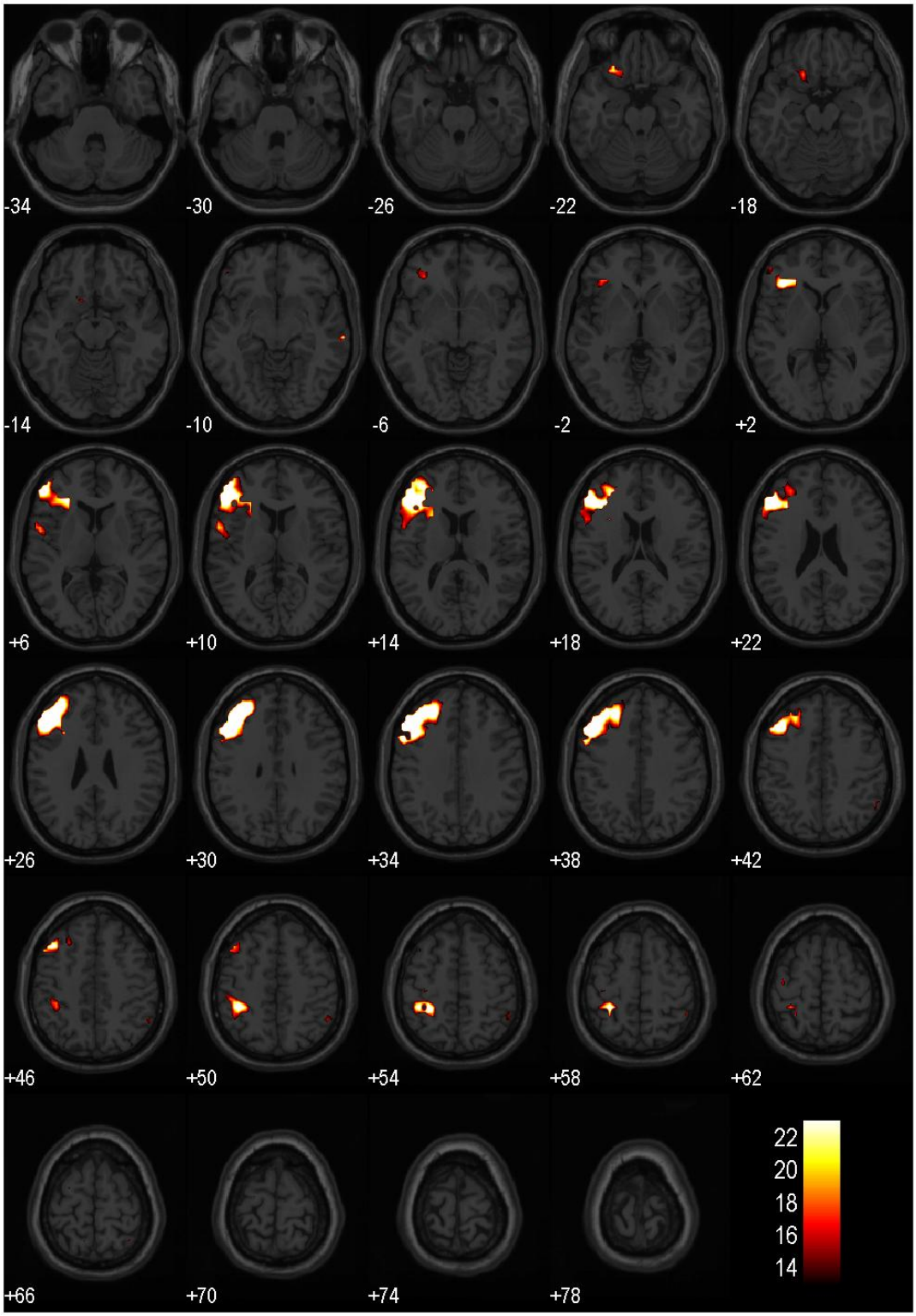

Figure F.4 *Statistical map of TMS pulses of 115% RMT delivered to the left DLPFC contrasted with TMS pulses of 60% RMT (P < 0.05, FWE corrected). The TMS coil isocenter was located* ***inside*** *the left DLPFC. DLPFC: dorsolateral prefrontal cortex.*

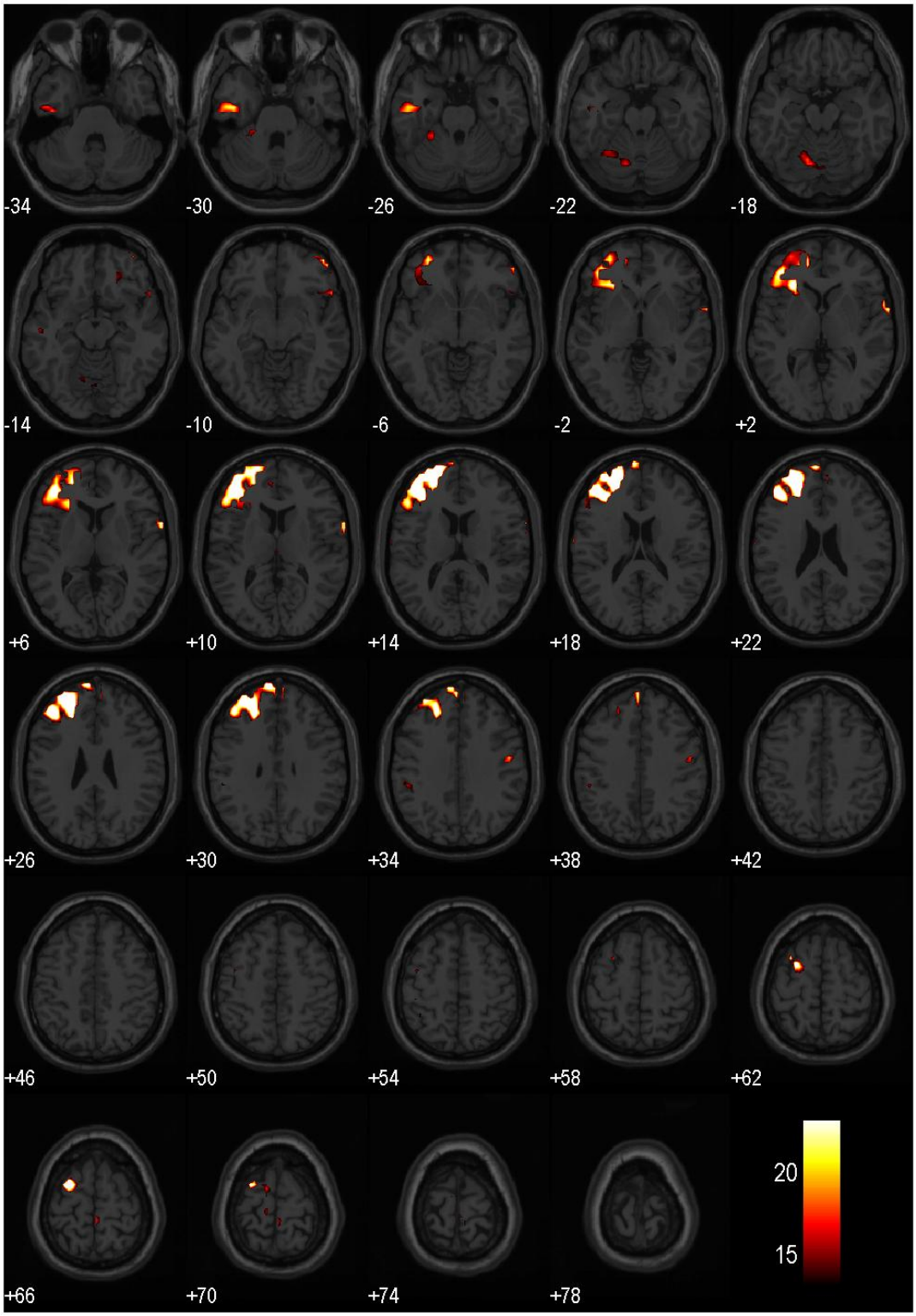

Figure F.5 *Statistical map of TMS pulses of 115% RMT delivered to the left DLPFC contrasted with TMS pulses of 60% RMT (P < 0.05, FWE corrected). The TMS coil isocenter was located* ***inside*** *the left DLPFC. DLPFC: dorsolateral prefrontal cortex.*

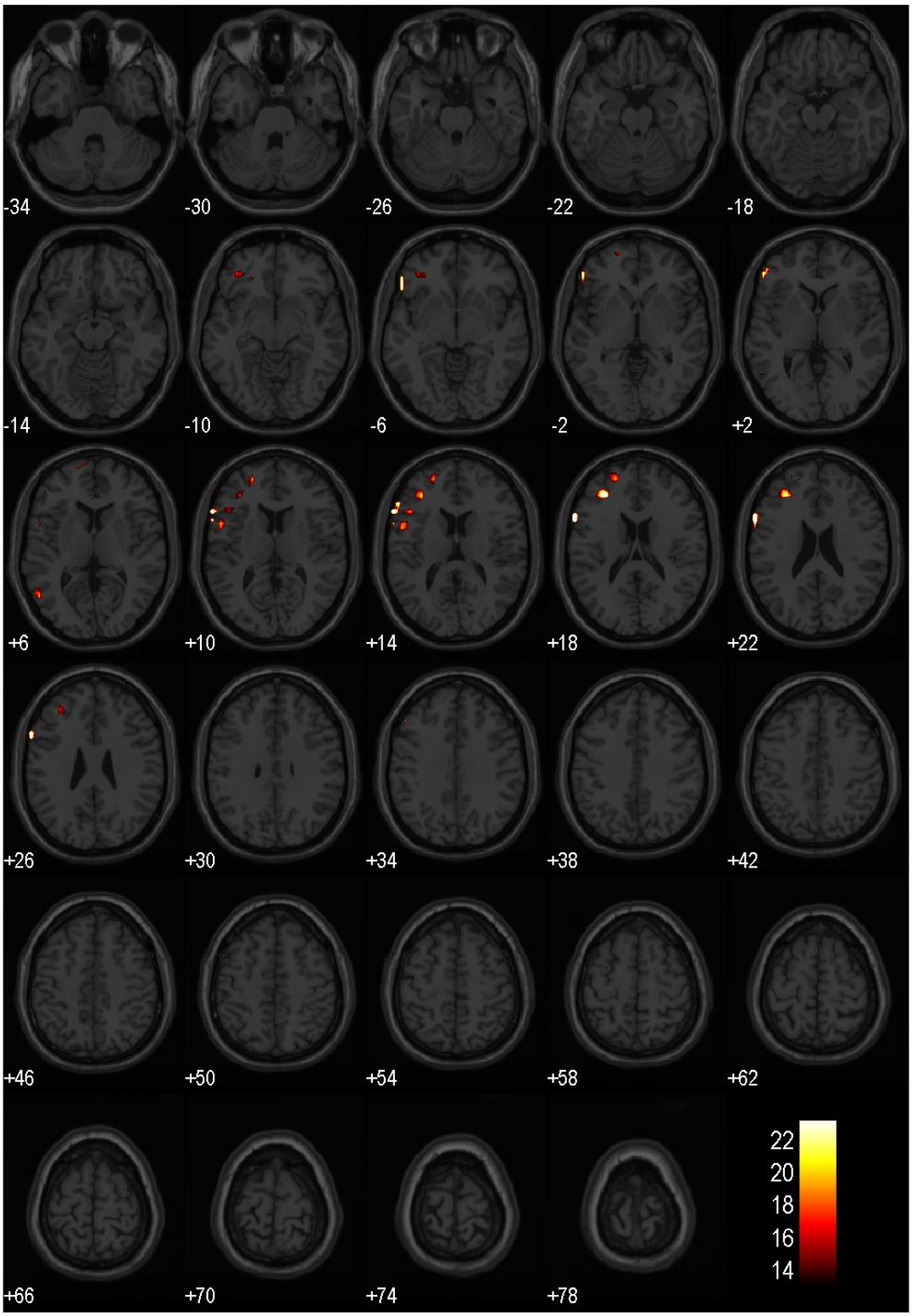

Figure F.6 *Statistical map of TMS pulses of 115% RMT delivered to the left DLPFC contrasted with TMS pulses of 60% RMT (P < 0.05, FWE corrected). The TMS coil isocenter was located* ***outside*** *the left DLPFC. DLPFC: dorsolateral prefrontal cortex.*

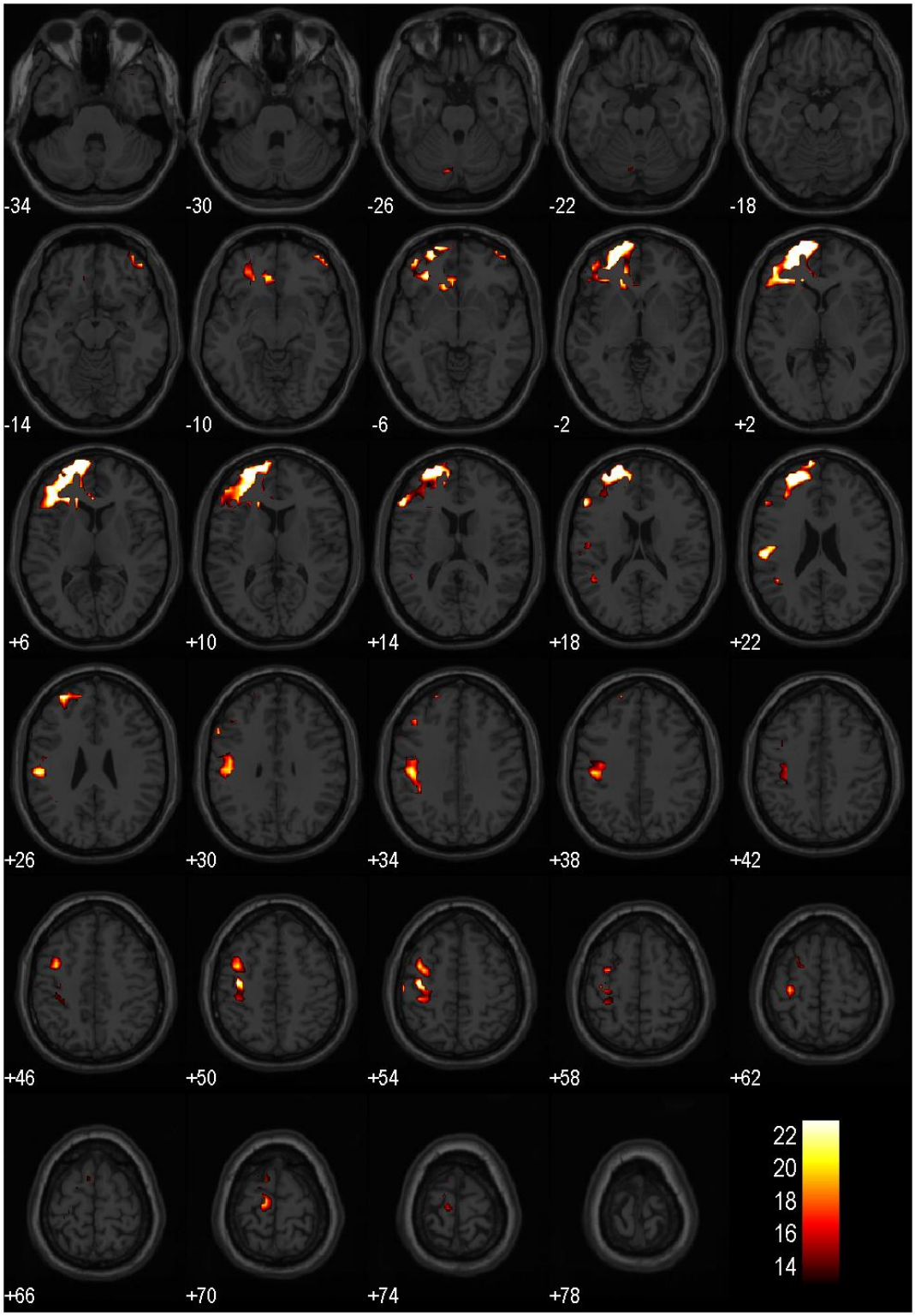

Figure F.7 *Statistical map of TMS pulses of 115% RMT delivered to the left DLPFC contrasted with TMS pulses of 60% RMT (P < 0.05, FWE corrected). The TMS coil isocenter was located* ***inside*** *the left DLPFC. DLPFC: dorsolateral prefrontal cortex.*